

CP violation of two-body hadronic Λ_b decays in the PQCD approach

Jia-Jie Han¹, Ji-Xin Yu¹ ^a, Ya Li² ^b, Hsiang-nan Li³ ^c,
 Jian-Peng Wang¹ ^d, Zhen-Jun Xiao⁴ ^e, Fu-Sheng Yu¹ ^f

¹*Frontiers Science Center for Rare Isotopes,
 and School of Nuclear Science and Technology,
 Lanzhou University, Lanzhou 730000, People's Republic of China*

²*Department of Physics, College of Sciences,
 Nanjing Agricultural University, Nanjing 210095, People's Republic of China*

³*Institute of Physics, Academia Sinica, Taipei, Taiwan 115, Republic of China*

⁴*Department of Physics and Institute of Theoretical Physics,
 Nanjing Normal University, Nanjing 210023, People's Republic of China*

We systematically investigate the CP -averaged branching ratios and CP violations (CPVs) for the two-body hadronic decays $\Lambda_b \rightarrow ph$, where h runs through the mesons π^- , ρ^- , a_1^- (1260), K^- , K^{*-} , K_1^- (1270) and K_1^- (1400), in the perturbative QCD approach to order α_s^2 in the strong coupling. Various topological amplitudes are obtained by incorporating subleading-twist hadron distribution amplitudes, which exhibit reasonable hierarchical patterns, sizable strong phases, and non-negligible higher-power corrections. The predicted direct CPVs in $\Lambda_b \rightarrow p\pi^-$, pK^- , different from those in similar B meson decays, are as small as the current data. The low CPV in $\Lambda_b \rightarrow p\pi^-$ results from the cancellation between the S - and P -wave CPVs, while the one in $\Lambda_b \rightarrow pK^-$ is determined by the tiny S -wave CPV. However, individual partial-wave CPVs can exceed 10%, consistent with direct CPVs in B meson decays. The CPVs in the $\Lambda_b \rightarrow pK_1^-$ (1270), pK_1^- (1400) channels are relatively larger. In particular, CPVs above 20% appear in the up-down asymmetries associated with the final-state angular distributions of $\Lambda_b \rightarrow pK_1^-$ (1270), pK_1^- (1400), followed by the secondary $K_1 \rightarrow K\pi\pi$ decays. These observables offer promising prospects for firmly establishing baryon CPVs. The decay asymmetry parameters of $\Lambda_b \rightarrow ph$ are also predicted for future experimental confrontations.

^a Corresponding author, Email: yujx18@lzu.edu.cn

^b Corresponding author, Email: liyakelly@163.com

^c Corresponding author, Email: hnli@phys.sinica.edu.tw

^d Corresponding author, Email: wangjp20@lzu.edu.cn

^e Corresponding author, Email: xiaozhenjun@njnu.edu.cn

^f Corresponding author, Email: yufsh@lzu.edu.cn

CONTENTS

I. Introduction	2
II. Framework	4
A. Effective Hamiltonian	4
B. Topological diagrams	5
C. Kinematics	6
D. Distribution amplitudes	7
E. Numerical integration	14
III. Numerical Results	16
A. Two-body $\Lambda_b \rightarrow ph$ decays	16
B. Quasi-two-body $\Lambda_b \rightarrow pV$ decays	29
C. Quasi-two-body $\Lambda_b \rightarrow pA$ decays	31
IV. Summary	37
Acknowledgements	38
A. Auxiliary functions	38
B. Decay amplitudes	39
C. Numerical results for $\Lambda_b \rightarrow pV, pA$ decays	52
References	69

I. INTRODUCTION

The explanation of the asymmetry between matter and antimatter in the Universe requires CP violations (CPVs), where C and P represent the charge-conjugation and parity, respectively. The standard model (SM) of particle physics provides the Cabibbo–Kobayashi–Maskawa (CKM) mechanism for generating CPVs, which is, however, too weak to account for the excess of matter. Additional sources of CPVs are thus needed, and their exploration has marked a long-term effort. CPVs have been observed in K [1], B [2, 3] and D [4] meson decays, and consistent with the SM predictions. However, they have not yet been firmly established in baryonic processes. Given that visible matter in the Universe is mainly composed of baryons, it is natural to search for CPVs in baryon systems.

Baryons cannot undergo mixing owing to baryon number conservation, and exhibit only direct CPVs in their decays. Experimental investigations of baryon CPVs have been extensively pursued by the BESIII, Belle and LHCb Collaborations [5–15]. The measured direct CPVs [14]

$$\begin{aligned} A_{CP}^{\text{dir}}(\Lambda_b^0 \rightarrow p\pi^-) &= (0.2 \pm 0.8 \pm 0.4)\%, \\ A_{CP}^{\text{dir}}(\Lambda_b^0 \rightarrow pK^-) &= (-1.1 \pm 0.7 \pm 0.4)\%, \end{aligned} \tag{1}$$

are compatible with null asymmetries within the precision of 1%. That is, the CPVs in Λ_b baryon decays are much lower than those in similar B meson decays, although both are induced by

the $b \rightarrow u\bar{u}q$ transitions, $q = d, s$. Recently, the LHCb reported the evidence of the CPV in $\Lambda_b^0 \rightarrow \Lambda^0 K^+ K^-$ [15] and the first observation of the baryon CPV in the $\Lambda_b^0 \rightarrow p K^- \pi^+ \pi^-$ mode [16], which motivates timely related theoretical studies.

Baryon processes, engaging more complicated dynamics than meson ones, impose a number of phenomenological challenges [17]. The non-zero spin of a baryon prompts at least two partial waves, such as the S - and P -wave amplitudes in $\Lambda_b \rightarrow p\pi^-, pK^-$, while there is only a single partial wave in B meson decays into two pseudoscalar mesons. The polarizations of initial and final states in a baryon decay enable the construction of more observables out of angular distributions of decay products [8, 18–21], which shed valuable insight on involved QCD dynamics. A baryon contains three valence quarks, demanding at least two hard gluons to propagate momentum transfer in its exclusive decay. More gluon exchanges may enhance higher-power contributions and modify the behavior of power expansions [22, 23]. Besides, there also exist additional topological diagrams, including color-commensurate W -emission and W -exchange diagrams, that serve as abundant sources of strong phases required for direct CPVs.

Several theoretical approaches have been proposed for analyzing two-body hadronic B meson decays: the QCD factorization (QCDF) [24, 25], the soft-collinear-effective theory (SCET) [26–28] and the perturbative QCD (PQCD) factorization [29–31]. The QCDF and SCET are based on the collinear factorization theorem, in which B meson transition form factors develop endpoint singularities if they were computed perturbatively. The PQCD is based on the k_T factorization theorem, in which the endpoint contribution is absorbed into a transverse-momentum-dependent distribution amplitude (DA) or resummed into a Sudakov factor. The factorizable emission, nonfactorizable emission, W -exchange and annihilation diagrams, being free of the endpoint singularities, are then computable. CPVs of two-body hadronic B meson decays have been successfully predicted in the PQCD [29–31]. However, rigorous and systematic formalisms for heavy baryon decays are still unavailable. The generalized factorization assumption was employed to estimate branching ratios of numerous bottom-baryon decays [32–34]. As to QCD-inspired methods, the QCDF was applied to Λ_b baryon decays under the diquark approximation [35, 36], and the $\Lambda_b \rightarrow p\pi, pK$ branching ratios were evaluated in the PQCD [37], but with the results being several times smaller than data.

The $\Lambda_b \rightarrow p$ transition form factors with reasonable subleading-twist hadron DAs were reproduced in the PQCD recently, and the outcomes agree with those from lattice QCD and other nonperturbative methods [23]. It indicates that exclusive heavy baryon decays can be examined reliably in this framework. We will perform a comprehensive analysis on the two-body hadronic decays $\Lambda_b \rightarrow ph$, where h runs through the pseudoscalar (P) mesons π, K , the vector (V) mesons ρ, K^* and the axil-vector (A) mesons $a_1(1260), K_1(1270), K_1(1400)$. A decay amplitude is expressed as a convolution of the hard kernel T_H with the Sudakov factor e^{-S} and the nonperturbative DAs Ψ_{Λ_b}, Ψ_p and Ψ_h [17],

$$\mathcal{A} = \int_0^1 [dx] \int [d^2 b] \Psi_{\Lambda_b} T_H \Psi_p \Psi_h e^{-S}, \quad (2)$$

where x are the quark momentum fractions, b are conjugate to the quark transverse momenta k_T , and S represents the Sudakov exponent. In principle, the threshold resummation factor S_t arising from the all-order organization of the large logarithms $\ln^2 x$ should be included. Since S_t has not been derived for heavy baryon decays, we set $S_t = 1$ conservatively as in our previous work [23]. For further details of the PQCD formalism and its applications to heavy baryon decays, refer to Refs. [23, 37].

It will be demonstrated that CPVs in individual partial waves of Λ_b decays can be as large as those in B meson decays, greater than 10%, but the cancellation between partial waves leaves no

significant deviation from zero. The sign of a partial-wave CPV depends on the location of the weak vertex in the penguin diagram that provides the dominant source of strong phases. We will illustrate such cancellation in a full QCD calculation for the $\Lambda_b \rightarrow p\pi^-$ decay. The partial-wave CPVs in the $\Lambda_b \rightarrow p\rho^-, pK^{*-}, pa_1^-(1260), pK_1^-(1270)$ modes also reach 10%, but cancel each other, turning in small net values. Stimulated by the above observation, we propose to search for the CPVs in the up-down asymmetries associated with the angular distributions of the $\Lambda_b \rightarrow pa_1(1260), pK_1(1270), pK_1(1400)$ decay products. They are found to be of the order of 20%, granting an extraordinary opportunity to establish CPVs in the baryon sector. Our work unveils the distinct dynamics responsible for CPVs in bottom baryon and meson decays, and suggests to detect the former through partial-wave related CPV observables in angular distributions.

The remainder of this paper is arranged as follows. In Sec. II we present the effective Hamiltonian and classify the topologies of Feynman diagrams relevant to the considered channels. We specify the inputs for the factorization formula in Eq. (2), i.e., DAs of various twists for the Λ_b baryon, the proton and the mesons. The numerical algorithm for handling integrable singularities present in the factorization formulas is elaborated. The outcomes for the branching ratios and CPVs, and their phenomenological implications are discussed in Sec. III, which is divided into three subsections focusing on decays into pseudoscalar, vector and axial-vector mesons. Sec. IV summarizes our findings and sketches future perspectives. Appendix A contains the auxiliary functions as the hard kernels under the Fourier transformation from the k_T space to the b space. Appendix B gathers the $\Lambda_b \rightarrow ph$ decay amplitudes for the Feynman diagrams. Only one Feynman diagram is picked in each topology for simplicity. Appendix C displays the numerical results for the $\Lambda_b \rightarrow pV, pA$ amplitudes.

II. FRAMEWORK

A. Effective Hamiltonian

The weak effective Hamiltonian for the two-body hadronic Λ_b baryon decays is given by

$$\mathcal{H}_W = \frac{G_F}{\sqrt{2}} \left\{ V_{ub} V_{uq}^* [C_1(\mu) O_1^u(\mu) + C_2(\mu) O_2^u(\mu)] - V_{tb} V_{tq}^* \left[\sum_{i=3}^{10} C_i(\mu) O_i(\mu) \right] \right\}, \quad (3)$$

with the Fermi constants $G_F = 1.166 \times 10^{-5}$ GeV $^{-2}$ and the light quarks $q = d, s$. The local four-quark operators O_i read

$$\begin{aligned} O_1^u &= (\bar{u}_\alpha b_\beta)_{V-A} (\bar{q}_\beta u_\alpha)_{V-A}, & O_2^u &= (\bar{u}_\alpha b_\alpha)_{V-A} (\bar{q}_\beta u_\beta)_{V-A}, \\ O_3 &= (\bar{q}_\alpha b_\alpha)_{V-A} \sum_{q'} (\bar{q}'_\beta q'_\beta)_{V-A}, & O_4 &= (\bar{q}_\beta b_\alpha)_{V-A} \sum_{q'} (\bar{q}'_\alpha q'_\beta)_{V-A}, \\ O_5 &= (\bar{q}_\alpha b_\alpha)_{V-A} \sum_{q'} (\bar{q}'_\beta q'_\beta)_{V+A}, & O_6 &= (\bar{q}_\beta b_\alpha)_{V-A} \sum_{q'} (\bar{q}'_\alpha q'_\beta)_{V+A}, \\ O_7 &= \frac{3}{2} (\bar{q}_\alpha b_\alpha)_{V-A} \sum_{q'} e_{q'} (\bar{q}'_\beta q'_\beta)_{V+A}, & O_8 &= \frac{3}{2} (\bar{q}_\beta b_\alpha)_{V-A} \sum_{q'} e_{q'} (\bar{q}'_\alpha q'_\beta)_{V+A}, \\ O_9 &= \frac{3}{2} (\bar{q}_\alpha b_\alpha)_{V-A} \sum_{q'} e_{q'} (\bar{q}'_\beta q'_\beta)_{V-A}, & O_{10} &= \frac{3}{2} (\bar{q}_\beta b_\alpha)_{V-A} \sum_{q'} e_{q'} (\bar{q}'_\alpha q'_\beta)_{V-A}, \end{aligned} \quad (4)$$

where α and β are the color indices, the active quarks cover $q' = u, d, s, c, b$, and $(\bar{q}_\alpha q'_\beta)_{V \mp A} = \bar{q}_\alpha \gamma_\mu (1 \mp \gamma_5) q'_\beta$ denote the left- and right-handed currents. The expressions of the scale-dependent Wilson coefficients C_i can be found in Ref. [30, 38], whose values at the three specific renormalization scales $\mu = m_b/2, m_b$ and $3m_b/2, m_b = 4.8$ GeV being the b quark mass, to leading-logarithm accuracy in QCD are listed in Table I. The variation of the Wilson coefficients in the scale μ constitutes one of the sources of theoretical uncertainties in our analysis.

TABLE I: Wilson coefficients at the renormalization scales $\mu = m_b/2, m_b$ and $3m_b/2$ with $m_b = 4.8$ GeV to leading-logarithm accuracy.

μ	C_1	C_2	$C_3(10^{-2})$	$C_4(10^{-2})$	$C_5(10^{-2})$	$C_6(10^{-2})$	$C_7(10^{-3})$	$C_8(10^{-3})$	$C_9(10^{-3})$	$C_{10}(10^{-3})$
$m_b/2$	-0.39	1.19	1.94	-3.90	1.15	-5.20	1.05	0.63	-9.49	3.13
m_b	-0.27	1.12	1.26	-2.70	0.85	-3.26	1.09	0.40	-8.95	2.16
$3m_b/2$	-0.22	1.09	0.98	-2.16	0.71	-2.49	1.10	0.30	-8.71	1.71

B. Topological diagrams

The topological-diagram approach [39] has been successfully applied to predictions for observables in charm hadron decays [40, 41]. Topological diagrams, which include full strong interaction, are categorized according to the weak vertex insertion and quark flows. Those for the $\Lambda_b \rightarrow ph$ decays with the meson h being formed by $\bar{u}d$ or $\bar{u}s$ quarks are shown in Fig. 1. Four types of tree diagrams are identified [17]:

- T , the external- W emission diagram, which can be separated into the factorizable piece T^f and the non-factorizable piece T^{nf} ;
- C_2 , the internal- W emission diagram, which is also called the color-commensurate W -emission diagram in some references;
- E_2 , the W -exchange diagram, where the quark from the weak vertex goes into the meson h ;
- B , the bow-tie W -exchange diagram, where the light spectator quark goes into the meson h .

The topologies C_2, E_2 and B , existing in baryon decays, have no counterparts in meson decays. There are six types of penguin diagrams [17]:

- PC_1, PC_2, PE_1^u and PB , whose quark flows are related to those of the tree diagrams T, C_2, E_2 and B , respectively, by the Feriz transformation. The PC_1 topology can be further classified into the factorizable piece PC_1^f and the non-factorizable piece PC_1^{nf} ;
- PE_1^d and PE_2 , which are related to each other through the Feriz transformation without the corresponding tree diagrams.

The T^f diagram dominates the tree contributions to the $\Lambda_b \rightarrow ph$ decays as a consequence of the color transparency mechanism, and can be well estimated by the factorization hypothesis. All

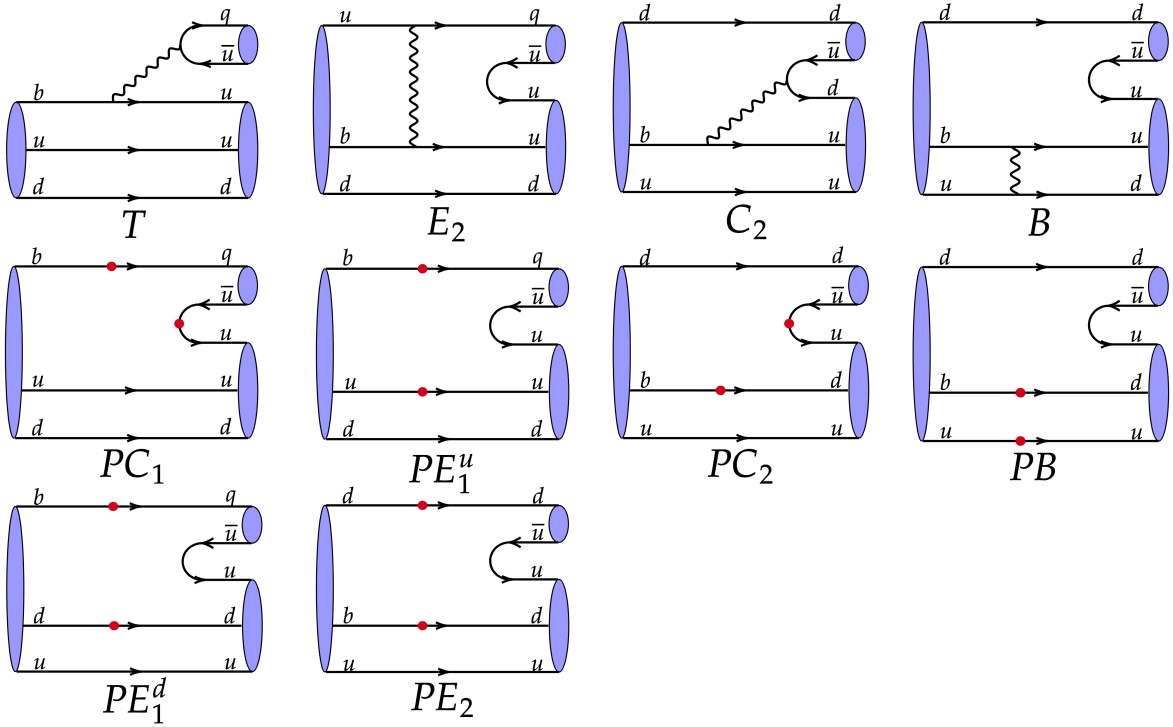


FIG. 1: Topological diagrams contributing to the $\Lambda_b \rightarrow ph$ decays.

the other tree topologies give nonfactorizable contributions. Following the power counting rules in the SCET, we attain the hierarchy among the various tree topologies [42]

$$\frac{|C_2|}{|T|} \sim \frac{|E_2|}{|T|} \sim \frac{|B|}{|T|} \sim \mathcal{O}\left(\frac{\Lambda_{\text{QCD}}}{m_b}\right)^2, \quad (5)$$

with the QCD scale Λ_{QCD} .

C. Kinematics

We adopt the light-cone coordinates for assigning the kinematic variables of the $\Lambda_b \rightarrow ph$ decays. The initial Λ_b baryon momentum p_{Λ_b} , the proton momentum p_p and the meson momentum q are chosen, in the rest frame of the Λ_b baryon, as

$$\begin{aligned} p_{\Lambda_b} &= \frac{m_{\Lambda_b}}{\sqrt{2}}(1, 1, \mathbf{0}_T), \\ p_p &= \frac{m_{\Lambda_b}}{\sqrt{2}}(\eta^+, \eta^-, \mathbf{0}_T), \\ q &= p_{\Lambda_b} - p_p = \frac{m_{\Lambda_b}}{\sqrt{2}}(1 - \eta^+, 1 - \eta^-, \mathbf{0}_T), \end{aligned} \quad (6)$$

where the variables

$$\eta^\pm = \left[m_{\Lambda_b}^2 - m_h^2 + m_p^2 \pm \sqrt{(m_{\Lambda_b}^2 - m_h^2 + m_p^2)^2 - 4m_{\Lambda_b}^2 m_p^2} \right] / (2m_{\Lambda_b}^2), \quad (7)$$

are determined by the momentum conservation with the Λ_b baryon (proton, meson) mass m_{Λ_b} (m_p , m_h). The longitudinal and transverse polarization vectors of a spin-1 final-state meson,

$$\epsilon_L = \frac{m_h}{\sqrt{2}m_{\Lambda_b}}(\eta^+ - 1, 1 - \eta^-, \mathbf{0}_T), \quad \epsilon_T = (0, 0, \mathbf{1}_T), \quad (8)$$

are fixed by the normalization and orthogonality conditions, which respect $\epsilon_L^2 = -1$ and $\epsilon_L \cdot q = 0$.

The valence quark momenta in the three involved hadrons are parameterized as

$$\begin{aligned} k_1 &= \left(\frac{m_{\Lambda_b}}{\sqrt{2}}, \frac{m_{\Lambda_b}}{\sqrt{2}}x_1, \mathbf{k}_{1T} \right), & k_2 &= \left(0, \frac{m_{\Lambda_b}}{\sqrt{2}}x_2, \mathbf{k}_{2T} \right), & k_3 &= \left(0, \frac{m_{\Lambda_b}}{\sqrt{2}}x_3, \mathbf{k}_{3T} \right), \\ k'_1 &= \left(\frac{m_{\Lambda_b}}{\sqrt{2}}\eta^+x'_1, 0, \mathbf{k}'_{1T} \right), & k'_2 &= \left(\frac{m_{\Lambda_b}}{\sqrt{2}}\eta^+x'_2, 0, \mathbf{k}'_{2T} \right), & k'_3 &= \left(\frac{m_{\Lambda_b}}{\sqrt{2}}\eta^+x'_3, 0, \mathbf{k}'_{3T} \right), \\ q_1 &= \left(0, \frac{m_{\Lambda_b}}{\sqrt{2}}y(1 - \eta^-), \mathbf{q}_T \right), & q_2 &= \left(0, \frac{m_{\Lambda_b}}{\sqrt{2}}(1 - y)(1 - \eta^-), -\mathbf{q}_T \right), \end{aligned} \quad (9)$$

where k_1 is the b quark momentum, and the other momenta are designated in the Feynman diagrams in Appendix B. The momentum fractions $x_{1,2,3}^{(\prime)}$ and the transverse momenta $\mathbf{k}_{1T,2T,3T}^{(\prime)}$ obey

$$\sum_{i=1}^3 x_i^{(\prime)} = 1, \quad \sum_{i=1}^3 \mathbf{k}_{iT}^{(\prime)} = 0, \quad (10)$$

respectively. We stress that the quark momenta in the Λ_b baryon should be parametrized as

$$k_1 = \left(\frac{m_{\Lambda_b}}{\sqrt{2}}(1 - x_3), \frac{m_{\Lambda_b}}{\sqrt{2}}(1 - x_2), \mathbf{k}_{1T} \right), \quad k_2 = \left(0, \frac{m_{\Lambda_b}}{\sqrt{2}}x_2, \mathbf{k}_{2T} \right), \quad k_3 = \left(\frac{m_{\Lambda_b}}{\sqrt{2}}x_3, 0, \mathbf{k}_{3T} \right), \quad (11)$$

to maintain the virtuality of hard gluons as evaluating the topologies C_2 , B , PC_2 and PB . This special kinematic assignment is allowed in view that light quarks in a Λ_b baryon are soft, and their momenta can point to different directions in principle.

D. Distribution amplitudes

The Λ_b baryon DAs are defined by the matrix elements of nonlocal operators sandwiched between the vacuum and the Λ_b baryon state. The general Lorentz structures of these matrix elements can be found in [43–46],

$$\begin{aligned} (Y_{\Lambda_b})_{\alpha\beta\gamma}(x_i, \mu) &\equiv \frac{1}{2\sqrt{2}N_c} \int \prod_{l=2}^3 \frac{dz_l^- dz_l}{(2\pi)^3} e^{ik_l \cdot z_l} \epsilon^{ijk} \langle 0 | T[b_\alpha^i(0) u_\beta^j(z_2) d_\gamma^k(z_3)] | \Lambda_b \rangle \\ &= \frac{1}{8\sqrt{2}N_c} \left\{ f_{\Lambda_b}^{(1)}(\mu) [M_1(x_2, x_3) \gamma_5 C^T]_{\gamma\beta} + f_{\Lambda_b}^{(2)}(\mu) [M_2(x_2, x_3) \gamma_5 C^T]_{\gamma\beta} \right\} [u_{\Lambda_b}]_\alpha, \end{aligned} \quad (12)$$

where N_c is the number of colors, i', j', k' are the color indices, α, β, γ are the Dirac indices, the normalization constants $f_{\Lambda_b}^{(1)} \approx f_{\Lambda_b}^{(2)} \equiv f_{\Lambda_b} = 0.022 \pm 0.001 \text{ GeV}^3$ are quoted from the leading-order sum-rule result [47], C stands for the charge conjugation matrix, and u_{Λ_b} is the Λ_b baryon spinor. The DAs in Eq. (12) are decomposed into

$$\begin{aligned} M_1(x_2, x_3) &= \frac{\not{q}\not{q}}{4} \psi_3^{+-}(x_2, x_3) + \frac{\not{q}\not{q}}{4} \psi_3^{-+}(x_2, x_3), \\ M_2(x_2, x_3) &= \frac{\not{q}}{\sqrt{2}} \psi_2(x_2, x_3) + \frac{\not{q}}{\sqrt{2}} \psi_4(x_2, x_3), \end{aligned} \quad (13)$$

with the light-like vectors $n = (1, 0, \mathbf{0}_T)$ and $\bar{n} = (0, 1, \mathbf{0}_T)$. The models with the exponential ansatz [44] are employed

$$\begin{aligned}
\psi_2(x_2, x_3) &= \frac{x_2 x_3}{\omega_0^4} m_{\Lambda_b}^4 e^{-(x_2+x_3)m_{\Lambda_b}/\omega_0}, \\
\psi_3^{+-}(x_2, x_3) &= \frac{2x_2}{\omega_0^3} m_{\Lambda_b}^3 e^{-(x_2+x_3)m_{\Lambda_b}/\omega_0}, \\
\psi_3^{-+}(x_2, x_3) &= \frac{2x_3}{\omega_0^3} m_{\Lambda_b}^3 e^{-(x_2+x_3)m_{\Lambda_b}/\omega_0}, \\
\psi_4(x_2, x_3) &= \frac{1}{\omega_0^2} m_{\Lambda_b}^2 e^{-(x_2+x_3)m_{\Lambda_b}/\omega_0},
\end{aligned} \tag{14}$$

where the parameter ω_0 , with the typical value lower than 1 GeV, measures the average energy of the two light quarks in a Λ_b baryon. We extract ω_0 from the LHCb data for the $\Lambda_b \rightarrow p\mu\bar{\nu}_\mu$ and $\Lambda_b \rightarrow pD_s^-$ branching ratios, $Br(\Lambda_b \rightarrow p\mu\bar{\nu}_\mu) = (4.1 \pm 1.0) \times 10^{-4}$ and $Br(\Lambda_b \rightarrow pD_s^-) = (12.5 \pm 1.3) \times 10^{-6}$. The former for a semileptonic mode depends on the $\Lambda_b \rightarrow p$ transition form factors, and the latter involves only the T topology. The comparison between the data and our predictions for various ω_0 sets the conservative range $\omega_0 = 0.7 \pm 0.1$ GeV as exhibited in Fig. 2, which is higher than the one chosen in light-cone sum rules [45, 48]. The common extraction $\omega_0 \approx 0.7$ GeV from the two disparate pieces of data supports the consistency of our framework.

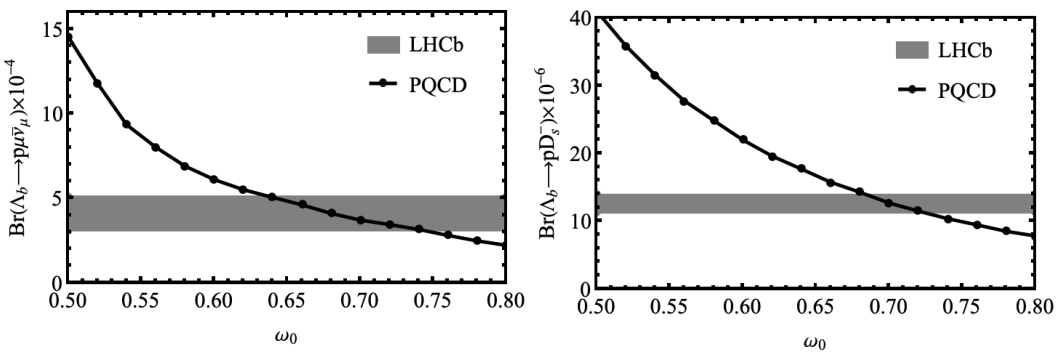


FIG. 2: Dependencies of $Br(\Lambda_b \rightarrow p\mu\bar{\nu}_\mu)$ (left) and $Br(\Lambda_b \rightarrow pD_s^-)$ (right) on ω_0 .

The final-state proton DAs up to twist 6 have been defined in Ref. [49] through the corresponding

momentum-space projector

$$\begin{aligned}
(\bar{Y}_P)_{\alpha\beta\gamma}(x'_i, \mu) &\equiv \frac{1}{2\sqrt{2}N_c} \int \prod_{l=2}^3 \frac{dz_l^- dz_l}{(2\pi)^3} e^{ik'_l \cdot z_l} e^{i'j'k'} \langle p(p') | T[\bar{u}_\alpha^{i'}(0) \bar{u}_\beta^{j'}(z_2) \bar{d}_\gamma^{k'}(z_3)] | 0 \rangle \\
&= \frac{-1}{8\sqrt{2}N_c} \left\{ S_1 m_p C_{\beta\alpha} (\bar{N}^+ \gamma_5)_\gamma + S_2 m_p C_{\beta\alpha} (\bar{N}^- \gamma_5)_\gamma + P_1 m_p (C\gamma_5)_{\beta\alpha} \bar{N}_\gamma^+ \right. \\
&\quad + P_2 m_p (C\gamma_5)_{\beta\alpha} \bar{N}_\gamma^- + V_1 (C\cancel{P})_{\beta\alpha} (\bar{N}^+ \gamma_5)_\gamma + V_2 (C\cancel{P})_{\beta\alpha} (\bar{N}^- \gamma_5)_\gamma \\
&\quad + V_3 \frac{m_p}{2} (C\gamma_\perp)_{\beta\alpha} (\bar{N}^+ \gamma_5 \gamma^\perp)_\gamma + V_4 \frac{m_p}{2} (C\gamma_\perp)_{\beta\alpha} (\bar{N}^- \gamma_5 \gamma^\perp)_\gamma + V_5 \frac{m_p^2}{2Pz} (C\cancel{\not{z}})_{\beta\alpha} (\bar{N}^+ \gamma_5)_\gamma \\
&\quad + V_6 \frac{m_p^2}{2Pz} (C\cancel{\not{z}})_{\beta\alpha} (\bar{N}^- \gamma_5)_\gamma + A_1 (C\gamma_5 \cancel{P})_{\beta\alpha} (\bar{N}^+)_\gamma + A_2 (C\gamma_5 \cancel{P})_{\beta\alpha} (\bar{N}^-)_\gamma \\
&\quad + A_3 \frac{m_p}{2} (C\gamma_5 \gamma_\perp)_{\beta\alpha} (\bar{N}^+ \gamma^\perp)_\gamma + A_4 \frac{m_p}{2} (C\gamma_5 \gamma_\perp)_{\beta\alpha} (\bar{N}^- \gamma^\perp)_\gamma + A_5 \frac{m_p^2}{2Pz} (C\gamma_5 \cancel{\not{z}})_{\beta\alpha} (\bar{N}^+)_\gamma \\
&\quad + A_6 \frac{m_p^2}{2Pz} (C\gamma_5 \cancel{\not{z}})_{\beta\alpha} (\bar{N}^-)_\gamma - T_1 (iC\sigma_{\perp P})_{\beta\alpha} (\bar{N}^+ \gamma_5 \gamma^\perp)_\gamma - T_2 (iC\sigma_{\perp P})_{\beta\alpha} (\bar{N}^- \gamma_5 \gamma^\perp)_\gamma \\
&\quad - T_3 \frac{m_p}{Pz} (iC\sigma_{Pz})_{\beta\alpha} (\bar{N}^+ \gamma_5)_\gamma - T_4 \frac{m_p}{Pz} (iC\sigma_{zP})_{\beta\alpha} (\bar{N}^- \gamma_5)_\gamma - T_5 \frac{m_p^2}{2Pz} (iC\sigma_{\perp z})_{\beta\alpha} (\bar{N}^+ \gamma_5 \gamma^\perp)_\gamma \\
&\quad - T_6 \frac{m_p^2}{2Pz} (iC\sigma_{\perp z})_{\beta\alpha} (\bar{N}^- \gamma_5 \gamma^\perp)_\gamma + T_7 \frac{m_p}{2} (C\sigma_{\perp\perp'})_{\beta\alpha} (\bar{N}^+ \gamma_5 \sigma^{\perp\perp'})_\gamma \\
&\quad \left. + T_8 \frac{m_p}{2} (C\sigma_{\perp\perp'})_{\beta\alpha} (\bar{N}^- \gamma_5 \sigma^{\perp\perp'})_\gamma \right\}, \tag{15}
\end{aligned}$$

with the color indices i', j', k' . The light-like vector P is written, in terms of the proton momentum p_p and the light-like vector z , as

$$P^\mu = p_p^\mu - \frac{1}{2} z^\mu \frac{m_p^2}{Pz}, \tag{16}$$

with $Pz \sim p_p z \sim 1$, and the shorthand notation $\sigma_{Pz} = \sigma^{\nu\mu} P_\nu z_\mu$ has been used. Furthermore, $\bar{N}^+ = \bar{N} \cancel{P}/(2Pz)$ and $\bar{N}^- = \bar{N} \cancel{P}/(2Pz)$ are introduced to represent the "large" and "small" components of the proton spinor \bar{N} , respectively. The symbol \perp labels the projection perpendicular to z or P , and the contraction $\gamma_\perp \gamma^\perp = \gamma^\mu g_{\mu\nu}^\perp \gamma^\nu$ is perceived with $g_{\mu\nu}^\perp = g_{\mu\nu} - (P_\mu z_\nu + z_\mu P_\nu)/Pz$. The functions V_i , A_i , T_i , S_i and P_i are classified according to their twists:

- Twist-3 DAs

$$\begin{aligned}
V_1(x'_i) &= 120 x'_1 x'_2 x'_3 [\phi_3^0 + \phi_3^+(1 - 3x'_3)], \\
A_1(x'_i) &= 120 x'_1 x'_2 x'_3 (x'_2 - x'_1) \phi_3^-, \\
T_1(x'_i) &= 120 x'_1 x'_2 x'_3 [\phi_3^0 + \frac{1}{2}(\phi_3^- - \phi_3^+)(1 - 3x'_3)]; \tag{17}
\end{aligned}$$

- Twist-4 DAs

$$\begin{aligned}
V_2(x'_i) &= 24 x'_1 x'_2 [\phi_4^0 + \phi_4^+(1 - 5x'_3)], \\
V_3(x'_i) &= 12 x'_3 [\psi_4^0(1 - x'_3) + \psi_4^-(x'^2_1 + x'^2_2 - x'_3(1 - x'_3)) + \psi_4^+(1 - x'_3 - 10x'_1 x'_2)], \\
A_2(x'_i) &= 24 x'_1 x'_2 (x'_2 - x'_1) \phi_4^-,
\end{aligned}$$

$$\begin{aligned}
A_3(x'_i) &= 12x'_3(x'_2 - x'_1)[(\psi_4^0 + \psi_4^+) + \psi_4^-(1 - 2x'_3)], \\
T_2(x'_i) &= 24x'_1x'_2[\xi_4^0 + \xi_4^+(1 - 5x'_3)], \\
T_3(x'_i) &= 6x'_3[(\xi_4^0 + \phi_4^0 + \psi_4^0)(1 - x'_3) + (\xi_4^- + \phi_4^- - \psi_4^-)(x'^2_1 + x'^2_2 - x'_3(1 - x'_3)) \\
&\quad + (\xi_4^+ + \phi_4^+ + \psi_4^+)(1 - x'_3 - 10x'_1x'_2)], \\
T_7(x'_i) &= 6x'_3[(-\xi_4^0 + \phi_4^0 + \psi_4^0)(1 - x'_3) + (-\xi_4^- + \phi_4^- - \psi_4^-)(x'^2_1 + x'^2_2 - x'_3(1 - x'_3)) \\
&\quad + (-\xi_4^+ + \phi_4^+ + \psi_4^+)(1 - x'_3 - 10x'_1x'_2)], \\
S_1(x'_i) &= 6x'_3(x'_2 - x'_1)[(\xi_4^0 + \phi_4^0 + \psi_4^0 + \xi_4^+ + \phi_4^+ + \psi_4^+) + (\xi_4^- + \phi_4^- - \psi_4^-)(1 - 2x'_3)], \\
P_1(x'_i) &= 6x'_3(x'_2 - x'_1)[(\xi_4^0 - \phi_4^0 - \psi_4^0 + \xi_4^+ - \phi_4^+ - \psi_4^+) + (\xi_4^- - \phi_4^- + \psi_4^-)(1 - 2x'_3)];
\end{aligned} \tag{18}$$

- Twist-5 DAs

$$\begin{aligned}
V_4(x'_i) &= 3[\psi_5^0(1 - x'_3) + \psi_5^-(2x'_1x'_2 - x'_3(1 - x'_3)) + \psi_5^+(1 - x'_3 - 2(x'^2_1 + x'^2_2))], \\
V_5(x'_i) &= 6x'_3[\phi_5^0 + \phi_5^+(1 - 2x'_3)], \\
A_4(x'_i) &= 3(x'_2 - x'_1)[- \psi_5^0 + \psi_5^-x'_3 + \psi_5^+(1 - 2x'_3)], \\
A_5(x'_i) &= 6x'_3(x'_2 - x'_1)\phi_5^-, \\
T_4(x'_i) &= \frac{3}{2}[(\xi_5^0 + \psi_5^0 + \phi_5^0)(1 - x'_3) + (\xi_5^- + \phi_5^- - \psi_5^-)(2x'_1x'_2 - x'_3(1 - x'_3)) \\
&\quad + (\xi_5^+ + \phi_5^+ + \psi_5^+)(1 - x'_3 - 2(x'^2_1 + x'^2_2))], \\
T_5(x'_i) &= 6x'_3[\xi_5^0 + \xi_5^+(1 - 2x'_3)], \\
T_8(x'_i) &= \frac{3}{2}[(\psi_5^0 + \phi_5^0 - \xi_5^0)(1 - x'_3) + (\phi_5^- - \phi_5^- - \xi_5^-)(2x'_1x'_2 - x'_3(1 - x'_3)) \\
&\quad + (\phi_5^+ + \phi_5^+ - \xi_5^+)(1 - x'_3 - 2(x'^2_1 + x'^2_2))], \\
S_2(x'_i) &= \frac{3}{2}(x'_2 - x'_1)[-(\psi_5^0 + \phi_5^0 + \xi_5^0) + (\xi_5^- + \phi_5^- - \psi_5^0)x'_3 + (\xi_5^+ + \phi_5^+ + \psi_5^0)(1 - 2x'_3)], \\
P_2(x'_i) &= \frac{3}{2}(x'_2 - x'_1)[(\psi_5^0 + \phi_5^0 - \xi_5^0) + (\xi_5^- - \phi_5^- + \psi_5^0)x'_3 + (\xi_5^+ - \phi_5^+ - \psi_5^0)(1 - 2x'_3)];
\end{aligned} \tag{19}$$

- Twist-6 DAs

$$\begin{aligned}
V_6(x'_i) &= 2[\phi_6^0 + \phi_6^+(1 - 3x'_3)], \\
A_6(x'_i) &= 2(x'_2 - x'_1)\phi_6^-, \\
T_6(x'_i) &= 2[\phi_6^0 + \frac{1}{2}(\phi_6^- - \phi_6^+)(1 - 3x'_3)].
\end{aligned} \tag{21}$$

The values of $\phi_i^{\pm,0}$, $\psi_i^{\pm,0}$ and $\xi_i^{\pm,0}$ are connected to the eight independent parameters f_N , λ_1 , λ_2 , V_1^d , A_1^u , f_1^d , f_2^d and f_1^u [49],

$$\begin{aligned}
\phi_3^0 &= \phi_6^0 = f_N, & \phi_4^0 &= \phi_5^0 = \frac{1}{2}(\lambda_1 + f_N), \\
\xi_4^0 &= \xi_5^0 = \frac{1}{6}\lambda_2, & \psi_4^0 &= \psi_5^0 = \frac{1}{2}(f_N - \lambda_1),
\end{aligned}$$

$$\begin{aligned}
\phi_4^- &= \frac{5}{4} (\lambda_1(1 - 2f_1^d - 4f_1^u) + f_N(2A_1^u - 1)), \\
\phi_4^+ &= \frac{1}{4} (\lambda_1(3 - 10f_1^d) - f_N(10V_1^d - 3)), \\
\psi_4^- &= -\frac{5}{4} (\lambda_1(2 - 7f_1^d + f_1^u) + f_N(A_1^u + 3V_1^d - 2)), \\
\psi_4^+ &= -\frac{1}{4} (\lambda_1(-2 + 5f_1^d + 5f_1^u) + f_N(2 + 5A_1^u - 5V_1^d)), \\
\xi_4^- &= \frac{5}{16} \lambda_2(4 - 15f_2^d), \quad \xi_4^+ = \frac{1}{16} \lambda_2(4 - 15f_2^d), \\
\phi_5^- &= \frac{5}{3} (\lambda_1(f_1^d - f_1^u) + f_N(2A_1^u - 1)), \\
\phi_5^+ &= -\frac{5}{6} (\lambda_1(4f_1^d - 1) + f_N(3 + 4V_1^d)), \\
\psi_5^- &= \frac{5}{3} (\lambda_1(f_1^d - f_1^u) + f_N(2 - A_1^u - 3V_1^d)), \\
\psi_5^+ &= -\frac{5}{6} (\lambda_1(-1 + 2f_1^d + 2f_1^u) + f_N(5 + 2A_1^u - 2V_1^d)), \\
\xi_5^- &= -\frac{5}{4} \lambda_2 f_2^d, \quad \xi_5^+ = \frac{5}{36} \lambda_2(2 - 9f_2^d), \\
\phi_6^- &= \frac{1}{2} (\lambda_1(1 - 4f_1^d - 2f_1^u) + f_N(1 + 4A_1^u)), \\
\phi_6^+ &= -\frac{1}{2} (\lambda_1(1 - 2f_1^d) + f_N(4V_1^d - 1)). \tag{22}
\end{aligned}$$

These parameters have been derived in QCD sum rules (QCDSR) [49, 50] and lattice QCD (LQCD) [51], whose results are summarized in Table II. They come with large uncertainties, reflecting our limited knowledge on baryon DAs. We will take the set of parameters from QCDSR [50] for the numerical investigations.

TABLE II: The eight independent parameters for Eq. (22) at the scale 1 GeV from QCDSR and LQCD.

	$f_N(\text{GeV}^2)$	$\lambda_1(\text{GeV}^2)$	$\lambda_2(\text{GeV}^2)$	V_1^d
QCDSR(2001)[49]	$(5.3 \pm 0.5) \times 10^{-3}$	$-(2.7 \pm 0.9) \times 10^{-2}$	$(5.1 \pm 1.9) \times 10^{-2}$	0.23 ± 0.03
QCDSR(2006)[50]	$(5.0 \pm 0.5) \times 10^{-3}$	$-(2.7 \pm 0.9) \times 10^{-2}$	$(5.4 \pm 1.9) \times 10^{-2}$	0.23 ± 0.03
LQCD(2019)[51]	$(3.54 \pm 0.06) \times 10^{-3}$	$-(4.49 \pm 0.42) \times 10^{-2}$	$(9.34 \pm 0.48) \times 10^{-2}$	0.19 ± 0.22
	A_1^u	f_1^d	f_2^d	f_1^u
QCDSR(2001)[49]	0.38 ± 0.15	0.6 ± 0.2	0.15 ± 0.06	0.22 ± 0.15
QCDSR(2006)[50]	0.38 ± 0.15	0.4 ± 0.05	0.22 ± 0.05	0.07 ± 0.05
LQCD(2019)[51]	0.30 ± 0.32

The DAs for a pseudoscalar meson are expanded, up to twist 3, as [52–55]

$$\begin{aligned}
\Phi_{\pi(K)}(q, y) &= \int d^4z e^{-iyq \cdot z} \langle \pi(K)(q) | \bar{q}_\beta(z) u_\alpha(0) | 0 \rangle \\
&= \frac{i}{\sqrt{2N_C}} \left[\gamma_5 \not{q} \phi_{\pi(K)}^A(y) + m_0^{\pi(K)} \gamma_5 \phi_{\pi(K)}^P(y) + m_0^{\pi(K)} \gamma_5 (\not{q} - 1) \phi_{\pi(K)}^T(y) \right]_{\alpha\beta}, \tag{23}
\end{aligned}$$

where $m_0^{\pi(K)} = m_{\pi(K)}^2 / (m_u + m_{d(s)})$, m_u (m_d , m_s) being the u (d , s) quark mass, is the chiral scale associated with the pseudoscalar meson, and the momentum fraction y is carried by the *quark* in the meson. The DAs are parameterized as [56, 57],

$$\begin{aligned}\phi_{\pi(K)}^A(y) &= \frac{f_{\pi(K)}}{2\sqrt{2N_c}} 6y(1-y) \left[1 + a_1^{\pi(K)} C_1^{3/2}(2y-1) + a_2^{\pi(K)} C_2^{3/2}(2y-1) + a_4^{\pi(K)} C_4^{3/2}(2y-1) \right], \\ \phi_{\pi(K)}^P(y) &= \frac{f_{\pi(K)}}{2\sqrt{2N_c}} \left[1 + \left(0.45 - \frac{5}{2} \rho_{\pi(K)}^2 \right) C_2^{1/2}(2y-1) \right. \\ &\quad \left. - 3 \left(-0.045 + \frac{9}{20} \rho_{\pi(K)}^2 (1 + 6a_2^{\pi(K)}) \right) C_4^{1/2}(2y-1) \right], \\ \phi_{\pi(K)}^T(y) &= \frac{f_{\pi(K)}}{2\sqrt{2N_c}} (1-2y) \left[1 + 6 \left(0.0975 - \frac{7}{20} \rho_{\pi(K)}^2 - \frac{3}{5} \rho_{\pi(K)}^2 a_2^{\pi(K)} \right) (1 - 10y + 10y^2) \right],\end{aligned}\tag{24}$$

with the decay constant $f_{\pi(K)} = 0.13$ (0.16) GeV, the Gegenbauer polynomials C_n^ν , $\nu = 1/2, 3/2$ and $n = 1, 2, 4$, and the other parameters [56, 57],

$$\begin{aligned}a_1^\pi &= 0, & a_1^K &= 0.06, \\ a_2^\pi &= 0.25 \pm 0.15, & a_2^K &= 0.25 \pm 0.15, \\ a_4^\pi &= -0.015, & a_4^K &= 0, \\ m_\pi &= 0.14 \text{ GeV}, & m_K &= 0.494 \text{ GeV}, \\ m_0^\pi &= (1.4 \pm 0.1) \text{ GeV}, & m_0^K &= (1.6 \pm 0.1) \text{ GeV}, \\ \rho_\pi &= \frac{m_\pi}{m_0^\pi}, & \rho_K &= \frac{m_K}{m_0^K}.\end{aligned}\tag{25}$$

The vector meson DAs are defined by [58]

$$\begin{aligned}\Phi_V^L(q, \epsilon_L^*, y) &= \int d^4z e^{-iyq\cdot z} \langle V(q, \epsilon_L^*) | \bar{q}_\beta(z) u_\alpha(0) | 0 \rangle \\ &= \frac{-1}{\sqrt{2N_c}} [m_V \not{\epsilon}_L^* \phi_V(y) + \not{\epsilon}_L^* \not{q} \phi_V^t(y) + m_V \phi_V^s(y)]_{\alpha\beta},\end{aligned}\tag{26}$$

$$\begin{aligned}\Phi_V^T(q, \epsilon_T^*, y) &= \int d^4z e^{-iyq\cdot z} \langle V(q, \epsilon_T^*) | \bar{q}_\beta(z) u_\alpha(0) | 0 \rangle \\ &= \frac{-1}{\sqrt{2N_c}} [m_V \not{\epsilon}_T^* \phi_V^v(y) + \not{\epsilon}_T^* \not{q} \phi_V^T(y) + m_V i \epsilon_{\mu\nu\rho\sigma} \gamma_5 \gamma^\mu \epsilon_T^{*\nu} v^\rho n^\sigma \phi_V^a(y)]_{\alpha\beta},\end{aligned}\tag{27}$$

with the vector meson mass m_V . The twist-2 DAs are also expanded int terms of the Gegenbauer polynomials,

$$\begin{aligned}\phi_V(y) &= \frac{3f_V}{\sqrt{2N_c}} y(1-y) \left[1 + a_1^{\parallel} C_1^{3/2}(2y-1) + a_2^{\parallel} C_2^{3/2}(2y-1) \right], \\ \phi_V^T(y) &= \frac{3f_V^T}{\sqrt{2N_c}} y(1-y) \left[1 + a_1^{\perp} C_1^{3/2}(2y-1) + a_2^{\perp} C_2^{3/2}(2y-1) \right].\end{aligned}\tag{28}$$

The asymptotic forms are assumed for the twist-3 DAs, [59],

$$\phi_V^t(y) = \frac{3f_V^T}{2\sqrt{2N_c}} (2y-1)^2,$$

$$\begin{aligned}
\phi_V^s(y) &= \frac{3f_V^T}{2\sqrt{2N_c}}(1-2y), \\
\phi_V^v(y) &= \frac{3f_V}{8\sqrt{2N_c}}(1+(2y-1)^2), \\
\phi_V^a(y) &= \frac{3f_V}{4\sqrt{2N_c}}(1-2y).
\end{aligned} \tag{29}$$

The Gegenbauer moments a_n in the above expansions have been obtained in QCDSR [60–63], which, together with the decay constants, are collected in Table III.

TABLE III: Inputs of the decay constants (in MeV) and the Gegenbauer moments for the vector meson DAs.

f_ρ	f_ρ^T	f_{K^*}	$f_{K^*}^T$
209 ± 2	165 ± 9	217 ± 5	185 ± 10
$a_{1\rho}^\parallel$	$a_{1\rho}^\perp$	$a_{1K^*}^\parallel$	$a_{1K^*}^\perp$
0	0	0.03 ± 0.02	0.04 ± 0.03
$a_{2\rho}^\parallel$	$a_{2\rho}^\perp$	$a_{2K^*}^\parallel$	$a_{2K^*}^\perp$
0.15 ± 0.07	0.14 ± 0.06	0.11 ± 0.09	0.10 ± 0.08

The DAs for an axial-vector with the quantum number $J^P = 1^+$ are introduced through [58],

$$\begin{aligned}
\Phi_A^L(q, \epsilon_L^*, y) &= \int d^4z e^{-iyq\cdot z} \langle A(q, \epsilon_L^*) | \bar{q}_\beta(z) u_\alpha(0) | 0 \rangle \\
&= \frac{-i}{\sqrt{2N_c}} [m_A \gamma_5 \not{\epsilon}_L^* \phi_A(y) + \not{\epsilon}_L^* \not{q} \gamma_5 \phi_A^t(y) + m_A \gamma_5 \phi_A^s(y)]_{\alpha\beta},
\end{aligned} \tag{30}$$

$$\begin{aligned}
\Phi_A^T(q, \epsilon_T^*, y) &= \int d^4z e^{-iyq\cdot z} \langle A(q, \epsilon_T^*) | \bar{q}_\beta(z) u_\alpha(0) | 0 \rangle \\
&= \frac{-i}{\sqrt{2N_c}} [m_A \gamma_5 \not{\epsilon}_T^* \phi_A^v(y) + \not{\epsilon}_T^* \not{q} \gamma_5 \phi_A^T(y) + m_A i \epsilon_{\mu\nu\rho\sigma} \gamma^\mu \epsilon_T^{*\nu} v^\rho n^\sigma \phi_A^a(y)]_{\alpha\beta},
\end{aligned} \tag{31}$$

with the axial-vector meson mass m_A . The twist-2 and twist-3 DAs read

$$\begin{aligned}
\phi_A(y) &= \frac{3f_A}{\sqrt{2N_c}} y(1-y) \left[a_{0A}^\parallel + 3a_{1A}^\parallel (2y-1) + \frac{3}{2} a_{2A}^\parallel (5(2y-1)^2 - 1) \right], \\
\phi_A^T(y) &= \frac{3f_A}{\sqrt{2N_c}} y(1-y) \left[a_{0A}^\perp + 3a_{1A}^\perp (2y-1) + \frac{3}{2} a_{2A}^\perp (5(2y-1)^2 - 1) \right],
\end{aligned} \tag{32}$$

and

$$\begin{aligned}
\phi_A^t(y) &= \frac{f_A}{2\sqrt{2N_c}} \left[3a_{0A}^\perp (2y-1)^2 + \frac{3}{2} a_{1A}^\perp (2y-1)(3(2y-1)^2 - 1) \right], \\
\phi_A^s(y) &= \frac{3f_A}{2\sqrt{2N_c}} (a_{0A}^\perp - a_{1A}^\perp - 2a_{0A}^\perp y + 6a_{1A}^\perp y - 6a_{1A}^\perp y^2), \\
\phi_A^v(y) &= \frac{f_A}{2\sqrt{2N_c}} \left[\frac{3}{4} a_{0A}^\parallel (1 + (2y-1)^2) + \frac{3}{2} a_{1A}^\parallel (2y-1)^3 \right],
\end{aligned}$$

TABLE IV: Same as Table III but for the axial-vector meson DAs.

$f_{a_1(1260)}$	$a_{0a_1(1260)}^{\parallel}$	$a_{1a_1(1260)}^{\parallel}$	$a_{2a_1(1260)}^{\parallel}$
238 ± 10	1	0	-0.02 ± 0.02
$a_{0a_1(1260)}^{\perp}$	$a_{1a_1(1260)}^{\perp}$	$a_{2a_1(1260)}^{\perp}$	
0	-1.04 ± 0.34	0	
$f_{K_{1A}}$	$a_{0K_{1A}}^{\parallel}$	$a_{1K_{1A}}^{\parallel}$	$a_{2K_{1A}}^{\parallel}$
250 ± 13	1	0.00 ± 0.26	-0.05 ± 0.03
$a_{0K_{1A}}^{\perp}$	$a_{1K_{1A}}^{\perp}$	$a_{2K_{1A}}^{\perp}$	
0.08 ± 0.09	-1.08 ± 0.48	0.02 ± 0.20	
$f_{K_{1B}}$	$a_{0K_{1B}}^{\parallel}$	$a_{1K_{1B}}^{\parallel}$	$a_{2K_{1B}}^{\parallel}$
190 ± 10	0.14 ± 0.15	-1.95 ± 0.45	0.02 ± 0.10
$a_{0K_{1B}}^{\perp}$	$a_{1K_{1B}}^{\perp}$	$a_{2K_{1B}}^{\perp}$	
1	0.17 ± 0.22	-0.02 ± 0.22	

$$\phi_A^a(y) = \frac{3f_A}{4\sqrt{2N_c}}(a_{0A}^{\parallel} - a_{1A}^{\parallel} - 2a_{0A}^{\parallel}y + 6a_{1A}^{\parallel}y - 6a_{1A}^{\parallel}y^2), \quad (33)$$

respectively. The associated decay constants and Gegenbauer moments are listed in Table IV.

The physical mass eigenstates $K_1(1270)$ and $K_1(1400)$ are considered to be the mixtures of the $K_{1A}(^3P_1)$ and $K_{1B}(^1P_1)$ states with the mixing angle θ_{K_1} :

$$\begin{pmatrix} |K_1(1270)\rangle \\ |K_1(1400)\rangle \end{pmatrix} = \begin{pmatrix} \sin \theta_{K_1} & \cos \theta_{K_1} \\ \cos \theta_{K_1} & -\sin \theta_{K_1} \end{pmatrix} \begin{pmatrix} |K_{1A}\rangle \\ |K_{1B}\rangle \end{pmatrix}, \quad (34)$$

in which θ_{K_1} is chosen as the typical values 30° and 60° suggested in Refs.[64–67].

For reader's reference, we present the explicit expressions for the relevant Gegenbauer polynomials $C_n^{\nu}(t)$,

$$\begin{aligned} C_1^{3/2}(t) &= 3t, \\ C_2^{1/2}(t) &= \frac{1}{2}(3t^2 - 1), \\ C_2^{3/2}(t) &= \frac{3}{2}(5t^2 - 1), \\ C_4^{1/2}(t) &= \frac{1}{8}(3 - 30t^2 + 35t^4), \\ C_4^{3/2}(t) &= \frac{15}{8}(1 - 14t^2 + 21t^4), \end{aligned} \quad (35)$$

and the definitions of the meson decay constants,

$$\begin{aligned} \langle P|(\bar{q}q')_{V\mp A}|0\rangle &= \pm if_P p_\mu, & \langle P|(\bar{q}q')_{S\mp P}|0\rangle &= \pm if_P m_{0P}, \\ \langle V|(\bar{q}q')_{V\mp A}|0\rangle &= f_V m_V \epsilon_\mu^*, & \langle V|(\bar{q}q')_{S\mp P}|0\rangle &= 0, \\ \langle A|(\bar{q}q')_{V\mp A}|0\rangle &= \mp if_A m_A \epsilon_\mu^*, & \langle A|(\bar{q}q')_{S\mp P}|0\rangle &= 0. \end{aligned} \quad (36)$$

E. Numerical integration

The PQCD factorization formulas and the auxiliary functions from Fourier transformation in Appendices A and B are extremely complicated, containing $11 \sim 13$ dimensional integrations.

Computing high dimensional integrals effectively and making precise predictions for heavy baryon decays thus remain a numerical challenge. Various algorithms have been proposed, among which the VEGAS+ is one of the most widely used in particle physics. The classic VEGAS performs a multidimensional Monte Carlo integration based on adaptive importance sampling, originally developed by G.P. Lepage [68]. It then evolved to the VEGAS+ by incorporating a second strategy known as adaptive stratified sampling [69]. It is believed that the VEGAS+ is much more efficient for handling integrands with multiple peaks compared to the VEGAS. See Ref. [69] and references therein for more details of the VEGAS+ algorithm.

When applying the VEGAS+ to the integrations involved in this work, we encounter a subtlety, which can be illustrated by taking the diagram $T(d5)$ in Fig. 15 as an example. This diagram gives a non-factorizable amplitude with the auxiliary function F_4 . The numerical outcomes from the VEGAS+ for the $T(d5)$ contributions after 15 iterations are plotted in Fig. 3, where the number of samples increases from 10^4 to 10^8 . It is observed that the statistical errors in the imaginary parts decrease as $1/\sqrt{N_{ev}}$, consistent with the characteristics of a Monte Carlo algorithm. However, the real parts do not converge, meaning that the VEGAS+ is ineffective for the real parts.

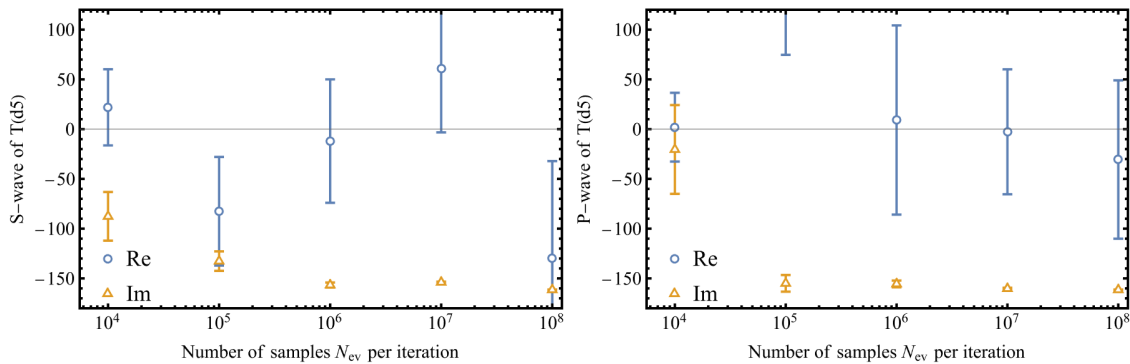


FIG. 3: (left) Numerical results of the $T(d5)$ contribution to the S -wave from the VEGAS+ after 15 iterations with increasing numbers of samples; (right) same as the left panel but for the P -wave.

We find that the real parts of the diagrams with the auxiliary function F_1 can be accurately acquired, but those depending on $F_{2,3,4}$ cannot. To elaborate the issue, we introduce the functions $B^{(1)}(x) \equiv K_0(\sqrt{x})\Theta(x) + \frac{i\pi}{2}H_0^{(1)}(\sqrt{-x})\Theta(-x)$ and $B^{(2)}(x) \equiv K_1(\sqrt{x})\Theta(x) - \frac{i\pi}{2}H_1^{(1)}(\sqrt{-x})\Theta(-x)$, where the step function $\Theta(x)$ equals 1 when $x > 0$ and 0 otherwise. The former (latter) corresponds to the Bessel function appearing in F_1 ($F_{2,3,4}$). As described in Fig. 4, both $B^{(1)}(x)$ and $B^{(2)}(x)$ are singular at $x = 0$ with the limits,

$$\begin{aligned} \lim_{x \rightarrow 0^-} B^{(1)}(x) &= -\lim_{x \rightarrow 0^-} \log(\sqrt{-x}) + \frac{i\pi}{2}, \\ \lim_{x \rightarrow 0^+} B^{(1)}(x) &= -\lim_{x \rightarrow 0^+} \log(\sqrt{x}), \\ \lim_{x \rightarrow 0^-} B^{(2)}(x) &= \lim_{x \rightarrow 0^-} \frac{-1}{\sqrt{-x}}, \\ \lim_{x \rightarrow 0^+} B^{(2)}(x) &= \lim_{x \rightarrow 0^+} \frac{1}{\sqrt{x}}. \end{aligned} \tag{37}$$

The real part of $B^{(1)}(x)$ behaves like $\log(\sqrt{|x|})$ on both sides of $x = 0$, which can be well managed by the VEGAS+. However, the real part of $B^{(2)}(x)$ approaches $\pm\infty$ from the two sides of $x = 0$, whose incomplete cancellation causes the numerical instability.

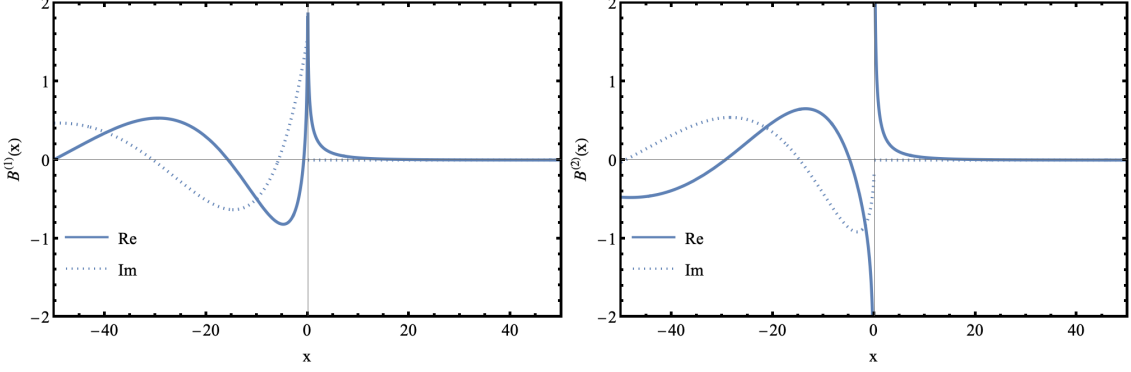


FIG. 4: The Bessel functions $B^{(1)}$ (left) and $B^{(2)}$ (right).

The aforementioned divergences of $B^{(2)}$ ought to cancel, since they are from an integrable singularity as shown in Eq. (37); the integrand takes the same values in magnitude but with opposite signs at $x = \epsilon$ and $x = -\epsilon$, where ϵ is a tiny parameter. We then decompose the function $B^{(2)}(x)$ into two terms, $B^{(2)}(x) - \text{Sign}(x)/\sqrt{|x|}$ and $\text{Sign}(x)/\sqrt{|x|}$, as depicted in Fig. 5. The former is finite everywhere, whose integration is convergent and can be evaluated reliably by the VEGAS+. The latter is divergent at $x = 0$ but antisymmetric about the origin. Therefore, the contributions to its integral from the intervals $(-\epsilon, 0)$ and $(0, \epsilon)$ in x are expected to cancel exactly and negligible. This operation replaces the integrations involving $F_{2,3,4}$ by the sum of two pieces, one with $B^{(2)}(x) - \text{Sign}(x)/\sqrt{|x|}$ in the entire range of x and the other with $\text{Sign}(x)/\sqrt{|x|}$ in the region outside $(-\epsilon, \epsilon)$. It has been checked that the cut parameter ϵ within the range $0.0005 \sim 0.005$ leads to accurate outcomes with controllable uncertainties. Here we set $\epsilon = 0.001$, for which the errors in the real parts of the $T(d5)$ contributions indeed decrease as $1/\sqrt{N_{ev}}$, as indicated in Fig. 6. It confirms the effectiveness of our algorithm.

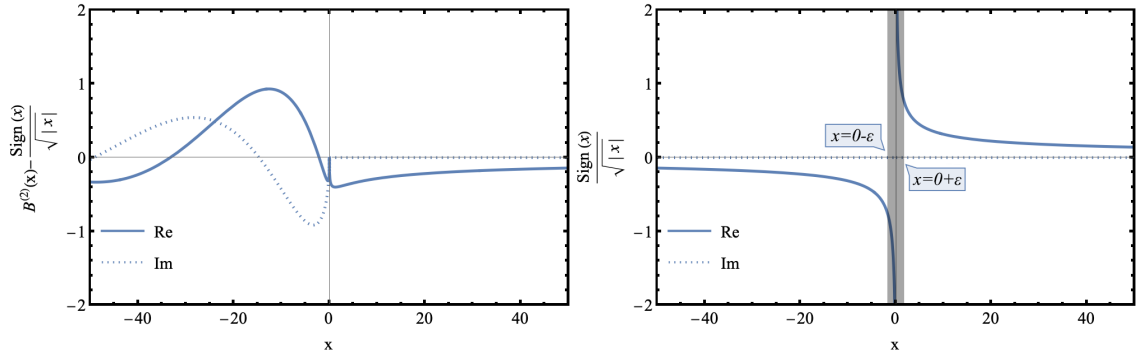


FIG. 5: The function $B^{(2)}(x) - \text{Sign}(x)/\sqrt{|x|}$ (left) ; the function $\text{Sign}(x)/\sqrt{|x|}$ (right).

III. NUMERICAL RESULTS

A. Two-body $\Lambda_b \rightarrow ph$ decays

We start with the invariant amplitude of the $\Lambda_b(\frac{1}{2}^+) \rightarrow p(\frac{1}{2}^+)h(0^-)$ decay [70], $h = \pi^-$ or K^- ,

$$\mathcal{A} = i\bar{u}_p(p_p)(S + P\gamma_5)u_{\Lambda_b}(p_{\Lambda_b}), \quad (38)$$

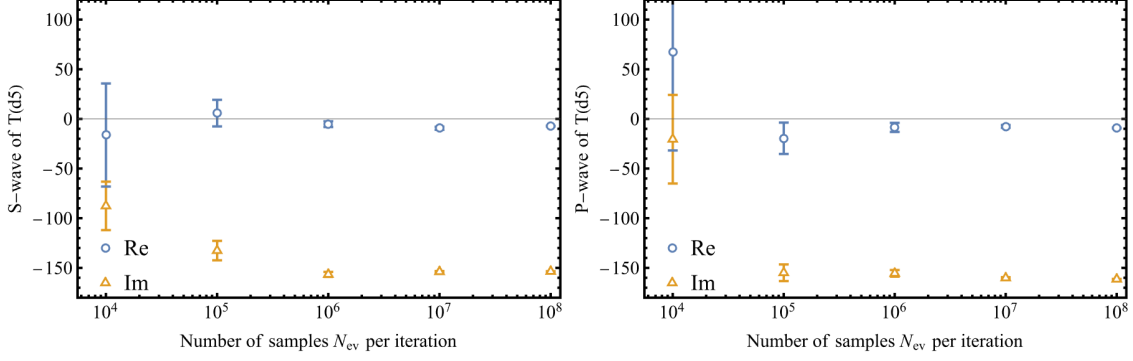


FIG. 6: Same as Fig. 3 but the integrals are treated under our algorithm.

where u_p is the proton spinor, and S (P) denotes the parity-violating S -wave (parity-conserving P -wave) amplitude. CPVs are generated by the interference between the contributions of the *tree* operators \mathcal{T} and the *penguin* operators \mathcal{P} . The S - and P -wave amplitudes are split into [17]

$$\begin{aligned} S &= \lambda_{\mathcal{T}}|S_{\mathcal{T}}|e^{i\delta_{\mathcal{T}}^S} + \lambda_{\mathcal{P}}|S_{\mathcal{P}}|e^{i\delta_{\mathcal{P}}^S}, \\ P &= \lambda_{\mathcal{T}}|P_{\mathcal{T}}|e^{i\delta_{\mathcal{T}}^P} + \lambda_{\mathcal{P}}|P_{\mathcal{P}}|e^{i\delta_{\mathcal{P}}^P}, \end{aligned} \quad (39)$$

where δ 's represent the strong phases, and $\lambda_{\mathcal{T}} = V_{ub}V_{ud(s)}^*$ and $\lambda_{\mathcal{P}} = V_{tb}V_{td(s)}^*$ are the products of the CKM matrix elements. It is reminded that the S -wave amplitude flips sign under the C transformation, but the P -wave one does not [18],

$$\begin{aligned} S \rightarrow \bar{S} &= -\lambda_{\mathcal{T}}^*|S_{\mathcal{T}}|e^{i\delta_{\mathcal{T}}^S} - \lambda_{\mathcal{P}}^*|S_{\mathcal{P}}|e^{i\delta_{\mathcal{P}}^S}, \\ P \rightarrow \bar{P} &= \lambda_{\mathcal{T}}^*|P_{\mathcal{T}}|e^{i\delta_{\mathcal{T}}^P} + \lambda_{\mathcal{P}}^*|P_{\mathcal{P}}|e^{i\delta_{\mathcal{P}}^P}. \end{aligned} \quad (40)$$

It is equivalent to formulate the decay $\Lambda_b \rightarrow ph$ in terms of the helicity amplitudes, defined as

$$H_{\lambda_p, \lambda_h} = \langle p(\lambda_p)h(\lambda_h)|H_W|\Lambda_b(\lambda_{\Lambda_b})\rangle. \quad (41)$$

The Λ_b spin component obeys $\lambda_{\Lambda_b} = \lambda_p - \lambda_h$ with the proton helicity λ_p and the meson spin λ_h . The helicity amplitudes H_{λ_p, λ_h} are related to the partial-wave amplitudes via

$$\begin{aligned} H_{1/2,0} &= -iM_+S + iM_-P, \\ H_{-1/2,0} &= -iM_+S - iM_-P, \end{aligned} \quad (42)$$

with the coefficients $M_{\pm}^2 \equiv (m_{\Lambda_b} \pm m_p)^2 - m_h^2 = 2m_{\Lambda_b}(E_p \pm m_p)$, E_p being the proton energy.

We calculate the contributions from all diagrams to the invariant amplitudes $S_{\mathcal{T}, \mathcal{P}}$ and $P_{\mathcal{T}, \mathcal{P}}$ in Eq. (39), including their strong phases, for the $\Lambda_b \rightarrow p\pi^-$, pK^- decays in the PQCD approach. The results can be transformed into the helicity amplitudes in Eq. (42) straightforwardly. It is worth mentioning that the nonfactorizable diagrams from the topologies PC_2 and PE_1^u are evaluated for the first time. Our predictions for the $\Lambda_b \rightarrow p\pi^-$ (pK^-) amplitudes are presented in Tables V and VI (VII and VIII), where only the central values are given for clarity.

The contributions to the decay amplitudes have been categorized according to topologies in the above tables. The external- W emission topology T is further divided into the factorizable part T^f and the non-factorizable part T^{nf} , and the same division applies to the PC_1 topology. The

topological amplitudes, excluding the CKM matrix elements, respect the hierarchy relations,

$$\begin{aligned} |T^f| &\gg |E_2| \gtrsim |PC_1^f| \gtrsim |T^{nf}| > |C_2| > |PC_2| > |B| \\ &\gtrsim |PE_1^u| > |PE_1^d| \sim |PB| \sim |PE_2| \sim |PC_1^{nf}| \quad (\text{S wave}), \\ |T^f| &\gg |T^{nf}| \gg |E_2| > |C_2| > |B| > |PC_2| \gtrsim |PC_1^{nf}| \\ &\gtrsim |PE_1^u| > |PC_1^f| > |PE_1^d| \sim |P^B| \sim |PE_2| \quad (\text{P wave}), \end{aligned} \quad (43)$$

with the explicit relative ratios,

$$\begin{aligned} \frac{|C_2|}{|T|} &= 0.042, \quad \frac{|E_2|}{|T|} = 0.095, \quad \frac{|B|}{|T|} = 0.014 \quad (\text{S wave}), \\ \frac{|C_2|}{|T|} &= 0.041, \quad \frac{|E_2|}{|T|} = 0.072, \quad \frac{|B|}{|T|} = 0.024 \quad (\text{P wave}), \end{aligned} \quad (44)$$

for the $\Lambda_b \rightarrow p\pi^-$ mode. Likewise, we have

$$\begin{aligned} |T^f| &\gg |E_2| \gtrsim |PC_1^f| \gtrsim |T^{nf}| > |PE_1^u| > |PE_1^d| > |PC_1^{nf}| \quad (\text{S wave}), \\ |T^f| &\gg |T^{nf}| \gg |E_2| > |PC_1^{nf}| \gtrsim |PE_1^u| > |PC_1^f| > |PE_1^d| \quad (\text{P wave}), \end{aligned} \quad (45)$$

$$\frac{|E_2|}{|T|} = 0.104 \quad (\text{S wave}), \quad \frac{|E_2|}{|T|} = 0.076 \quad (\text{P wave}). \quad (46)$$

for the $\Lambda_b \rightarrow pK^-$ mode. It is seen that Eqs. (43) and (45) are consistent with those from the SCET [42].

The $\Lambda_b \rightarrow p\pi^-, pK^-$ decays share the same topologies T and E_2 , allowing a quantitative assessment on the $SU(3)_F$ flavor symmetry breaking effects. The ratios

$$\begin{aligned} \frac{|T^f(pK)|}{|T^f(p\pi)|} &= 1.22, \quad \frac{|T^{nf}(pK)|}{|T^{nf}(p\pi)|} = 1.03, \quad \frac{|E_2(pK)|}{|E_2(p\pi)|} = 1.33 \quad (\text{S wave}), \\ \frac{|T^f(pK)|}{|T^f(p\pi)|} &= 1.23, \quad \frac{|T^{nf}(pK)|}{|T^{nf}(p\pi)|} = 1.28, \quad \frac{|E_2(pK)|}{|E_2(p\pi)|} = 1.29 \quad (\text{P wave}). \end{aligned} \quad (47)$$

imply that the $SU(3)_F$ breaking effects reach roughly 30%, similar to the case of B meson decays [71]. The breaking effects primarily originate from the meson decay constants in the factorizable T_f topology because of $|T^f(pK)|/|T^f(p\pi)| \approx f_K/f_\pi$, and from the meson DAs in the other topologies.

A hierarchy relation exists between the helicity amplitudes $H_{-1/2,0}$ and $H_{1/2,0}$ from the factorizable topology T^f , as manifested in Tables. VI and VIII. The proton spin tends to be anti-parallel to its momentum due to the chiral current ($V - A$) in weak interaction, granting the dominance of $H_{-1/2,0}$ over $H_{1/2,0}$.

Tables. V and VII and the hierarchy relations in Eqs. (43) and (45) declare that the factorizable penguin contribution to the P -wave is much lower than to the S -wave, i.e., $|PC_1^f|^{P\text{-wave}} \ll |PC_1^f|^{S\text{-wave}}$. This feature is attributed to the current structures of the penguin operators; the matrix element for the factorizable penguin PC_1^f from the $(V - A) \otimes (V - A)$ operators like O_4 is written, in the factorization hypothesis, as

$$\begin{aligned} \langle p\pi^- | O_4 | \Lambda_b \rangle &= \langle p\pi^- | (\bar{d}_\alpha b_\beta)_{V-A} (\bar{u}_\beta u_\alpha)_{V-A} | \Lambda_b \rangle \\ &= \langle \pi^- | (\bar{d}u)_{V-A} | 0 \rangle [\langle p | (\bar{u}b)_V | \Lambda_b \rangle - \langle p | (\bar{u}b)_A | \Lambda_b \rangle]. \end{aligned} \quad (48)$$

TABLE V: Invariant amplitudes of the $\Lambda_b \rightarrow p\pi^-$ decay classified by topologies without the CKM matrix elements.

$\Lambda_b \rightarrow p\pi^-$	$ S $	$\delta^S(^{\circ})$	Real(S)	Imag(S)	$ P $	$\delta^P(^{\circ})$	Real(P)	Imag(P)
T^f	707.17	0.00	707.17	0.00	1004.44	0.00	1004.44	0.00
T^{nf}	51.72	-96.64	-5.98	-51.38	267.72	-97.92	-36.90	-265.17
$T^f + T^{nf}$	703.07	-4.19	701.19	-51.38	1003.22	-15.33	967.54	-265.17
C_2	29.37	154.96	-26.61	12.43	41.51	179.80	-41.51	0.14
E_2	66.94	-145.26	-55.01	-38.14	72.58	119.94	-36.23	62.89
B	10.40	112.64	-4.00	9.60	23.65	-122.56	-12.73	-19.93
Tree	619.26	-6.26	615.57	-67.49	904.75	-14.21	877.08	-222.06
PC_1^f	58.44	0.00	58.44	0.00	2.90	0.00	2.90	0.00
PC_1^{nf}	1.24	-115.38	-0.53	-1.12	11.16	-95.25	-1.02	-11.11
$PC_1^f + PC_1^{nf}$	57.91	-1.11	57.90	-1.12	11.27	-80.38	1.88	-11.11
PC_2	13.36	-116.10	-5.88	-12.00	14.93	71.96	4.62	14.20
PE_1^u	9.48	-87.62	0.39	-9.47	8.83	114.44	-3.65	8.04
PB	1.36	-51.30	0.85	-1.06	1.55	-159.86	-1.46	-0.53
$PE_1^d + PE_2$	3.87	-98.18	-0.55	-3.83	1.41	-12.55	1.37	-0.31
Penguin	59.45	-27.54	52.71	-27.49	10.65	74.93	2.77	10.28

For the $(V - A) \otimes (V + A)$ operators like O_6 , the corresponding matrix element is approximated by

$$\begin{aligned}
 \langle p\pi^- | O_6 | \Lambda_b \rangle &= \langle p\pi^- | (\bar{d}_\alpha b_\beta)_{V-A} (\bar{u}_\beta u_\alpha)_{V+A} | \Lambda_b \rangle \\
 &= -2 \langle \pi^- | (\bar{d}u)_{S+P} | 0 \rangle \langle p | (\bar{u}b)_{S-P} | \Lambda_b \rangle \\
 &= \langle \pi^- | (\bar{d}u)_{V-A} | 0 \rangle \left[\frac{2m_\pi^2}{(m_b - m_u)(m_u + m_d)} \langle p | (\bar{u}b)_V | \Lambda_b \rangle \right. \\
 &\quad \left. + \frac{2m_\pi^2}{(m_b + m_u)(m_u + m_d)} \langle p | (\bar{u}b)_A | \Lambda_b \rangle \right] \\
 &= \langle \pi^- | (\bar{d}u)_{V-A} | 0 \rangle (R_1^\pi \langle p | (\bar{u}b)_V | \Lambda_b \rangle + R_2^\pi \langle p | (\bar{u}b)_A | \Lambda_b \rangle),
 \end{aligned} \tag{49}$$

with the chiral factors $R_1^\pi \equiv \frac{2m_\pi^2}{(m_b - m_u)(m_u + m_d)}$ and $R_2^\pi \equiv \frac{2m_\pi^2}{(m_b + m_u)(m_u + m_d)}$.

The S - and P -wave PC_1^f amplitudes then read

$$\begin{aligned}
 (PC_1^f)^{S\text{-wave}} &= -\frac{G_F}{\sqrt{2}} f_h V_{tb} V_{td}^* \left[\frac{C_3}{3} + C_4 + \frac{C_9}{3} + C_{10} + R_1^\pi \left(\frac{C_5}{3} + C_6 + \frac{C_7}{3} + C_8 \right) \right] \\
 &\quad \left[f_1(m_h^2)(m_{\Lambda_b} - m_p) + f_3(m_h^2)m_h^2 \right], \\
 (PC_1^f)^{P\text{-wave}} &= -\frac{G_F}{\sqrt{2}} f_h V_{tb} V_{td}^* \left[\frac{C_3}{3} + C_4 + \frac{C_9}{3} + C_{10} - R_2^\pi \left(\frac{C_5}{3} + C_6 + \frac{C_7}{3} + C_8 \right) \right] \\
 &\quad \left[g_1(m_h^2)(m_{\Lambda_b} + m_p) - g_3(m_h^2)m_h^2 \right],
 \end{aligned} \tag{50}$$

TABLE VI: Helicity amplitudes of the $\Lambda_b \rightarrow p\pi^-$ decay classified by topologies without the CKM matrix elements.

$\Lambda_b \rightarrow p\pi^-$	$ H_{\frac{1}{2},0} $	$\delta(H_{\frac{1}{2},0})^\circ$	$\text{Real}(H_{\frac{1}{2},0})$	$\text{Imag}(H_{\frac{1}{2},0})$	$ H_{-\frac{1}{2},0} $	$\delta(H_{-\frac{1}{2},0})^\circ$	$\text{Real}(H_{-\frac{1}{2},0})$	$\text{Imag}(H_{-\frac{1}{2},0})$
T^f	65.30	90.00	0.00	65.30	9344.10	-90.00	0.00	-9344.10
T^{nf}	914.77	-8.40	904.96	-133.62	1593.23	172.35	-1579.06	212.04
$T^f + T^{nf}$	907.53	-4.32	904.96	-68.32	9267.57	-99.81	-1579.06	-9132.06
C_2	83.29	-13.80	80.89	-19.87	378.05	77.44	82.24	369.00
E_2	577.41	160.66	-544.83	191.24	532.44	85.22	44.34	530.59
B	159.82	-12.04	156.30	-33.35	91.09	109.50	-30.40	85.87
Tree	601.38	6.66	597.33	69.70	8280.47	-100.32	-1482.88	-8146.61
PC_1^f	369.76	-90.00	0.00	-369.76	396.97	-90.00	0.00	-396.97
PC_1^{nf}	44.70	-1.64	44.68	-1.28	60.01	172.07	-59.43	8.28
$PC_1^f + PC_1^{nf}$	373.72	-83.13	44.68	-371.04	393.21	-98.69	-59.43	-388.69
PC_2	157.24	157.48	-145.25	60.24	20.86	125.84	-12.21	16.91
PE_1^u	101.73	-168.84	-99.80	-19.70	28.48	149.33	-24.50	14.53
PB	13.17	-109.70	-4.44	-12.40	9.53	172.34	-9.45	1.27
$PE_1^d + PE_2$	25.76	157.05	-23.72	10.04	26.73	-173.96	-26.58	-2.81
Penguin	403.75	-124.47	-228.52	-332.85	382.37	-110.22	-132.18	-358.80

respectively, where the form factors $f_{1,3}$ and $g_{1,3}$ are defined in terms of the matrix element $\langle p|\bar{u}\gamma_\mu b|\Lambda_b\rangle = \bar{u}_p(f_1\gamma_\mu + f_2i\sigma_{\mu\nu}q^\nu + f_3q_\mu)u_{\Lambda_b}$ and $\langle p|\bar{u}\gamma_\mu\gamma_5 b|\Lambda_b\rangle = \bar{u}_p(g_1\gamma_\mu + g_2i\sigma_{\mu\nu}q^\nu + g_3q_\mu)\gamma_5 u_{\Lambda_b}$. The chiral factors $R_{1,2}^\pi$ are of $\mathcal{O}(1)$, so the negative sign of the R_2^π piece in the second expression of Eq. (50) results in destruction. As a consequence, the S -wave PC_1^f is enhanced, while the P -wave one is suppressed.

It is observed from the amplitudes in Appendix B that specific combinations of the hadron DAs may produce opposite signs between the S and P waves. For instance, Eq. (B9) from the combination of the Λ_b twist-2, proton twist-3 and meson twist-2 DAs yields

$$\begin{aligned} & M_{T_{nf}(c7)}^{(V-A)\otimes(V-A)}(\Lambda_b \text{ twist-2-proton twist-3-meson twist-2}) \\ &= 8m_{\Lambda_b}^4(x_3 - y)(-2A_1\psi_2(-1 + x_2 + y) + 2\psi_2(2T_1 + V_1)(-1 + x_2 + y))\phi_m^A \\ &+ 8m_{\Lambda_b}^4(x_3 - y)(-2A_1\psi_2(-1 + x_2 + y) + 2\psi_2(2T_1 + V_1)(-1 + x_2 + y))\phi_m^A\gamma_5, \end{aligned} \quad (51)$$

where the S -wave (first) piece and the P -wave (second) piece have the same sign. Nevertheless, the two partial waves are opposite in sign in the combination of the Λ_b twist-3, proton twist-3 and meson twist-2 DAs,

$$\begin{aligned} & M_{T_{nf}(c7)}^{(V-A)\otimes(V-A)}(\Lambda_b \text{ twist-3+proton twist-3+meson twist-2}) \\ &= 8m_{\Lambda_b}^4(x_3 - y)(A_1\psi_3^{-+}x'_2 + V_1\psi_3^{-+}x'_2)\phi_m^A \\ &- 8m_{\Lambda_b}^4(x_3 - y)(A_1\psi_3^{-+}x'_2 + V_1\psi_3^{-+}x'_2)\phi_m^A\gamma_5. \end{aligned} \quad (52)$$

This distinction arises from the different numbers of γ_5 for the S and P waves endowed by the vector and axial-vector currents in weak interaction and by the Dirac structures of the hadron DAs.

TABLE VII: Same as Table **V** but for the $\Lambda_b \rightarrow pK^-$ decay.

$\Lambda_b \rightarrow pK^-$	$ S $	$\delta^S(^{\circ})$	Real(S)	Imag(S)	$ P $	$\delta^P(^{\circ})$	Real(P)	Imag(P)
T^f	865.44	0.00	865.44	0.00	1230.64	0.00	1230.64	0.00
T^{nf}	53.41	-102.81	-11.84	-52.08	343.23	-96.76	-40.43	-340.84
$T^f + T^{nf}$	855.18	-3.49	853.60	-52.08	1238.05	-15.98	1190.21	-340.84
E_2	89.06	-138.10	-66.28	-59.48	94.13	122.31	-50.31	79.56
Tree	795.18	-8.06	787.31	-111.55	1169.46	-12.91	1139.90	-261.28
PC_1^f	76.43	0.00	76.43	0.00	3.30	180.00	-3.30	0.00
PC_1^{nf}	1.14	-134.10	-0.79	-0.82	13.85	-94.36	-1.05	-13.81
$PC_1^f + PC_1^{nf}$	75.64	-0.62	75.64	-0.82	14.48	-107.50	-4.35	-13.81
PE_1^u	11.80	-89.53	0.10	-11.80	11.02	115.62	-4.76	9.93
PE_1^d	7.53	-101.53	-1.50	-7.38	2.67	51.53	1.66	2.09
Penguin	76.88	-15.08	74.23	-20.00	7.66	-166.53	-7.45	-1.79

TABLE VIII: Same as Table **VI** but for the $\Lambda_b \rightarrow pK^-$ decay.

$\Lambda_b \rightarrow pK^-$	$ H_{\frac{1}{2},0} $	$\delta(H_{\frac{1}{2},0})^{\circ}$	Real($H_{\frac{1}{2},0}$)	Imag($H_{\frac{1}{2},0}$)	$ H_{-\frac{1}{2},0} $	$\delta(H_{-\frac{1}{2},0})^{\circ}$	Real($H_{-\frac{1}{2},0}$)	Imag($H_{-\frac{1}{2},0}$)
T^f	71.74	90.00	0.00	71.74	11397.55	-90.00	0.00	-11397.55
T^{nf}	1252.42	-5.08	1247.50	-110.90	1947.26	172.15	-1929.02	265.90
$T^f + T^{nf}$	1248.12	-1.80	1247.50	-39.17	11297.55	-99.83	-1929.02	-11131.65
E_2	785.62	165.31	-759.92	199.29	668.39	91.58	-18.44	668.13
Tree	513.20	18.18	487.58	160.12	10643.20	-100.54	-1947.46	-10463.51
PC_1^f	515.50	-90.00	0.00	-515.50	484.74	-90.00	0.00	-484.74
PC_1^{nf}	59.00	0.28	59.00	0.29	70.45	171.76	-69.72	10.10
$PC_1^f + PC_1^{nf}$	518.58	-83.47	59.00	-515.22	479.73	-98.36	-69.72	-474.64
PE_1^u	125.61	-169.53	-123.52	-22.83	37.72	145.13	-30.95	21.57
PE_1^d	60.63	163.13	-58.02	17.60	38.56	176.88	-38.51	2.10
Penguin	534.68	-103.25	-122.54	-520.44	471.96	-107.15	-139.17	-450.97

We survey all combinations of the DAs, and decide the relative signs between the S - and P -wave amplitudes as exhibited in Table **IX**, where the symbol ‘+’ (‘−’) means the same (opposite) sign. It is interesting that the relative sign between the S and P waves alternates with the twists of the Λ_b or proton DAs. This feature holds for all Feynman diagrams and all types of weak interaction vertices. The net interference between the S - and P -wave amplitudes for a topology is then determined by the dominant Feynman diagram and DA combination involved. This accounts for the notable fluctuation of the strong phases in Tables **V** and **VII**. The different strong phases impact the predictions for CPVs, which will be explored in the following subsections.

With the obtained amplitudes, we predict the various observables associated with the $\Lambda_b \rightarrow p\pi^-, pK^-$ decays as elaborated below. The outcomes are assembled in Table **X**, where the first

meson twist-2	proton twist-3	proton twist-4	proton twist-5	proton twist-6
Λ_b twist-2	+	-	+	-
Λ_b twist-3	-	+	-	+
Λ_b twist-4	+	-	+	-
meson twist-3	proton twist-3	proton twist-4	proton twist-5	proton twist-6
Λ_b twist-2	-	+	-	+
Λ_b twist-3	+	-	+	-
Λ_b twist-4	-	+	-	+

TABLE IX: Relative signs between the S - and P -wave amplitudes for various twist combinations of the Λ_b and proton DAs.

three errors are from the inputs in the Λ_b , proton and meson DAs, respectively, and the fourth one stems from varying the renormalization scale of the Wilson coefficients in Table I. The uncertainties from the CKM matrix elements are negligible relative to the above sources.

TABLE X: Observables associated with the $\Lambda_b \rightarrow p\pi^-$, pK^- decays. The percentages in the parentheses stand for the proportions of the partial-wave CPVs to the direct CPVs.

$Br(\times 10^{-6})$			
$\Lambda_b \rightarrow p\pi^-$	$3.34^{+2.53+1.33+0.10+0.47}_{-1.30-1.10-0.11-0.14}$		
$\Lambda_b \rightarrow pK^-$	$2.83^{+2.17+1.17+0.49+2.19}_{-1.05-0.92-0.37-0.66}$		
	A_{CP}^{dir}	$A_{CP}^S(\kappa_S)$	$A_{CP}^P(\kappa_P)$
$\Lambda_b \rightarrow p\pi^-$	$0.05^{+0.00+0.00+0.00+0.02}_{-0.02-0.01-0.02-0.01}$	$0.17^{+0.01+0.01+0.03+0.04}_{-0.04-0.04-0.07-0.04}$ (49%)	$-0.06^{+0.01+0.03+0.02+0.00}_{-0.02-0.03-0.03-0.01}$ (51%)
$\Lambda_b \rightarrow pK^-$	$-0.06^{+0.01+0.01+0.02+0.00}_{-0.01-0.01-0.01-0.00}$	$-0.05^{+0.02+0.02+0.04+0.00}_{-0.02-0.01-0.03-0.00}$ (94%)	$-0.21^{+0.07+0.23+0.29+0.04}_{-0.15-0.33-0.27-0.01}$ (6%)
	α	A_{CP}^α	$\langle \alpha \rangle$
$\Lambda_b \rightarrow p\pi^-$	$-0.94^{+0.00+0.02+0.01+0.03}_{-0.02-0.02-0.02-0.02}$	$0.02^{+0.00+0.01+0.00+0.01}_{-0.01-0.01-0.01-0.01}$	$-0.96^{+0.00+0.01+0.01+0.02}_{-0.00-0.01-0.01-0.01}$
$\Lambda_b \rightarrow pK^-$	$0.23^{+0.04+0.02+0.10+0.15}_{-0.03-0.05-0.12-0.07}$	$0.04^{+0.02+0.02+0.01+0.01}_{-0.02-0.03-0.01-0.01}$	$0.20^{+0.02+0.01+0.11+0.14}_{-0.02-0.02-0.12-0.06}$
	β	A_{CP}^β	$\langle \beta \rangle$
$\Lambda_b \rightarrow p\pi^-$	$0.34^{+0.00+0.05+0.01+0.07}_{-0.06-0.06-0.06-0.05}$	$0.22^{+0.00+0.00+0.03+0.07}_{-0.01-0.01-0.04-0.03}$	$0.12^{+0.00+0.05+0.03+0.00}_{-0.05-0.05-0.04-0.02}$
$\Lambda_b \rightarrow pK^-$	$-0.39^{+0.03+0.08+0.08+0.12}_{-0.01-0.04-0.07-0.01}$	$-0.44^{+0.01+0.01+0.02+0.08}_{-0.00-0.00-0.01-0.04}$	$0.05^{+0.03+0.08+0.07+0.04}_{-0.01-0.05-0.07-0.02}$
	γ	A_{CP}^γ	$\langle \gamma \rangle$
$\Lambda_b \rightarrow p\pi^-$	$0.09^{+0.02+0.04+0.04+0.04}_{-0.04-0.06-0.06-0.01}$	$0.11^{+0.01+0.02+0.03+0.03}_{-0.02-0.03-0.04-0.02}$	$-0.02^{+0.01+0.02+0.01+0.01}_{-0.02-0.04-0.01-0.00}$
$\Lambda_b \rightarrow pK^-$	$0.89^{+0.02+0.04+0.04+0.00}_{-0.01-0.02-0.05-0.01}$	$0.02^{+0.02+0.05+0.04+0.00}_{-0.01-0.03-0.04-0.00}$	$0.87^{+0.00+0.01+0.02+0.00}_{-0.00-0.01-0.02-0.01}$

The decay width is written as

$$\Gamma = \frac{p_c}{8\pi m_{\Lambda_b}^2} \{ M_+^2 |S|^2 + M_-^2 |P|^2 \} = \frac{p_c}{16\pi m_{\Lambda_b}^2} (|H_{1/2,0}|^2 + |H_{-1/2,0}|^2), \quad (53)$$

where

$$p_c = \sqrt{[(m_{\Lambda_b} + m_p)^2 - m_h^2][(m_{\Lambda_b} - m_p)^2 - m_h^2]/(2m_{\Lambda_b})}, \quad (54)$$

is the momentum of either the proton or the meson in the rest frame of the Λ_b baryon. The predicted $\Lambda_b \rightarrow p\pi^-$ and $\Lambda_b \rightarrow pK^-$ branching ratios are a bit lower than the data $Br(\Lambda_b \rightarrow p\pi^-) =$

$(4.6 \pm 0.8) \times 10^{-6}$ and $Br(\Lambda_b \rightarrow pK^-) = (5.5 \pm 1.0) \times 10^{-6}$. We suspect that the discrepancy is attributed to higher-order corrections, in particular those to the non-factorizable topologies. The factorizable contributions have been more or less fixed by the measured $\Lambda_b \rightarrow p\mu\bar{\nu}_\mu$ and $\Lambda_b \rightarrow pD_s^-$ branching ratios. The uncertainty arising from the Wilson coefficients for the $\Lambda_b \rightarrow pK^-$ decay is larger than for $\Lambda_b \rightarrow p\pi^-$, suggesting that higher-order contributions are more important in penguin-dominant modes.

The $\Lambda_b \rightarrow p\pi^-, pK^-$ decays share the same inputs from the Λ_b and proton DAs, so the errors from these sources are suppressed in the difference of the branching ratios,

$$\begin{aligned}\Delta Br(\Lambda_b \rightarrow pK^-/\pi^-) &\equiv Br(\Lambda_b \rightarrow pK^-) - Br(\Lambda_b \rightarrow p\pi^-) \\ &= (-0.51^{+0.25+0.20+0.50+1.72}_{-0.36-0.17-0.38-0.52}) \times 10^{-6}.\end{aligned}\quad (55)$$

Though the errors from the meson DAs and the Wilson coefficients keep sizable, Eq. (55) indicates that the $\Lambda_b \rightarrow pK^-$ branching ratio is higher than the $\Lambda_b \rightarrow p\pi^-$ one. The discrepancy between Eq. (55) and the LHCb measurements may be also resolved by including higher-order corrections, as hinted by the crucial effects from varying the renormalization scale of the Wilson coefficients.

According to the definition for the direct CPV of the $\Lambda_b \rightarrow ph$ decay,

$$A_{CP}^{dir}(\Lambda_b \rightarrow ph) \equiv \frac{\Gamma(\Lambda_b \rightarrow ph) - \bar{\Gamma}(\bar{\Lambda}_b \rightarrow \bar{p}\bar{h})}{\Gamma(\Lambda_b \rightarrow ph) + \bar{\Gamma}(\bar{\Lambda}_b \rightarrow \bar{p}\bar{h})}, \quad (56)$$

we have the explicit expression

$$A_{CP}^{dir} = \frac{-2M_+^2|S_T|^2r_S \sin \Delta\phi \sin \Delta\delta_S - 2M_-^2|P_T|^2r_P \sin \Delta\phi \sin \Delta\delta_P}{M_+^2|S_T|^2(1+r_S^2+2r_S \cos \Delta\phi \cos \Delta\delta_S) + M_-^2|P_T|^2(1+r_P^2+2r_P \cos \Delta\phi \cos \Delta\delta_P)}, \quad (57)$$

where $r_S = |\lambda_P S_P|/|\lambda_T S_T|$ ($r_P = |\lambda_P P_P|/|\lambda_T P_T|$) is the ratio of the penguin amplitude to the tree amplitude for the S (P) wave, the difference of the weak phases $\Delta\phi \equiv \arg(\lambda_P) - \arg(\lambda_T)$ is identical for both waves, and $\Delta\delta_S = \delta_P^S - \delta_T^S$ ($\Delta\delta_P = \delta_P^P - \delta_T^P$) is the difference of the strong phases for the S (P) wave. It is trivial to construct the partial-wave CPVs,

$$\begin{aligned}A_{CP}^S &\equiv \frac{|S|^2 - |\bar{S}|^2}{|S|^2 + |\bar{S}|^2} = \frac{-2r_S \sin \Delta\phi \sin \Delta\delta_S}{1+r_S^2+2r_S \cos \Delta\phi \cos \Delta\delta_S}, \\ A_{CP}^P &\equiv \frac{|P|^2 - |\bar{P}|^2}{|P|^2 + |\bar{P}|^2} = \frac{-2r_P \sin \Delta\phi \sin \Delta\delta_P}{1+r_P^2+2r_P \cos \Delta\phi \cos \Delta\delta_P}.\end{aligned}\quad (58)$$

The net direct CPV is related to the partial-wave CPVs through [17]

$$\begin{aligned}A_{CP}^{dir} &= \frac{M_+^2(|S|^2 - |\bar{S}|^2) + M_-^2(|P|^2 - |\bar{P}|^2)}{M_+^2(|S|^2 + |\bar{S}|^2) + M_-^2(|P|^2 + |\bar{P}|^2)} \\ &= \kappa_S A_{CP}^S + \kappa_P A_{CP}^P,\end{aligned}\quad (59)$$

where the weights are given by

$$\begin{aligned}\kappa_S &\equiv \frac{|S|^2}{|S|^2 + \frac{M_-^2}{M_+^2} \frac{1+A_{CP}^S}{1+A_{CP}^P} |P|^2} = \frac{|S|^2}{|S|^2 + \kappa r_{CP} |P|^2}, \\ \kappa_P &\equiv \frac{\frac{M_-^2}{M_+^2} |P|^2}{\frac{1+A_{CP}^P}{1+A_{CP}^S} |S|^2 + \frac{M_-^2}{M_+^2} |P|^2} = \frac{\kappa |P|^2}{|S|^2/r_{CP} + \kappa |P|^2},\end{aligned}\quad (60)$$

with $\kappa \equiv M_-^2/M_+^2$ and $r_{CP} = (1 + A_{CP}^S)/(1 + A_{CP}^P)$. It states that the total direct CPV is the weighted average of the partial-wave CPVs.

It is observed in Table X that the partial-wave CPVs can exceed 10%, such as $A_{CP}^S(\Lambda_b \rightarrow p\pi) = 0.17$ and $A_{CP}^P(\Lambda_b \rightarrow pK) = -0.21$, similar to the direct CPVs in B meson decays. However, the destruction between the S -wave CPV (0.17) and the P -wave CPV (-0.06) in $\Lambda_b \rightarrow p\pi^-$ reduces the direct CPV to $0.05^{+0.02}_{-0.03}$. The central value of our prediction does not exactly match the data, but the destruction mechanism in this mode, which does not exist in the corresponding decay $B \rightarrow \pi\pi$, has been demonstrated unambiguously. The S -wave CPV in the penguin-dominated $\Lambda_b \rightarrow pK^-$ decay is small (-0.05) with the tiny strong phase $\Delta\delta_S = -7^\circ$, and the sizable P -wave CPV is down by the proportion $\kappa_P = 6\%$ because of $|P| \ll |S|$. The direct CPV $A_{CP}^{dir}(\Lambda_b \rightarrow pK) = -0.06^{+0.03}_{-0.02}$ turns out to diminish as well.

We emphasize that the aforementioned destruction mechanism was not noticed before. The previous studies based on the generalized factorization [32, 33, 72] and the QCDF [36] considered only the factorizable diagrams, i.e., T for the tree contributions and PC_1 for the penguin contributions. The associated partial-wave CPVs are always minor owing to either the small strong phase differences or the low weights of the penguin amplitudes. Here we point out the large relative strong phases from the PC_2 and PE_1^u diagrams, which are first realized in the PQCD formalism. They generate the strong phases for the S and P waves with opposite signs, whose cancellation is the mechanism responsible for the diminishing direct CPV in $\Lambda_b \rightarrow p\pi$.

To visualize the cancellation between the imaginary parts or the strong phases of the partial-wave amplitudes, we display the PC_2 , PE_1^u and PC_1 contributions to the $\Lambda_b \rightarrow p\pi^-$ decay in Fig. 7. It is evident that the combined $PC_2 + PE_1^u$ constitutes the dominant source of the strong phases, which destruct between the S and P waves. The diagram PC_1 mainly contributes to the magnitude of the S wave. The $\Lambda_b \rightarrow pK^-$ case is different as remarked before, where the diagram PE_1^u also gives the strong phases with opposite signs between the S and P waves. However, the dominant S -wave CPV governs the direct CPV in this mode.

We explain why the PC_2 and PE_1^u penguins generate the dominant strong phases with opposite signs between the S - and P -wave amplitudes. For simplicity, we ignore the electroweak penguins and concentrate on the QCD penguins. The distinction between the contributions of $O_{3,4}$ and $O_{1,2}$, both being the $(V - A) \otimes (V - A)$ operators, appears only in their Wilson coefficients, such that the strong phases of the penguin amplitudes from $O_{3,4}$ are close to those of the tree amplitudes. This claim is supported by the results in Tables XI and XII. Taking the $\Lambda_b \rightarrow p\pi^-$ decay as an example, we have $\delta^S = -6.26^\circ$ and -10.64° for the S -wave amplitudes from the tree and $O_{3,4}$ operators, respectively, and $\delta^P = -14.21^\circ$ and -12.75° for the P -wave ones from the tree and $O_{3,4}$ operators, respectively. It is also the case for $\Lambda_b \rightarrow pK^-$. The contributions from the $(V - A) \otimes (V + A)$ operators $O_{5,6}$ make the substantial strong phase differences between the penguin and tree amplitudes, which read $\delta^S = -40.61^\circ$ and $\delta^P = 153.58^\circ$ for the $p\pi^-$ mode in Table XI, and $\delta^S = -18.02^\circ$ and $\delta^P = 172.56^\circ$ for the pK^- mode in Table XII. Figure 8, depicting the S - and P -wave amplitudes from $O_{5,6}$, justifies our analytic argument for $S_{PC_2} \approx -P_{PC_2}$ and $S_{PE_1^u} \approx -P_{PE_1^u}$.

The underlying destruction between the partial-wave CPVs in the $\Lambda_b \rightarrow p\pi^-$ decay is manifested in Figure 9, for the ratio of $|P|^2/|S|^2 = 1.6$ obtained in this work. It shows the dependence of the net direct CPV on partial-wave CPVs, where the red spot corresponds to our prediction. The gray narrow band specifies the partial-wave CPVs allowed by the data of the direct CPV. We can perceive how the partial-wave CPVs affect the net CPV, and how close our prediction is to the data. It is noteworthy that the P wave of the decay $\Lambda_b \rightarrow pK^-$ reveals the highest partial-wave CPV, amounting to 21%, but with larger uncertainty compared to the S -wave CPV. The factorizable

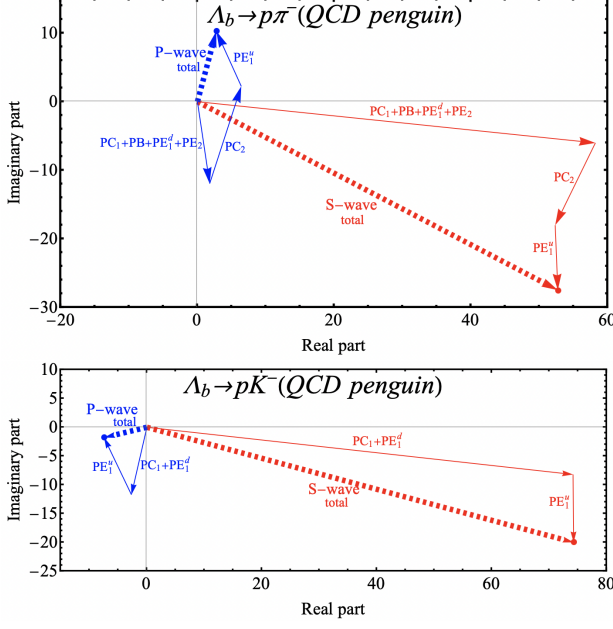


FIG. 7: QCD penguin contributions from each topological diagram to the $\Lambda_b \rightarrow p\pi^-$ decay (top) and to the $\Lambda_b \rightarrow pK^-$ decay (bottom) depicted in the complex plane. The red (blue) vectors represent the *S*-wave (*P*-wave) penguin contributions.

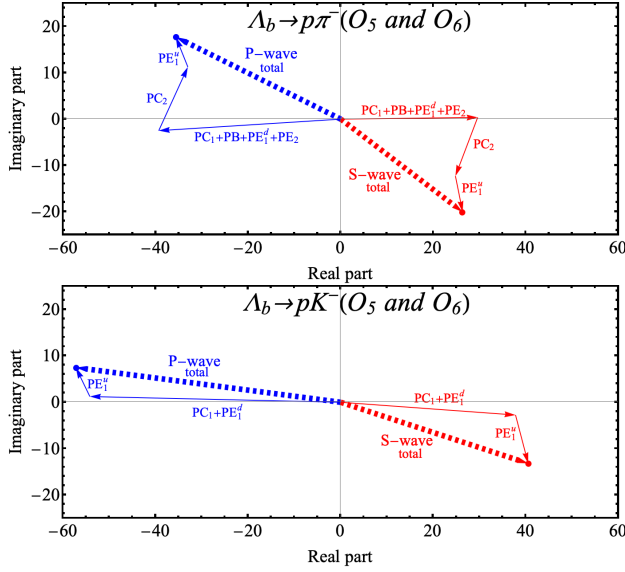


FIG. 8: O_5 and O_6 penguin contributions to the $\Lambda_b \rightarrow p\pi^-$ decay (top) and to the $\Lambda_b \rightarrow pK^-$ decay (bottom) depicted in the complex plane. The red (blue) vectors represent the *S*-wave (*P*-wave) penguin contributions.

penguin contributions play an essential role in the *S*-wave amplitude due to the chiral factors. These contributions, being less sensitive to the proton DAs, have smaller theoretical errors. By contrast, the non-factorizable penguin contributions, dominating the *P*-wave amplitude, suffer significant uncertainties from the proton and kaon DAs, which propagate into the *P*-wave CPVs.

$\Lambda_b \rightarrow p\pi^-$		$ S $	$\delta^S(\circ)$	$\text{Re}(S)$	$\text{Im}(S)$	$ P $	$\delta^P(\circ)$	$\text{Re}(P)$	$\text{Im}(P)$
Tree	T	703.07	-4.19	701.19	-51.38	1003.22	-15.33	967.54	-265.17
	C_2	29.37	154.96	-26.61	12.43	41.51	179.80	-41.51	0.14
	E_2	66.94	-145.26	-55.01	-38.14	72.58	119.94	-36.23	62.89
	B	10.40	112.64	-4.00	9.60	23.65	-122.56	-12.73	-19.93
	total	619.26	-6.26	615.57	-67.49	904.75	-14.21	877.08	-222.06
QCD Penguin	PC_1	59.36	-1.62	59.34	-1.68	13.41	-81.85	1.90	-13.27
	PC_2	13.95	-114.84	-5.86	-12.66	13.89	69.92	4.77	13.05
	PE_1^u	8.52	-93.30	-0.49	-8.51	10.23	112.10	-3.85	9.48
	PB	1.44	-39.65	1.11	-0.92	1.40	-162.08	-1.33	-0.43
	$PE_1^d + PE_2$	3.98	-101.17	-0.77	-3.90	1.35	7.65	1.34	0.18
	total	60.07	-27.41	53.33	-27.65	9.44	72.56	2.83	9.01
$O_{3,4}$	PC_1	30.41	-4.26	30.32	-2.26	43.11	-16.55	41.32	-12.28
	PC_2	1.05	179.78	-1.05	0.00	1.68	-154.82	-1.52	-0.71
	PE_1^u	2.18	-159.87	-2.05	-0.75	3.28	112.54	-1.26	3.03
	PB	0.36	103.90	-0.09	0.35	0.38	-114.38	-0.16	-0.35
	$PE_1^d + PE_2$	2.42	-93.34	-0.14	-2.42	1.61	86.32	0.10	1.60
	total	27.47	-10.64	27.00	-5.07	39.46	-12.75	38.49	-8.71
$O_{5,6}$	PC_1	29.02	1.15	29.02	0.58	39.44	-178.56	-39.42	-0.99
	PC_2	13.54	-110.82	-4.81	-12.66	15.13	65.45	6.29	13.76
	PE_1^u	7.92	-78.61	1.56	-7.76	6.95	111.88	-2.59	6.45
	PB	1.74	-46.52	1.20	-1.27	1.17	-176.00	-1.17	-0.08
	$PE_1^d + PE_2$	1.61	-113.22	-0.63	-1.48	1.89	-48.96	1.24	-1.42
	total	34.69	-40.61	26.33	-22.58	39.82	153.58	-35.66	17.72

TABLE XI: Results of the topological amplitudes for the $\Lambda_b \rightarrow p\pi^-$ decay in units of 10^{-9} without the CKM matrix elements. The QCD penguin contributions are further broken down into those from the $O_{3,4}$ and $O_{5,6}$ operators. The magnitudes and strong phases of each topological diagram are grouped in the columns of $|S|$, $\delta^S(\circ)$, $|P|$ and $\delta^P(\circ)$.

The difference of the direct CPVs is given by

$$\Delta A_{CP}^{dir}(\Lambda_b \rightarrow pK^-/\pi^-) \equiv A_{CP}^{dir}(\Lambda_b \rightarrow pK^-) - A_{CP}^{dir}(\Lambda_b \rightarrow p\pi^-) = -0.11^{+0.02+0.02+0.03+0.02}_{-0.01-0.00-0.01-0.02}, \quad (61)$$

which slightly deviates from the measured value around -0.01 . As mentioned in Sec. I and Ref. [23], the threshold resummation factor for heavy baryon decays, which smooths the endpoint behavior of hard kernels and modifies tree and penguin contributions differently, has not been taken into account in the present framework. Implementing this factor may achieve more accurate predictions, improve the agreement with experimental data, and advance our understanding of the decay dynamics accordingly.

We define the decay parameters for $\Lambda_b \rightarrow p\pi^-, pK^-$ [73],

$$\alpha = -\frac{2\kappa_c \text{Re}(S^* P)}{|S|^2 + \kappa_c^2 |P|^2}, \quad \beta = -\frac{2\kappa_c \text{Im}(S^* P)}{|S|^2 + \kappa_c^2 |P|^2}, \quad \gamma = \frac{|S|^2 - \kappa_c^2 |P|^2}{|S|^2 + \kappa_c^2 |P|^2}, \quad (62)$$

$\Lambda_b \rightarrow pK^-$		$ S $	$\delta^S(^{\circ})$	$\text{Re}(S)$	$\text{Im}(S)$	$ P $	$\delta^P(^{\circ})$	$\text{Re}(P)$	$\text{Im}(P)$
Tree	T	855.18	-3.49	853.60	-52.08	1238.05	-15.98	1190.21	-340.84
	E_2	89.06	-138.10	-66.28	-59.48	94.13	122.31	-50.31	79.56
	total	795.18	-8.06	787.31	-111.55	1169.46	-12.91	1139.90	-261.28
QCD Penguin	PC_1	76.08	-0.81	76.07	-1.07	15.03	-106.59	-4.29	-14.40
	PE_1^u	11.88	-88.70	0.27	-11.88	11.41	114.21	-4.68	10.41
	PE_1^d	7.46	-100.12	-1.31	-7.34	2.08	60.60	1.02	1.81
	total	77.72	-15.13	75.03	-20.29	8.25	-164.60	-7.95	-2.19
$O_{3,4}$	PC_1	37.18	-4.11	37.09	-2.66	53.10	-17.42	50.67	-15.89
	PE_1^u	2.86	-149.71	-2.47	-1.44	4.48	111.71	-1.66	4.17
	PE_1^d	3.00	-92.18	-0.11	-3.00	2.08	83.11	0.25	2.06
	total	35.23	-11.64	34.51	-7.11	50.20	-11.10	49.26	-9.66
$O_{5,6}$	PC_1	39.01	2.33	38.98	1.59	54.98	178.45	-54.96	1.49
	PE_1^u	10.79	-75.30	2.74	-10.44	6.93	115.83	-3.02	6.24
	PE_1^d	4.50	-105.46	-1.20	-4.34	0.81	-18.16	0.77	-0.25
	total	42.61	-18.02	40.52	-13.18	57.70	172.56	-57.21	7.47

TABLE XII: Same as Table V but for the $\Lambda_b \rightarrow pK^-$ decay.

with the coefficient $\kappa_c = p_c/(E_p + m_p) = \sqrt{(E_p - m_p)/(E_p + m_p)}$, and their associated CP asymmetries and averages,

$$\begin{aligned} A_{CP}^{\alpha} &= \frac{\alpha + \bar{\alpha}}{2}, & A_{CP}^{\beta} &= \frac{\beta + \bar{\beta}}{2}, & A_{CP}^{\gamma} &= \frac{\gamma - \bar{\gamma}}{2}, \\ \langle \alpha \rangle &= \frac{\alpha - \bar{\alpha}}{2}, & \langle \beta \rangle &= \frac{\beta - \bar{\beta}}{2}, & \langle \gamma \rangle &= \frac{\gamma + \bar{\gamma}}{2}. \end{aligned} \quad (63)$$

The numerical outcomes for the above observables are supplied in table X, among which the CP asymmetries A_{CP}^{β} are prominent for both the $\Lambda_b \rightarrow p\pi^-$, pK^- modes. However, the information on the Λ_b baryon and proton polarizations is needed to measure these parameters, which are experimentally inaccessible by now.

The proton and meson masses have been retained in the kinematic variables and hard kernels in the current analysis. To quantify the impact of these supposed higher-power contributions, we neglect the proton and pion masses, and recalculate the $\Lambda_b \rightarrow p\pi^-$ decay amplitudes. The resultant branching ratio 3.65×10^{-6} and direct CPV 0.09 in Table XIII evince that the light-hadron masses produce 15% and 50% effects, respectively, relative to the corresponding values in Table X. This test manifests the importance of power corrections in heavy baryon decays.

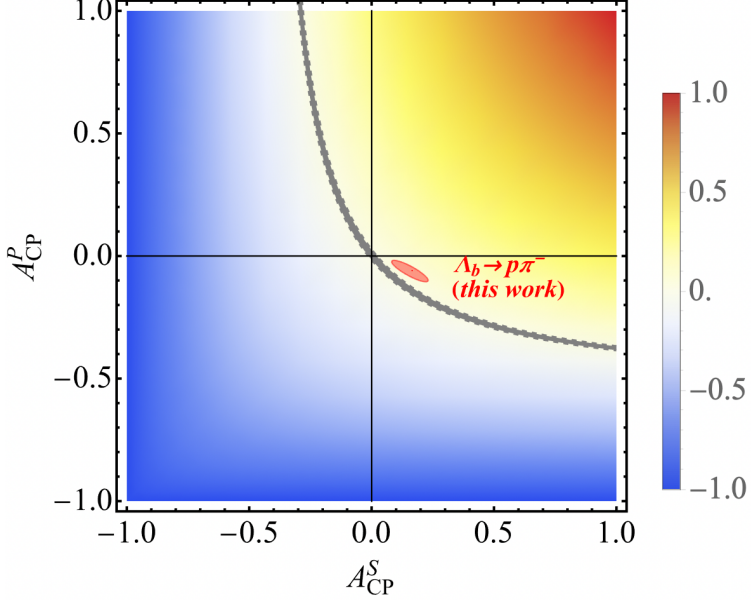


FIG. 9: Dependence of the net direct CPV on partial-wave CPVs, where the red spot corresponds to our prediction. The gray narrow band specifies the partial-wave CPVs allowed by the data of the direct CPV of $\Lambda_b \rightarrow p\pi^-$.

TABLE XIII: Same as table V but without the proton and meson masses in kinematics.

$\Lambda_b \rightarrow p\pi^-$	$ S $	$\phi(S)^\circ$	Real(S)	Imag(S)	$ P $	$\phi(P)^\circ$	Real(P)	Imag(P)
T_f	839.84	0.00	839.84	0.00	850.10	0.00	850.10	0.00
T_{nf}	62.83	-100.16	-11.08	-61.84	240.42	-97.09	-29.69	-238.58
$T_f + T_{nf}$	831.06	-4.27	828.75	-61.84	854.39	-16.21	820.41	-238.58
C'	35.65	162.64	-34.02	10.64	32.99	-176.98	-32.95	-1.74
E_2	84.36	-141.20	-65.75	-52.86	51.84	128.88	-32.54	40.35
B	17.54	104.24	-4.32	17.00	13.74	-124.50	-7.78	-11.32
Tree	729.88	-6.85	724.66	-87.06	776.44	-15.79	747.14	-211.29
$P_f^{C_1}$	67.66	0.00	67.66	0.00	2.61	0.00	2.61	0.00
$P_{nf}^{C_1}$	1.83	-109.17	-0.60	-1.73	9.87	-92.94	-0.51	-9.86
$P_f^{C_1} + P_{nf}^{C_1}$	67.08	-1.48	67.06	-1.73	10.08	-77.93	2.11	-9.86
P^{C_2}	17.24	-116.06	-7.57	-15.49	13.63	67.60	5.19	12.60
$P^{E_1^u}$	11.22	-90.55	-0.11	-11.22	7.06	112.49	-2.70	6.52
P^B	1.30	-42.87	0.96	-0.89	1.40	-170.77	-1.38	-0.22
$P^{E_1^d} + P^{E_2}$	4.68	-101.65	-0.95	-4.59	1.62	-12.75	1.58	-0.36
Penguin	68.39	-29.72	59.39	-33.91	9.92	61.02	4.81	8.68

B. Quasi-two-body $\Lambda_b \rightarrow pV$ decays

The $\Lambda_b \rightarrow pV$ decay amplitudes for longitudinally and transversely polarized vector mesons $V = \rho^-, K^{*-}$ are decomposed into

$$\begin{aligned}\mathcal{A}^L &= \bar{u}_p \left(A_1^L \gamma^\mu \gamma_5 + A_2^L \frac{p_p^\mu}{m_{\Lambda_b}} \gamma_5 + B_1^L \gamma^\mu + B_2^L \frac{p_p^\mu}{m_{\Lambda_b}} \right) u_{\Lambda_b} \epsilon_{L\mu}^*, \\ \mathcal{A}^T &= \bar{u}_p (A_1^T \gamma^\mu \gamma_5 + B_1^T \gamma^\mu) u_{\Lambda_b} \epsilon_{T\mu}^*,\end{aligned}\quad (64)$$

with the longitudinal (transverse) polarization vector $\epsilon_{L(T)}$. The polarization amplitudes $A_1^{L,T}, A_2^L, B_1^{L,T}$ and B_2^L form the partial-wave amplitudes

$$\begin{aligned}S^L &= -A_1^L, \\ S^T &= -A_1^T, \\ P_1 &= -\frac{p_c}{E_V} \left(\frac{m_{\Lambda_b} + m_p}{E_p + m_p} B_1^L + B_2^L \right), \\ P_2 &= \frac{p_c}{E_p + m_p} B_1^T, \\ D &= -\frac{p_c^2}{E_V(E_p + m_p)} (A_1^L - A_2^L),\end{aligned}\quad (65)$$

and the helicity amplitudes

$$\begin{aligned}H_{\frac{1}{2},1} &= -\sqrt{2} M_+ A_1^T - \sqrt{2} M_- B_1^T, \\ H_{-\frac{1}{2},-1} &= \sqrt{2} M_+ A_1^T - \sqrt{2} M_- B_1^T, \\ H_{\frac{1}{2},0} &= (M_+ (m_{\Lambda_b} - m_p) A_1^L - M_- p_c A_2^L + M_- (m_{\Lambda_b} + m_p) B_1^L + M_+ p_c B_2^L) / m_V, \\ H_{-\frac{1}{2},0} &= (-M_+ (m_{\Lambda_b} - m_p) A_1^L + M_- p_c A_2^L + M_- (m_{\Lambda_b} + m_p) B_1^L + M_+ p_c B_2^L) / m_V,\end{aligned}\quad (66)$$

with the vector meson energy E_V .

Given the numerical results in Appendix C for the above amplitudes, the $\Lambda_b \rightarrow pV$ decay width is derived via

$$\begin{aligned}\Gamma &= \frac{p_c}{4\pi} \frac{E_p + m_p}{m_{\Lambda_b}} \left\{ 2(|S^T|^2 + |P_2|^2) + \frac{E_V^2}{m_V^2} (|S^L + D|^2 + |P_1|^2) \right\} \\ &= \frac{p_c}{16\pi m_{\Lambda_b}^2} (|H_{1/2,1}|^2 + |H_{-1/2,-1}|^2 + |H_{1/2,0}|^2 + |H_{-1/2,0}|^2).\end{aligned}\quad (67)$$

The associated partial-wave CPVs are defined as in Eq. (58), in terms of which the direct CPV is decomposed [17],

$$A_{CP}^{dir} \approx \kappa_{ST} A_{CP}^{ST} + \kappa_{P_1} A_{CP}^{P_1} + \kappa_{P_2} A_{CP}^{P_2} + \kappa_{D+S^L} A_{CP}^{D+S^L}, \quad (68)$$

with the weights

$$\begin{aligned}\kappa_{ST} &= \frac{2|S^T|^2}{\Pi}, \quad \kappa_{P_1} = \frac{E_V^2 |P_1|^2}{m_V^2 \Pi}, \\ \kappa_{P_2} &= \frac{2|P_2|^2}{\Pi}, \quad \kappa_{D+S^L} = \frac{E_V^2 |D + S^L|^2}{m_V^2 \Pi}, \\ \Pi &\equiv 2|S^T|^2 + 2|P_2|^2 + E_V^2 |D + S^L|^2 + E_V^2 |P_1|^2.\end{aligned}\quad (69)$$

TABLE XIV: Same as Table X but for the $\Lambda_b \rightarrow p\rho^-, pK^{*-}$ decays.

	$Br(\times 10^{-6})$	A_{CP}^{dir}	$A_{CP}^{ST}(\kappa_{ST})$
$\Lambda_b \rightarrow p\rho^-$	$9.66^{+6.23+3.23+0.21+1.89}_{-3.50-3.03-1.20-0.75}$	$0.03^{+0.02+0.01+0.00+0.02}_{-0.02-0.03-0.03-0.02}$	$0.01^{+0.00+0.00+0.00+0.00+0.00}_{-0.01-0.02-0.02-0.02}(7\%)$
$\Lambda_b \rightarrow pK^{*-}$	$2.83^{+1.77+0.46+0.37+0.63}_{-1.29-1.23-0.53-0.66}$	$-0.05^{+0.04+0.07+0.01+0.05}_{-0.11-0.07-0.06-0.08}$	$-0.15^{+0.06+0.09+0.02+0.05}_{-0.00-0.04-0.05-0.00}(6\%)$
	$A_{CP}^{S^L+D}(\kappa_{SL+D})$	$A_{CP}^{P_1}(\kappa_{P_1})$	$A_{CP}^{P_2}(\kappa_{P_2})$
$\Lambda_b \rightarrow p\rho^-$	$0.02^{+0.03+0.04+0.02+0.05}_{-0.02-0.02-0.00-0.00}(44\%)$	$0.03^{+0.04+0.00+0.00+0.00}_{-0.05-0.04-0.10-0.05}(45\%)$	$0.17^{+0.00+0.00+0.01+0.03}_{-0.02-0.03-0.03-0.04}(4\%)$
$\Lambda_b \rightarrow pK^{*-}$	$0.27^{+0.02+0.06+0.05+0.03}_{-0.17-0.11-0.02-0.18}(33\%)$	$-0.23^{+0.05+0.07+0.02+0.05}_{-0.11-0.11-0.09-0.03}(55\%)$	$-0.14^{+0.01+0.00+0.02+0.01}_{-0.04-0.09-0.02-0.03}(6\%)$
	α	A_{CP}^α	$\langle \alpha \rangle$
$\Lambda_b \rightarrow p\rho^-$	$-0.83^{+0.02+0.01+0.00+0.00}_{-0.02-0.05-0.04-0.01}$	$-0.01^{+0.01+0.01+0.01+0.00}_{-0.00-0.00-0.01-0.00}$	$-0.83^{+0.01+0.01+0.01+0.00}_{-0.02-0.05-0.04-0.01}$
$\Lambda_b \rightarrow pK^{*-}$	$-1.00^{+0.01+0.01+0.00+0.01}_{-0.00-0.00-0.00-0.00}$	$-0.00^{+0.00+0.00+0.00+0.00}_{-0.00-0.00-0.00-0.00}$	$-1.00^{+0.00+0.01+0.00+0.00}_{-0.00-0.00-0.00-0.00}$
	β	A_{CP}^β	$\langle \beta \rangle$
$\Lambda_b \rightarrow p\rho^-$	$-0.98^{+0.05+0.07+0.05+0.06}_{-0.00-0.00-0.00-0.00}$	$0.00^{+0.01+0.02+0.01+0.02}_{-0.00-0.00-0.00-0.00}$	$-0.99^{+0.04+0.05+0.04+0.04}_{-0.00-0.00-0.00-0.00}$
$\Lambda_b \rightarrow pK^{*-}$	$-0.90^{+0.07+0.17+0.11+0.00}_{-0.03-0.03-0.00-0.03}$	$-0.02^{+0.04+0.06+0.04+0.01}_{-0.00-0.04-0.00-0.00}$	$-0.88^{+0.06+0.11+0.08+0.00}_{-0.03-0.06-0.00-0.04}$
	γ	A_{CP}^γ	$\langle \gamma \rangle$
$\Lambda_b \rightarrow p\rho^-$	$-0.11^{+0.01+0.01+0.01+0.01}_{-0.01-0.01-0.02-0.00}$	$-0.01^{+0.00+0.00+0.00+0.00}_{-0.00-0.00-0.00-0.00}$	$-0.10^{+0.01+0.01+0.01+0.00}_{-0.01-0.01-0.02-0.00}$
$\Lambda_b \rightarrow pK^{*-}$	$-0.12^{+0.01+0.00+0.02+0.00}_{-0.06-0.05-0.03-0.05}$	$0.02^{+0.01+0.03+0.01+0.01}_{-0.02-0.02-0.01-0.01}$	$-0.14^{+0.01+0.01+0.02+0.00}_{-0.04-0.07-0.04-0.04}$
	Λ	A_{CP}^Λ	$\langle \Lambda \rangle$
$\Lambda_b \rightarrow p\rho^-$	$-0.96^{+0.05+0.06+0.04+0.05}_{-0.00-0.00-0.00-0.00}$	$0.00^{+0.01+0.02+0.01+0.02}_{-0.00-0.00-0.00-0.00}$	$-0.97^{+0.04+0.04+0.03+0.04}_{-0.00-0.00-0.00-0.00}$
$\Lambda_b \rightarrow pK^{*-}$	$-0.91^{+0.06+0.15+0.09+0.00}_{-0.02-0.02-0.00-0.03}$	$-0.01^{+0.03+0.06+0.03+0.01}_{-0.00-0.03-0.00-0.00}$	$-0.90^{+0.05+0.09+0.07+0.00}_{-0.03-0.05-0.01-0.03}$
	\mathcal{J}	$A_{CP}^{\mathcal{J}}$	$\langle \mathcal{J} \rangle$
$\Lambda_b \rightarrow p\rho^-$	$1.66^{+0.04+0.04+0.02+0.02}_{-0.03-0.03-0.05-0.00}$	$-0.01^{+0.01+0.01+0.01+0.00}_{-0.01-0.01-0.01-0.00}$	$1.67^{+0.03+0.04+0.02+0.02}_{-0.05-0.03-0.05-0.00}$
$\Lambda_b \rightarrow pK^{*-}$	$1.67^{+0.02+0.00+0.04+0.00}_{-0.14-0.12-0.08-0.12}$	$0.04^{+0.02+0.05+0.02+0.01}_{-0.06-0.04-0.02-0.03}$	$1.63^{+0.01+0.03+0.04+0.00}_{-0.08-0.15-0.09-0.09}$

The predictions for the branching ratios and CPVs of the $\Lambda_b \rightarrow p\rho^-, pK^{*-}$ decays are collected in Table XIV. Unlike $\Lambda_b \rightarrow p\pi^-, pK^-$, whose branching ratios are of the same order, the $\Lambda_b \rightarrow p\rho^-$ branching ratio is greater than the pK^{*-} one by a factor of 3. The operators $O_{5,6,7,8}$ do not contribute to the factorizable penguin topologies as shown in Eq. (36). Hence, the enhancement of the penguin amplitudes by the chiral factor in Eq. (50) is absent in the $\Lambda_b \rightarrow pK^{*-}$ decay.

It is found that the $D + S^L$ and P_1 components dominate the direct CPVs because of the enhancement factor E_V/m_V . The partial-wave CPVs of the $\Lambda_b \rightarrow pV$ decays also exceed 10%; the P_2 -wave CPVs of $\Lambda_b \rightarrow p\rho^-$ reaches 17%; the $(D + S^L)$ -wave CPV of $\Lambda_b \rightarrow pK^{*-}$ is even as large as 27%. However, the direct CPVs of these modes are all minor for the similar reasons. The relative sign of the partial-wave amplitudes in the $\Lambda_b \rightarrow pK^{*-}$ decay can be argued in the same manner. Their tiny direct CPVs trace back to the destruction between the major $(D + S^L)$ - and P_1 -wave CPVs, like the $\Lambda_b \rightarrow p\pi^-$ case. For the $\Lambda_b \rightarrow p\rho^-$ decay, the two dominant partial-wave CPVs are small, leading to a negligible direct CPV.

The decay asymmetry parameters are expressed, in terms of the helicity amplitudes, as

$$\begin{aligned} \alpha &= \frac{|H_{1/2,1}|^2 - |H_{-1/2,-1}|^2}{|H_{1/2,1}|^2 + |H_{-1/2,-1}|^2}, \quad \beta = \frac{|H_{1/2,0}|^2 - |H_{-1/2,0}|^2}{|H_{1/2,0}|^2 + |H_{-1/2,0}|^2}, \quad \gamma = \frac{|H_{1/2,1}|^2 - |H_{-1/2,-1}|^2}{|H_{1/2,0}|^2 + |H_{-1/2,0}|^2}, \\ \Lambda &= \frac{|H_{1/2,1}|^2 - |H_{-1/2,-1}|^2 + |H_{1/2,0}|^2 - |H_{-1/2,0}|^2}{|H_{1/2,1}|^2 + |H_{-1/2,-1}|^2 + |H_{1/2,0}|^2 + |H_{-1/2,0}|^2}, \end{aligned} \quad (70)$$

which satisfy $\Lambda = (\beta + \alpha\gamma)/(1 + \gamma)$. The associated CPVs and averages are defined as in Eq. (63)

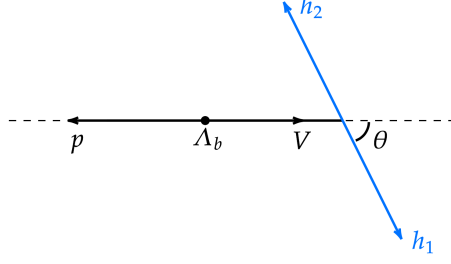


FIG. 10: Configuration of the $\Lambda_b \rightarrow pV \rightarrow ph_1h_2$ decay, where θ is the angle between h_1 in the V rest frame and the V momentum in the Λ_b rest frame.

and by

$$A_{CP}^{\Lambda} = \frac{\Lambda + \bar{\Lambda}}{2}, \quad \langle \Lambda \rangle = \frac{\Lambda - \bar{\Lambda}}{2}. \quad (71)$$

The results for the above quantities in Table XIV clearly imply that the CPVs of the decay asymmetry parameters are all consistent with zero.

Since a vector meson decays strongly with a finite width, what we worked on are actually the three-body decays $\Lambda_b \rightarrow p(\rho^- \rightarrow \pi^-\pi^0), p(K^{*-} \rightarrow K^-\pi^0)$. Motivated by the sizable partial-wave CPVs, we investigate the potential observables for identifying CPVs involved in the angle distributions for three-body decays. The angle distribution of $\Lambda_b \rightarrow pV \rightarrow ph_1h_2$ in Fig. 10 is formulated as

$$\begin{aligned} \frac{d\Gamma}{d\cos\theta} &\propto |H_{\frac{1}{2},0}|^2 + |H_{-\frac{1}{2},0}|^2 + |H_{-\frac{1}{2},-1}|^2 + |H_{\frac{1}{2},1}|^2 \\ &\quad + (2|H_{\frac{1}{2},0}|^2 + 2|H_{-\frac{1}{2},0}|^2 - |H_{-\frac{1}{2},-1}|^2 - |H_{\frac{1}{2},1}|^2)P_2 \\ &\propto 1 + \mathcal{J} \cdot P_2, \end{aligned} \quad (72)$$

where the observable

$$\mathcal{J} \equiv \frac{2|H_{\frac{1}{2},0}|^2 + 2|H_{-\frac{1}{2},0}|^2 - |H_{-\frac{1}{2},-1}|^2 - |H_{\frac{1}{2},1}|^2}{|H_{\frac{1}{2},0}|^2 + |H_{-\frac{1}{2},0}|^2 + |H_{-\frac{1}{2},-1}|^2 + |H_{\frac{1}{2},1}|^2}, \quad (73)$$

with the Legendre polynomial $P_2 = (3\cos^2\theta - 1)/2$ can be extracted from data fitting. The CPV and average for \mathcal{J} are written as

$$A_{CP}^{\mathcal{J}} = \frac{\mathcal{J} - \bar{\mathcal{J}}}{2}, \quad \langle \mathcal{J} \rangle = \frac{\mathcal{J} + \bar{\mathcal{J}}}{2}, \quad (74)$$

whose predictions are listed in Table XIV. Unfortunately, the CPVs $A_{CP}^{\mathcal{J}}$ in the $\Lambda_b \rightarrow p\rho^-, pK^{*-}$ decays are too tiny to search for experimentally.

C. Quasi-two-body $\Lambda_b \rightarrow pA$ decays

The decays $\Lambda_b \rightarrow pA$, with A denoting the axial-vector mesons $a_1^-(1260)$, $K_1^-(1270)$, $K_1^-(1400)$, share the same amplitude parametrization and observables as $\Lambda_b \rightarrow pV$ in the previous subsection.

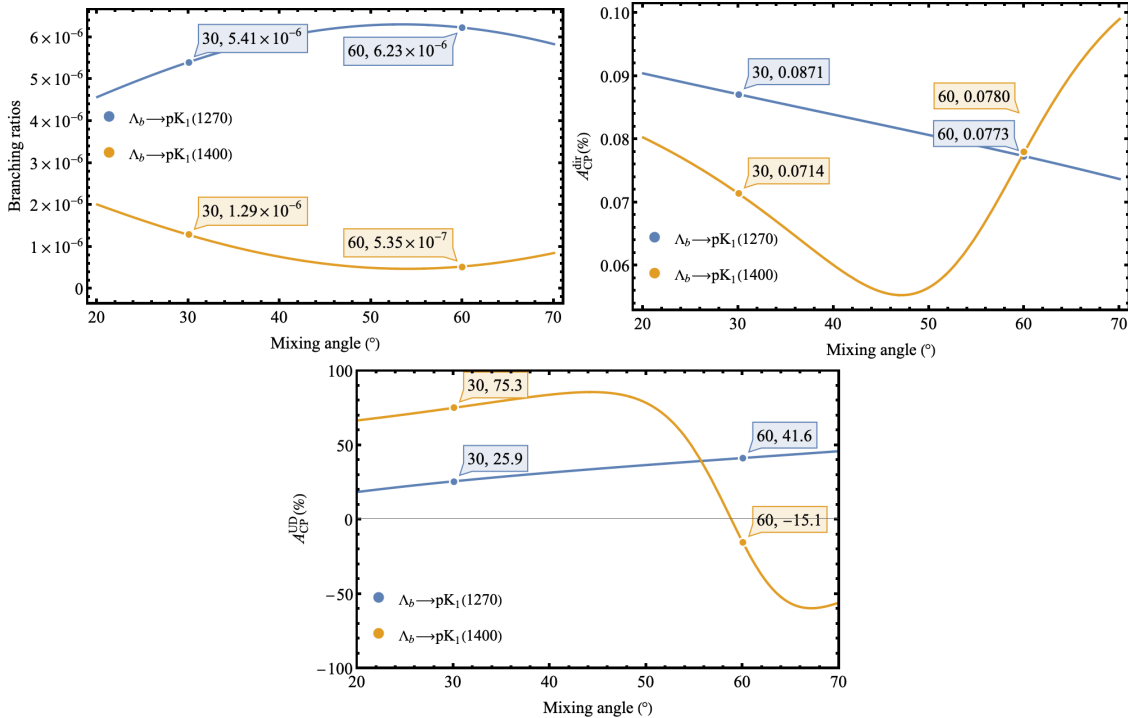


FIG. 11: (upper-left) Dependencies of the $\Lambda_b \rightarrow pK_1$ branching ratios on the mixing angle θ_K ; (upper-right) same as the up-left panel but for the direct CPVs; (bottom) same as the up-left panel but for the CPVs in the up-down asymmetry.

Because the $K_1(1270)$ - $K_1(1400)$ mixing angle θ_K is not yet well determined [67], we take the typical values $\theta_K = 30^\circ$ and 60° for illustration. It is seen that most of our predictions in Table XV are insensitive to θ_K . The predicted $\Lambda_b \rightarrow pa_1^-$ (1260) and $\Lambda_b \rightarrow pK_1^-$ (1270, 1400) branching ratios are of the order 10^{-6} , which can be verified experimentally. The partial-wave CPVs of the $\Lambda_b \rightarrow pa_1^-$ (1260), pK_1^- (1270), pK_1^- (1400) decays are significant, exceeding 50%. The opposite signs between the partial-wave CPVs turn in the minor direct CPV of $\Lambda_b \rightarrow pa_1^-$ (1260). The direct CPVs of $\Lambda_b \rightarrow pK_1(1270)^-, pK_1(1400)^-$ can deviate from zero, both of which are above $\pm 5\%$ in the range $20^\circ \sim 70^\circ$ of the mixing angle as plotted in Fig. 11.

The $\Lambda_b \rightarrow pa_1^-$ (1260), pK_1^- (1270), pK_1^- (1400) modes are actually the four-body decays, for a_1^- (1260) and K_1^- (1270, 1400) decay into $\pi^-\pi^+\pi^-$ and $K^-\pi^+\pi^-$, respectively. We propose the promising observables associated with the angle distributions of the final states in these multi-body Λ_b decays, which can be measured in the future. The angular distribution for the $\Lambda_b \rightarrow pA \rightarrow ph_1h_2h_3$ decay in Fig. 12 is given by [18]

$$\frac{d\Gamma}{d \cos \theta} \propto \frac{\left(|H_{1/2,1}|^2 + |H_{-1/2,-1}|^2\right) \frac{1+\cos^2 \theta}{2} + \left(|H_{1/2,0}|^2 + |H_{-1/2,0}|^2\right) \sin^2 \theta}{|H_{\frac{1}{2},0}|^2 + |H_{-\frac{1}{2},0}|^2 + |H_{-\frac{1}{2},-1}|^2 + |H_{\frac{1}{2},1}|^2} \\ + \frac{R \left(|H_{1/2,1}|^2 - |H_{-1/2,-1}|^2\right) \cos \theta}{|H_{\frac{1}{2},0}|^2 + |H_{-\frac{1}{2},0}|^2 + |H_{-\frac{1}{2},-1}|^2 + |H_{\frac{1}{2},1}|^2}, \quad (75)$$

with θ being the angle between the normal of the $A \rightarrow h_1h_2h_3$ decay plane and the A meson momentum in the Λ_b rest frame, i.e., $\cos \theta = \vec{n} \cdot \vec{p}_A = (\vec{p}_1 \times \vec{p}_2) \cdot \vec{p}_A$. The nonperturbative factor R parametrizes the effect and kinematics of the strong decay $A \rightarrow h_1h_2h_3$ [74], which will be

TABLE XV: Same as Table X but for the $\Lambda_b \rightarrow pA$ decays.

	$Br(\times 10^{-6})$	A_{CP}^{dir}	$A_{CP}^{ST}(\kappa_{ST})$
$\Lambda_b \rightarrow pa_1^-(1260)$	$11.06^{+8.21+3.88+0.91+1.73}_{-4.30-3.32-0.46-0.06}$	$-0.01^{+0.01+0.03+0.02+0.03}_{-0.00-0.01-0.02-0.00}$	$-0.22^{+0.04+0.07+0.05+0.04}_{-0.03-0.07-0.07-0.01}(6\%)$
$\Lambda_b \rightarrow pK_1^-(1270)(30^\circ)$	$5.48^{+3.63+1.94+0.27+2.49}_{-1.87-1.55-0.31-1.11}$	$0.09^{+0.03+0.07+0.03+0.01}_{-0.04-0.02-0.02-0.00}$	$0.34^{+0.00+0.01+0.01+0.00}_{-0.02-0.03-0.01-0.05}(8\%)$
$\Lambda_b \rightarrow pK_1^-(1400)(30^\circ)$	$1.25^{+0.59+0.33+0.13+0.64}_{-0.39-0.19-0.19-0.31}$	$0.06^{+0.03+0.05+0.03+0.00}_{-0.03-0.09-0.04-0.01}$	$0.71^{+0.05+0.06+0.03+0.03}_{-0.02-0.16-0.04-0.13}(13\%)$
$\Lambda_b \rightarrow pK_1^-(1270)(60^\circ)$	$6.28^{+3.97+1.93+0.18+2.79}_{-2.13-1.51-0.41-1.32}$	$0.07^{+0.01+0.03+0.03+0.01}_{-0.04-0.04-0.03-0.00}$	$0.46^{+0.00+0.00+0.02+0.01}_{-0.02-0.04-0.02-0.07}(9\%)$
$\Lambda_b \rightarrow pK_1^-(1400)(60^\circ)$	$0.53^{+0.33+0.38+0.09+0.36}_{-0.16-0.19-0.22-0.13}$	$0.08^{+0.11+0.09+0.12+0.00}_{-0.08-0.11-0.04-0.03}$	$0.07^{+0.00+0.41+0.08+0.22}_{-0.12-0.09-0.15-0.10}(3\%)$
	$A_{CP}^{S^L+D}(\kappa_{S^L+D})$	$A_{CP}^{P_1}(\kappa_{P_1})$	$A_{CP}^{P_2}(\kappa_{P_2})$
$\Lambda_b \rightarrow pa_1^-(1260)$	$-0.11^{+0.02+0.01+0.02+0.02}_{-0.00-0.01-0.07-0.03}(46\%)$	$0.18^{+0.03+0.02+0.04+0.09}_{-0.03-0.02-0.03-0.04}(40\%)$	$-0.24^{+0.01+0.05+0.04+0.03}_{-0.02-0.09-0.06-0.06}(8\%)$
$\Lambda_b \rightarrow pK_1^-(1270)(30^\circ)$	$-0.11^{+0.01+0.08+0.08+0.03}_{-0.04-0.06-0.03-0.00}(42\%)$	$0.19^{+0.10+0.13+0.05+0.02}_{-0.06-0.09-0.11-0.01}(42\%)$	$0.33^{+0.00+0.04+0.02+0.00}_{-0.02-0.03-0.02-0.03}(8\%)$
$\Lambda_b \rightarrow pK_1^-(1400)(30^\circ)$	$0.81^{+0.09+0.17+0.07+0.04}_{-0.12-0.14-0.11-0.00}(17\%)$	$-0.41^{+0.04+0.05+0.08+0.03}_{-0.07-0.05-0.11-0.04}(60\%)$	$0.78^{+0.04+0.11+0.09+0.05}_{-0.06-0.20-0.04-0.10}(10\%)$
$\Lambda_b \rightarrow pK_1^-(1270)(60^\circ)$	$0.06^{+0.01+0.08+0.07+0.03}_{-0.03-0.07-0.04-0.00}(37\%)$	$-0.07^{+0.05+0.06+0.04+0.01}_{-0.06-0.05-0.05-0.02}(45\%)$	$0.46^{+0.00+0.04+0.04+0.02}_{-0.01-0.03-0.02-0.06}(9\%)$
$\Lambda_b \rightarrow pK_1^-(1400)(60^\circ)$	$-0.82^{+0.14+0.19+0.12+0.21}_{-0.07-0.09-0.07-0.02}(30\%)$	$0.52^{+0.06+0.12+0.37+0.00}_{-0.01-0.14-0.03-0.07}(64\%)$	$-0.28^{+0.27+0.04+0.03+0.03}_{-0.07-0.36-0.25-0.16}(3\%)$
	α	A_{CP}^α	$\langle \alpha \rangle$
$\Lambda_b \rightarrow pa_1^-(1260)$	$-0.86^{+0.01+0.02+0.03+0.00}_{-0.03-0.05-0.05-0.03}$	$0.02^{+0.00+0.01+0.01+0.00}_{-0.00-0.01-0.00-0.00}$	$-0.88^{+0.01+0.02+0.04+0.00}_{-0.03-0.04-0.05-0.02}$
$\Lambda_b \rightarrow pK_1^-(1270)(30^\circ)$	$-1.00^{+0.00+0.00+0.00+0.00}_{-0.00-0.00-0.00-0.00}$	$0.00^{+0.00+0.00+0.00+0.00}_{-0.00-0.00-0.00-0.00}$	$-1.00^{+0.00+0.00+0.00+0.00}_{-0.00-0.00-0.00-0.00}$
$\Lambda_b \rightarrow pK_1^-(1400)(30^\circ)$	$-1.00^{+0.00+0.01+0.01+0.00}_{-0.00-0.00-0.00-0.00}$	$-0.01^{+0.01+0.01+0.01+0.00}_{-0.00-0.04-0.06-0.02}$	$-0.98^{+0.01+0.05+0.07+0.02}_{-0.01-0.01-0.01-0.00}$
$\Lambda_b \rightarrow pK_1^-(1270)(60^\circ)$	$-1.00^{+0.00+0.00+0.00+0.00}_{-0.00-0.00-0.00-0.00}$	$0.00^{+0.00+0.00+0.00+0.00}_{-0.00-0.00-0.00-0.00}$	$-1.00^{+0.00+0.00+0.01+0.00}_{-0.00-0.00-0.00-0.00}$
$\Lambda_b \rightarrow pK_1^-(1400)(60^\circ)$	$-0.96^{+0.01+0.10+0.10+0.04}_{-0.03-0.03-0.03-0.00}$	$-0.00^{+0.01+0.01+0.02+0.00}_{-0.00-0.02-0.01-0.01}$	$-0.96^{+0.00+0.09+0.08+0.05}_{-0.04-0.03-0.03-0.00}$
	β	A_{CP}^β	$\langle \beta \rangle$
$\Lambda_b \rightarrow pa_1^-(1260)$	$-0.98^{+0.01+0.02+0.01+0.03}_{-0.01-0.02-0.01-0.00}$	$-0.01^{+0.01+0.01+0.01+0.01}_{-0.01-0.01-0.01-0.00}$	$-0.97^{+0.01+0.01+0.02+0.02}_{-0.01-0.01-0.02-0.01}$
$\Lambda_b \rightarrow pK_1^-(1270)(30^\circ)$	$-0.99^{+0.00+0.03+0.03+0.00}_{-0.00-0.01-0.00-0.01}$	$0.00^{+0.00+0.02+0.00+0.00}_{-0.01-0.02-0.00-0.01}$	$-0.98^{+0.01+0.02+0.03+0.00}_{-0.00-0.00-0.00-0.00}$
$\Lambda_b \rightarrow pK_1^-(1400)(30^\circ)$	$-0.15^{+0.28+0.17+0.13+0.25}_{-0.10-0.10-0.16-0.09}$	$0.07^{+0.04+0.07+0.08+0.03}_{-0.01-0.02-0.04-0.03}$	$-0.22^{+0.24+0.17+0.10+0.22}_{-0.10-0.11-0.15-0.06}$
$\Lambda_b \rightarrow pK_1^-(1270)(60^\circ)$	$-0.95^{+0.04+0.06+0.04+0.01}_{-0.03-0.03-0.02-0.01}$	$0.00^{+0.00+0.01+0.01+0.00}_{-0.01-0.01-0.01-0.00}$	$-0.95^{+0.04+0.05+0.04+0.02}_{-0.02-0.03-0.01-0.01}$
$\Lambda_b \rightarrow pK_1^-(1400)(60^\circ)$	$-0.01^{+0.01+0.07+0.10+0.09}_{-0.06-0.17-0.28-0.18}$	$-0.26^{+0.09+0.09+0.03+0.03}_{-0.01-0.05-0.12-0.09}$	$0.25^{+0.12+0.07+0.11+0.06}_{-0.15-0.16-0.18-0.09}$
	γ	A_{CP}^γ	$\langle \gamma \rangle$
$\Lambda_b \rightarrow pa_1^-(1260)$	$-0.10^{+0.01+0.01+0.02+0.00}_{-0.01-0.02-0.02-0.01}$	$0.04^{+0.01+0.02+0.01+0.01}_{-0.01-0.01-0.00-0.00}$	$-0.14^{+0.01+0.01+0.02+0.00}_{-0.02-0.03-0.01-0.01}$
$\Lambda_b \rightarrow pK_1^-(1270)(30^\circ)$	$-0.24^{+0.04+0.03+0.02+0.01}_{-0.03-0.03-0.02-0.04}$	$-0.06^{+0.01+0.02+0.01+0.00}_{-0.01-0.01-0.01-0.00}$	$-0.18^{+0.03+0.02+0.01+0.00}_{-0.02-0.02-0.01-0.04}$
$\Lambda_b \rightarrow pK_1^-(1400)(30^\circ)$	$-0.61^{+0.15+0.23+0.13+0.00}_{-0.16-0.26-0.19-0.09}$	$-0.27^{+0.06+0.09+0.06+0.00}_{-0.07-0.08-0.09-0.05}$	$-0.34^{+0.08+0.14+0.07+0.00}_{-0.09-0.19-0.11-0.04}$
$\Lambda_b \rightarrow pK_1^-(1270)(60^\circ)$	$-0.32^{+0.06+0.06+0.02+0.00}_{-0.04-0.06-0.03-0.06}$	$-0.10^{+0.02+0.03+0.01+0.00}_{-0.02-0.01-0.01-0.01}$	$-0.22^{+0.04+0.04+0.01+0.00}_{-0.02-0.05-0.02-0.05}$
$\Lambda_b \rightarrow pK_1^-(1400)(60^\circ)$	$-0.05^{+0.02+0.02+0.01+0.02}_{-0.01-0.06-0.03-0.01}$	$0.01^{+0.01+0.03+0.03+0.00}_{-0.01-0.01-0.00-0.01}$	$-0.06^{+0.01+0.01+0.01+0.02}_{-0.01-0.08-0.06-0.01}$
	Λ	A_{CP}^Λ	$\langle \Lambda \rangle$
$\Lambda_b \rightarrow pa_1^-(1260)$	$-0.97^{+0.00+0.02+0.01+0.03}_{-0.01-0.02-0.01-0.00}$	$-0.01^{+0.01+0.01+0.01+0.01}_{-0.01-0.01-0.01-0.00}$	$-0.96^{+0.01+0.01+0.02+0.02}_{-0.01-0.01-0.02-0.01}$
$\Lambda_b \rightarrow pK_1^-(1270)(30^\circ)$	$-0.99^{+0.00+0.02+0.03+0.00}_{-0.00-0.01-0.00-0.01}$	$0.00^{+0.00+0.02+0.00+0.00}_{-0.01-0.02-0.00-0.01}$	$-0.99^{+0.01+0.01+0.02+0.00}_{-0.00-0.00-0.00-0.00}$
$\Lambda_b \rightarrow pK_1^-(1400)(30^\circ)$	$-0.47^{+0.14+0.16+0.06+0.14}_{-0.02-0.11-0.14-0.08}$	$-0.07^{+0.06+0.08+0.05+0.00}_{-0.02-0.04-0.04-0.03}$	$-0.40^{+0.17+0.09+0.08+0.15}_{-0.06-0.11-0.13-0.05}$
$\Lambda_b \rightarrow pK_1^-(1270)(60^\circ)$	$-0.96^{+0.03+0.05+0.03+0.01}_{-0.03-0.02-0.02-0.01}$	$0.00^{+0.00+0.01+0.00+0.00}_{-0.01-0.00-0.01-0.00}$	$-0.96^{+0.03+0.04+0.04+0.01}_{-0.02-0.02-0.01-0.01}$
$\Lambda_b \rightarrow pK_1^-(1400)(60^\circ)$	$-0.06^{+0.10+0.08+0.10+0.11}_{-0.07-0.17-0.29-0.18}$	$-0.23^{+0.09+0.08+0.03+0.02}_{-0.01-0.01-0.08-0.08}$	$0.18^{+0.11+0.07+0.11+0.09}_{-0.14-0.17-0.22-0.10}$
	a_{UD}	A_{CP}^{UD}	
$\Lambda_b \rightarrow pa_1^-(1260)$	$-0.09^{+0.00+0.01+0.02+0.00}_{-0.01-0.01-0.01-0.01}$	$-0.24^{+0.03+0.05+0.05+0.03}_{-0.03-0.09-0.06-0.06}$	
$\Lambda_b \rightarrow pK_1^-(1270)(30^\circ)$	$-0.19^{+0.03+0.02+0.01+0.01}_{-0.02-0.02-0.01-0.02}$	$0.26^{+0.02+0.03+0.01+0.00}_{-0.03-0.08-0.04-0.04}$	
$\Lambda_b \rightarrow pK_1^-(1400)(30^\circ)$	$-0.38^{+0.06+0.10+0.05+0.00}_{-0.06-0.09-0.07-0.03}$	$0.72^{+0.05+0.13+0.07+0.05}_{-0.05-0.23-0.03-0.12}$	
$\Lambda_b \rightarrow pK_1^-(1270)(60^\circ)$	$-0.24^{+0.04+0.04+0.01+0.00}_{-0.02-0.03-0.02-0.03}$	$0.40^{+0.02+0.03+0.02+0.01}_{-0.01-0.04-0.03-0.07}$	
$\Lambda_b \rightarrow pK_1^-(1400)(60^\circ)$	$-0.04^{+0.02+0.02+0.01+0.02}_{-0.01-0.05-0.03-0.01}$	$-0.19^{+0.12+0.14+0.00+0.06}_{-0.18-0.19-0.20-0.00}$	

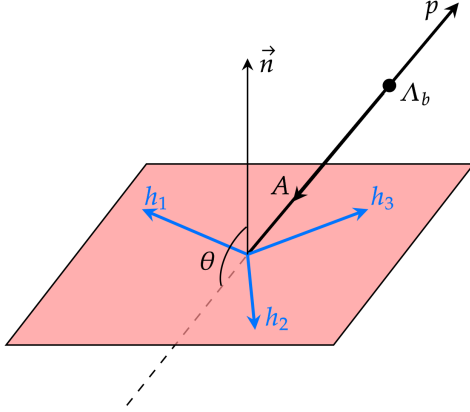


FIG. 12: Configuration of the $\Lambda_b \rightarrow pA \rightarrow ph_1h_2h_3$ decay, where θ is the angle between the normal of the $A \rightarrow h_1h_2h_3$ decay plane and the A meson momentum in the Λ_b rest frame.

canceled in the proposed CPV observable below. The up-down asymmetry is then constructed,

$$\begin{aligned} A_{UD} &= \frac{\Gamma(\cos \theta > 0) - \Gamma(\cos \theta < 0)}{\Gamma(\cos \theta > 0) + \Gamma(\cos \theta < 0)} \\ &= \frac{R (|H_{1/2,1}|^2 - |H_{-1/2,-1}|^2)}{(|H_{1/2,1}|^2 + |H_{-1/2,-1}|^2 + |H_{1/2,0}|^2 + |H_{-1/2,0}|^2)} \\ &\equiv R \cdot a_{UD}, \end{aligned} \quad (76)$$

which defines the R -independent CPV

$$A_{CP}^{UD} = \frac{A_{UD} + \bar{A}_{UD}}{A_{UD} - \bar{A}_{UD}}, \quad (77)$$

with $a_{UD} = \text{Re}(S^T P_2^*)$ and \bar{A}_{UD} representing the charge conjugate of A_{UD} .

The numerical outcomes for a_{UD} and A_{CP}^{UD} are gathered in Table XV and their dependencies on the mixing angle are displayed in Fig. 11, where A_{CP}^{UD} of the $\Lambda_b \rightarrow pK_1(1270)$ decay is more stable against the variation of the mixing angle. We highlight that A_{CP}^{UD} exceed 20% in the $\Lambda_b \rightarrow pA$ decays owing to the large strong phase difference between the S - and P -wave amplitudes. Therefore, A_{CP}^{UD} with controllable uncertainties serve as ideal observables for establishing CPVs in Λ_b baryon decays experimentally. The measurements of A_{CP}^{UD} are based on the four-body decays $\Lambda_b \rightarrow p\pi^+\pi^-\pi^-$ and $pK^-\pi^+\pi^-$ for $p\alpha_1(1260)$ and $pK_1(1270)$, respectively, both of which have abundant data at the LHCb.

The LHCb has announced the direct CPVs of the above modes from the Run 1 data corresponding to the integrated luminosity 3 fb^{-1} at the center-of-mass energies $\sqrt{s} = 7$ and 8 TeV [12]. The sum of particle and anti-particle channels gives the signal yields of $\Lambda_b \rightarrow p\alpha_1$ and pK_1 around 800 and 1000, respectively. The yields would be enhanced by four times with the Run 2 data from twice the integrated luminosity of 6 fb^{-1} and twice the cross section at a higher collision energy of $\sqrt{s} = 13 \text{ TeV}$. More b quarks and associated b -hadrons are produced at higher energies. As reported by the LHCb [75], the b -quark production cross sections are measured to be $72.0 \pm 0.3 \pm 6.8 \mu\text{b}$ at $\sqrt{s} = 7 \text{ TeV}$ and $144 \pm 1 \pm 21 \mu\text{b}$ at $\sqrt{s} = 13 \text{ TeV}$, respectively, showing an increase by a factor of two from Run 1 to Run 2. The number of signal events in Run 2 is thus expected to be four times greater than those in Run 1, with a factor of two from luminosities and another factor of two from

cross sections. Using the combined data of Run 1 and Run 2, we would get the signal yields five times higher relative to Run 1, which amount to 4000 and 5000 events for $\Lambda_b \rightarrow pa_1$ and pK_1 , respectively.

The trigger efficiencies for Run 3 are higher than those for Run 2, especially in the low p_T region, as indicated in Fig. 13. The red points mark the efficiencies for Run 3 in 2024, and the blue points mark those for Run 2. The gray bars display the Monte-Carlo candidates in acceptance. The number of signal events can be deduced by convoluting the gray bars with the red or blue points. The signal events in Run 3 are then found to be roughly twice as many as those in Run 2. This figure depicts the trigger efficiencies for hadronic B meson decays, which can be extrapolated to the case of hadronic Λ_b baryon decays. According to the plan [76], the LHCb will reach the integrated luminosity of 50 fb^{-1} at the end of Run 4. Since LHCb Run 3 is currently ongoing and its final integrated luminosity remains uncertain, we will estimate the signal events for the combined dataset of Run 3 and Run 4 by assuming that the conditions and performance of Run 4 are identical to those of Run 3. The ratio between the events from combined Run 3+4 and those from Run 2 is about $(50 - 9) \text{ fb}^{-1}/6 \text{ fb}^{-1} \times 2 \sim 14$, where the factor of 2 comes from the enhancement of trigger efficiencies for Run 3 [77] implied by Fig. 13. Taking into account the factor of 4 between the Run 2 and Run 1 data, the ratio of the events from Run 1+2+3+4 to those from Run 1 is nearly $1 + 4 + 4 \times 14 \sim 60$. That is, the total signal events of $\Lambda_b \rightarrow pa_1$ and pK_1 from the full Run 1+2+3+4 data can attain $800 \times 60 = 48000$ and $1000 \times 60 = 60000$, respectively.

TABLE XVI: Predictions for A_{UD} and A_{UD}^{CP} in the $\Lambda_b \rightarrow pa_1, pK_1$ decays.

	$\Lambda_b \rightarrow pa_1$	$\Lambda_b \rightarrow pK_1(\theta_K = 30^\circ)$	$\Lambda_b \rightarrow pK_1(\theta_K = 60^\circ)$
A_{UD}	$(-9^{+2}_{-2})\%$	$(-19^{+4}_{-4})\%$	$(-24^{+6}_{-5})\%$
A_{UD}^{CP}	$(-24^{+8}_{-13})\%$	$(+26^{+4}_{-10})\%$	$(+40^{+4}_{-9})\%$

Both the A_{UD} and A_{UD}^{CP} values are essential for evaluating the experimental sensitivities, whose predictions are provided in Table XVI. Recall the definition of A_{UD} ,

$$A_{UD} = \frac{\Gamma(\cos \theta > 0) - \Gamma(\cos \theta < 0)}{\Gamma(\cos \theta > 0) + \Gamma(\cos \theta < 0)} = \frac{N_> - N_<}{N_> + N_<}, \quad (78)$$

where N are the numbers of signal events with $N_> = N(\cos \theta > 0)$ and $N_< = N(\cos \theta < 0)$. The statistical error of A_{UD} follows the error propagation formula

$$\begin{aligned} \sigma_{A_{UD}} &= \sqrt{\left(\frac{\partial A_{UD}}{\partial N_>}\right)^2 \sigma_{N_>}^2 + \left(\frac{\partial A_{UD}}{\partial N_<}\right)^2 \sigma_{N_<}^2} \\ &= \sqrt{\left(\frac{2N_<}{(N_> + N_<)^2}\right)^2 \sigma_{N_>}^2 + \left(\frac{-2N_>}{(N_> + N_<)^2}\right)^2 \sigma_{N_<}^2}, \end{aligned} \quad (79)$$

with $\sigma_{N_>,<}$ being the statistical errors of $N_>,<$. The neglect of background events for a naive analysis leads to the approximate uncertainties $\sigma_{N_>} \approx \sqrt{N_>}$ and $\sigma_{N_<} \approx \sqrt{N_<}$. As a simple estimate of the uncertainties and experimental sensitivities, we assume $N_> = N_< = \bar{N}_> = \bar{N}_< = N_{\text{tot}}/4$, where $N_{\text{tot}} = 48000$ for $\Lambda_b \rightarrow pa_1$ and $N_{\text{tot}} = 60000$ for $\Lambda_b \rightarrow pK_1$. The statistical uncertainty of A_{UD} is then $\sigma_{A_{UD}} \approx \sqrt{2/N_{\text{tot}}}$, inferring the experimental uncertainties $\sigma_{A_{UD}}(\Lambda_b \rightarrow pa_1) \approx 0.65\%$ and $\sigma_{A_{UD}}(\Lambda_b \rightarrow pK_1) \approx 0.58\%$ from the full Run 1+2+3+4 data.

The background effects are expected to be less than 30% on $\sigma_{A_{UD}}$, as reflected by the LHCb data; the signal yields of $\Lambda_b \rightarrow p\pi\pi\pi$ are 6646 ± 105 corresponding to the integrated luminosity of 3 fb^{-1} in [8], and 27600 ± 200 for 6.6 fb^{-1} in [13], where the errors include background contributions. The uncertainties of the pure signal events $\sqrt{6646} = 81.5$ and $\sqrt{27600} = 166.1$ are lifted by 29% to 105 and by 20% to 200, respectively. Hence, the uncertainties are found to be $\sigma_{A_{UD}}(\Lambda_b \rightarrow pa_1) \approx 0.85\%$ and $\sigma_{A_{UD}}(\Lambda_b \rightarrow pK_1) \approx 0.75\%$, amplified by a factor of 1.3.

We then proceed to the statistical uncertainty of $A_{UD}^{CP} = (A_{UD} + \bar{A}_{UD})/(A_{UD} - \bar{A}_{UD})$. Note that the quantity \bar{A}_{UD} acquires an opposite sign relative to A_{UD} under the parity transformation, because A_{UD} is parity-odd. Analogous to Eq. (79), the uncertainty of A_{UD}^{CP} is derived from

$$\sigma_{A_{UD}^{CP}} = \sqrt{\left(\frac{\partial A_{UD}^{CP}}{\partial A_{UD}}\right)^2 \sigma_{A_{UD}}^2 + \left(\frac{\partial A_{UD}^{CP}}{\partial \bar{A}_{UD}}\right)^2 \sigma_{\bar{A}_{UD}}^2} \approx \frac{1}{\sqrt{2}|A_{UD}|} \sigma_{A_{UD}}, \quad (80)$$

where the last expression is justified by the assumptions $\bar{A}_{UD} = -A_{UD}$ and $\sigma_{\bar{A}_{UD}} = \sigma_{A_{UD}}$. The magnitude of A_{UD} is crucial for obtaining the uncertainty of A_{UD}^{CP} . The insertion of the central values of A_{UD} in Table XVI yields the statistical uncertainties of A_{UD}^{CP} , $\sigma_{A_{UD}^{CP}}(\Lambda_b \rightarrow pa_1) \approx \frac{0.85\%}{\sqrt{2} \times 9\%} = 6.7\%$, $\sigma_{A_{UD}^{CP}}(\Lambda_b \rightarrow pK_1(\theta_K = 30^\circ)) \approx \frac{0.75\%}{\sqrt{2} \times 19\%} = 2.8\%$ and $\sigma_{A_{UD}^{CP}}(\Lambda_b \rightarrow pK_1(\theta_K = 60^\circ)) \approx \frac{0.75\%}{\sqrt{2} \times 24\%} = 2.2\%$.

Considering the differences of event numbers between particles and antiparticles caused by direct CPVs, between $N_>$ and $N_<$ caused by A_{UD} , and between A_{UD} and \bar{A}_{UD} arising from A_{UD}^{CP} , we refine the above crude estimates, arriving at the uncertainties $\sigma_{A_{UD}^{CP}}(\Lambda_b \rightarrow pa_1) = 5.2\%$, $\sigma_{A_{UD}^{CP}}(\Lambda_b \rightarrow pK_1(\theta_K = 30^\circ)) = 3.8\%$ and $\sigma_{A_{UD}^{CP}}(\Lambda_b \rightarrow pK_1(\theta_K = 60^\circ)) = 3.5\%$. The decrease of $\sigma_{A_{UD}^{CP}}(\Lambda_b \rightarrow pa_1)$ and the increase of $\sigma_{A_{UD}^{CP}}(\Lambda_b \rightarrow pK_1)$ stem from the negativity of $A_{UD}^{CP}(\Lambda_b \rightarrow pa_1)$ and the positivity of $A_{UD}^{CP}(\Lambda_b \rightarrow pK_1)$, respectively. Referring to the predicted A_{UD}^{CP} in Table XVI, we conclude that the CPV induced by the up-down asymmetry in $\Lambda_b \rightarrow pK_1$ could attain a statistic significance greater than 5σ , while the CPV in $\Lambda_b \rightarrow pa_1$ is at the edge of 5σ .

At last, we come to the issue of systematic uncertainties. We can learn from the measurements of \hat{T} -odd triple-product-asymmetry CPVs of $\Lambda_b \rightarrow p\pi^-\pi^+\pi^-$ in [8] and [13], which are defined as $C_{\hat{T}} = \vec{p}_p \cdot (\vec{p}_{\pi_{\text{fast}}^-} \times \vec{p}_{\pi^+})$ for the \hat{T} -odd triple product of final-state particle momenta in the Λ_b rest frame. Note that the quasi-time reversal transformation \hat{T} reverses particle spins and momenta, while maintaining the initial and final states. The definitions of the triple product asymmetries (TPAs)

$$A_{\hat{T}} = \frac{N(C_{\hat{T}} > 0) - N(C_{\hat{T}} < 0)}{N(C_{\hat{T}} > 0) + N(C_{\hat{T}} < 0)}, \quad \bar{A}_{\hat{T}} = \frac{\bar{N}(-\bar{C}_{\hat{T}} > 0) - \bar{N}(-\bar{C}_{\hat{T}} < 0)}{\bar{N}(-\bar{C}_{\hat{T}} > 0) + \bar{N}(-\bar{C}_{\hat{T}} < 0)}, \quad (81)$$

are similar to that for the up-down asymmetries in Eq. (76). The \hat{T} -odd CP - and P -violating asymmetries,

$$a_{CP}^{\hat{T}\text{-odd}} = \frac{1}{2}(A_{\hat{T}} - \bar{A}_{\hat{T}}), \quad a_P^{\hat{T}\text{-odd}} = \frac{1}{2}(A_{\hat{T}} + \bar{A}_{\hat{T}}), \quad (82)$$

correspond to the numerator and the denominator, respectively, of the definition for A_{CP}^{UD} in Eq. (77).

It has been known that the main sources of systematic uncertainties in the TPA analysis include selection criteria, reconstruction and detector acceptance based on the control sample of $\Lambda_b^0 \rightarrow \Lambda_c^+(\rightarrow pK^-\pi^+)\pi^-$. The systematic uncertainties are evaluated as 0.32% for both $a_{CP}^{\hat{T}\text{-odd}}$ and $a_P^{\hat{T}\text{-odd}}$ with the Run 1 data in [8], and 0.2% with more data in [13]. The systematic uncertainties of both $A_{UD} + \bar{A}_{UD}$ and $A_{UD} - \bar{A}_{UD}$ can thus be taken as 0.2% under the assumption that it is unchanged

with more data samples. Using the error propagation formula with the fully positive correlation between $A_{UD} + \bar{A}_{UD}$ and $A_{UD} - \bar{A}_{UD}$, we obtain the systematic uncertainty of A_{CP}^{UD} as about $0.2\%/(2|A_{UD}|)$. Namely, the systematic uncertainties of A_{CP}^{UD} are 1.1% for $\Lambda_b \rightarrow pa_1$, 0.5% for $\Lambda_b \rightarrow pK_1(\theta_K = 30^\circ)$ and 0.4% for $\Lambda_b \rightarrow pK_1(\theta_K = 60^\circ)$, which are less than the statistic uncertainties. Therefore, there is a great chance to identify the order-of-20% $\sim 40\%$ up-down asymmetric CPVs in $\Lambda_b \rightarrow pa_1$ and pK_1 in the near future, and to establish CPVs in baryon decays.

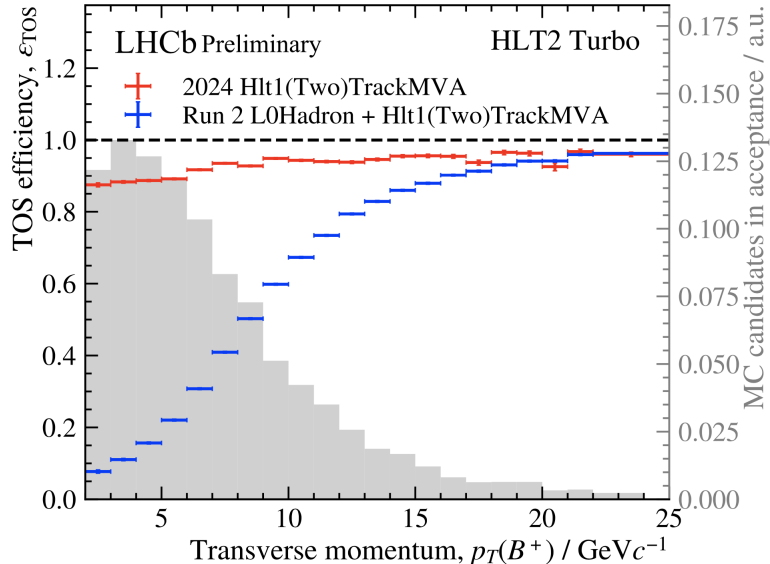


FIG. 13: Comparison of trigger efficiencies for LHCb Run 2 and Run 3 taken from the LHCb public website: <https://lbfence.cern.ch/alcsm/public/figure/details/3837>.

IV. SUMMARY

We have performed the first full QCD analysis on two-body hadronic $\Lambda_b \rightarrow ph$ decays in the PQCD approach. We calculated the various topological amplitudes, including their strong phases, by incorporating the higher-twist hadron DAs. It is found that the subleading power corrections are in fact sizable in heavy baryon decays.

Our predictions for the total and partial-wave CPVs of the considered modes are summarized and compared with the available data for bottom hadron decays in Fig. 14 [17]. We elucidated the mechanism responsible for the measured small CPVs in $\Lambda_b \rightarrow p\pi^-, pK^-$, in contrast to the sizable CPVs in the similar B meson decays. The partial-wave CPVs in $\Lambda_b \rightarrow p\pi^-$ attains 10% potentially, but the destruction between them leads to the tiny CPV. The direct CPV of $\Lambda_b \rightarrow pK^-$ is primarily attributed to the modest S -wave CPV.

We have extended our investigation to the CPVs in the modes with vector and axial-vector final states. The partial-wave CPVs of the $\Lambda_b \rightarrow pV$, pA decays also exceed 10%; for examples, the P_2 -wave CPVs of $\Lambda_b \rightarrow pp^-$ and $pa_1^-(1260)$ are 17% and -24% , respectively; the $(D + S^L)$ -wave CPV of $\Lambda_b \rightarrow pK^{*-}$ is 27%; the partial-wave CPVs of $\Lambda_b \rightarrow pK_1^-(1270)$ even amount to the order of 30%. Nevertheless, the direct CPVs of the $\Lambda_b \rightarrow pK^{*-}$, $pa_1^-(1260)$ and $pK_1(1270)$ decays diminish as well, which trace back to the strong cancellation of the major $(D + S^L)$ - and P_1 -wave CPVs, like the $\Lambda_b \rightarrow p\pi^-$ case.

Our work suggests that certain partial-wave CPVs in bottom baryon decays, especially those related to angular distributions, can be sufficiently significant and probed to establish baryon CPVs. The decay asymmetry parameters of two-body Λ_b modes are also predicted for future experimental confrontations. It opens avenues for deeply understanding the dynamics in heavy baryon decays and their CPVs. The rich data samples and complicated dynamics in multi-body bottom baryon decays offer remarkable prospects for exploring baryon CPVs.

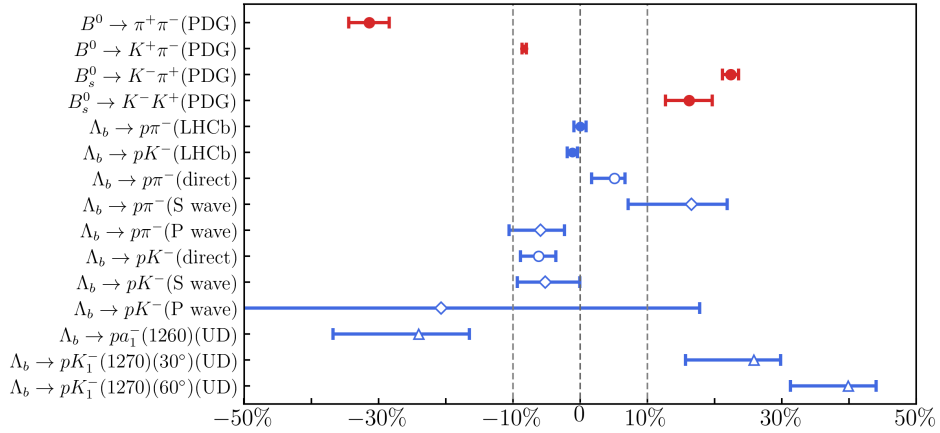


FIG. 14: CPVs measured in B meson and $\Lambda_b \rightarrow p\pi^-, pK^-$ decays, and our predictions.

ACKNOWLEDGEMENTS

We acknowledge Jun Hua, Yan-Qing Ma, Ding-Yu Shao and Jian Wang for their valuable comments. J.J.H. and J.X.Y. wish to thank Fan-Rong Xu for the warm hospitality during their visit to Jinan University. This work was supported in part by Natural Science Foundation of China under Grant No. 12335003, by the Fundamental Research Funds for the Central Universities under No. lzujbky-2023-stlt01, lzujbky-2023-it12, lzujbky-2024-oy02 and lzujbky-2025-eyt01, and by the Super Computing Center at Lanzhou University.

Appendix A: Auxiliary functions

The auxiliary functions $F_{1,2,3,4}$ as the results of the Fourier transformation of the hard decay kernels from the k_T space to the b space are collected below:

$$F_1(A, b) = \int d^2 k_T \frac{e^{i \mathbf{k}_T \cdot \mathbf{b}}}{k^2 + A} = 2\pi \left\{ K_0(\sqrt{Ab^2}) \Theta(A) + \frac{i\pi}{2} H_0^{(1)}(\sqrt{-Ab^2}) \Theta(-A) \right\}, \quad (\text{A1})$$

$$\begin{aligned} F_2(A, B, b) &= \int d^2 k_T \frac{e^{i \mathbf{k}_T \cdot \mathbf{b}}}{(k^2 + A)(k^2 + B)} \\ &= \int_0^1 dz \frac{\pi b}{\sqrt{|Z_1|}} \left\{ K_1(\sqrt{Z_1 b^2}) \Theta(Z_1) - \frac{i\pi}{2} H_1^{(1)}(\sqrt{-Z_1 b^2}) \Theta(-Z_1) \right\}, \end{aligned} \quad (\text{A2})$$

$$\begin{aligned}
F_3(A, B, C, b_1, b_2) &= \int d^2 k_{1T} \int d^2 k_{2T} \frac{e^{i(\mathbf{k}_{1T} \cdot \mathbf{b}_1 + \mathbf{k}_{2T} \cdot \mathbf{b}_2)}}{(k_1^2 + A)(k_2^2 + B)((k_1 + k_2)^2 + C)} \\
&= \int_0^1 \frac{dz_1 dz_2}{z_1(1-z_1)} \frac{\pi^2 \sqrt{X_2}}{\sqrt{|Z_2|}} \left\{ K_1(\sqrt{X_2 Z_2}) \Theta(Z_2) - \frac{i\pi}{2} H_1^{(1)}(\sqrt{-X_2 Z_2}) \Theta(-Z_2) \right\}, \tag{A3}
\end{aligned}$$

$$\begin{aligned}
F_4(A, B, C, D, b_1, b_2, b_3) &= \int d^2 k_{1T} \int d^2 k_{2T} \int d^2 k_{3T} \frac{e^{i(\mathbf{k}_{1T} \cdot \mathbf{b}_1 + \mathbf{k}_{2T} \cdot \mathbf{b}_2 + \mathbf{k}_{3T} \cdot \mathbf{b}_3)}}{(k_1^2 + A)(k_2^2 + B)(k_3^2 + C)((k_1 + k_2 + k_3)^2 + D)} \\
&= \int_0^1 \frac{dz_1 dz_2 dz_3}{z_1 z_2 (1-z_1)(1-z_2)} \frac{\pi^3 \sqrt{X_3}}{\sqrt{|Z_3|}} \left\{ K_1(\sqrt{X_3 Z_3}) \Theta(Z_3) - \frac{i\pi}{2} H_1^{(1)}(\sqrt{-X_3 Z_3}) \Theta(-Z_3) \right\}. \tag{A4}
\end{aligned}$$

In the above expressions $H_v^{(1)}(z)$ is the Hankel function of the first kind,

$$H_v^{(1)}(z) = J_v(z) + iY_v(z), \tag{A5}$$

where $J_v(z)$ ($Y_v(z)$) is the Bessel function of the first (second) kind, and $K_v(z)$ is the modified Bessel function of second kind. The variables Z_1, Z_2, Z_3 and X_2, X_3 read

$$\begin{aligned}
Z_1 &= Az + B(1-z), \\
Z_2 &= A(1-z_2) + \frac{z_2}{z_1(1-z_1)} [B(1-z_1) + Cz_1], \\
Z_3 &= A(1-z_3) + \frac{z_3}{z_2(1-z_2)} \left\{ B(1-z_2) + \frac{z_2}{z_1(1-z_1)} [C(1-z_1) + Dz_1] \right\}, \\
X_2 &= (b_1 - z_1 b_2)^2 + \frac{z_1(1-z_1)}{z_2} b_2^2, \\
X_3 &= [b_1 - b_2 z_2 - b_3 z_1(1-z_2)]^2 + \frac{z_2(1-z_2)}{z_3} (b_2 - b_3 z_1)^2 + \frac{z_1(1-z_1)z_2(1-z_2)}{z_2 z_3} b_3^2, \tag{A6}
\end{aligned}$$

with the Feynman parameters z 's. The above auxiliary functions appear in the PQCD factorization formulas for two-body hadronic Λ_b baryon decays.

Appendix B: Decay amplitudes

We present the PQCD factorization formula for each topological diagram, whose hard kernel involves two virtual gluons at the lowest order of the strong coupling α_s . The Feynman diagrams to be evaluated are shown in Figs. 15, 17, 16, 18 and 19, where the gluon in black stays fixed, while the gluon in red has one fixed end with another attaching to a cross at various locations. A Feynman diagram is labeled by the crossed vertex. For instance, the upper-left diagram in Fig. 15 is labeled as $a3$. We provide the formula for one typical diagram in each topology involved in the $\Lambda_b \rightarrow p\pi^-, pK^-$ decay. The amplitudes for the other modes $\Lambda_b \rightarrow p\rho^-, pK^{*-}, pa_1^-, pK_1^-$ from the same topology are similar, but with different meson DAs.

There are 40 Feynman diagrams from the T topology in Fig. 15, among which 16 are factorizable without hard gluons attaching to the emitted meson, and 24 are nonfactorizable. Applying the Feriz transformation to Fig. 15 and replacing the tree operators by the penguin ones, we acquire the

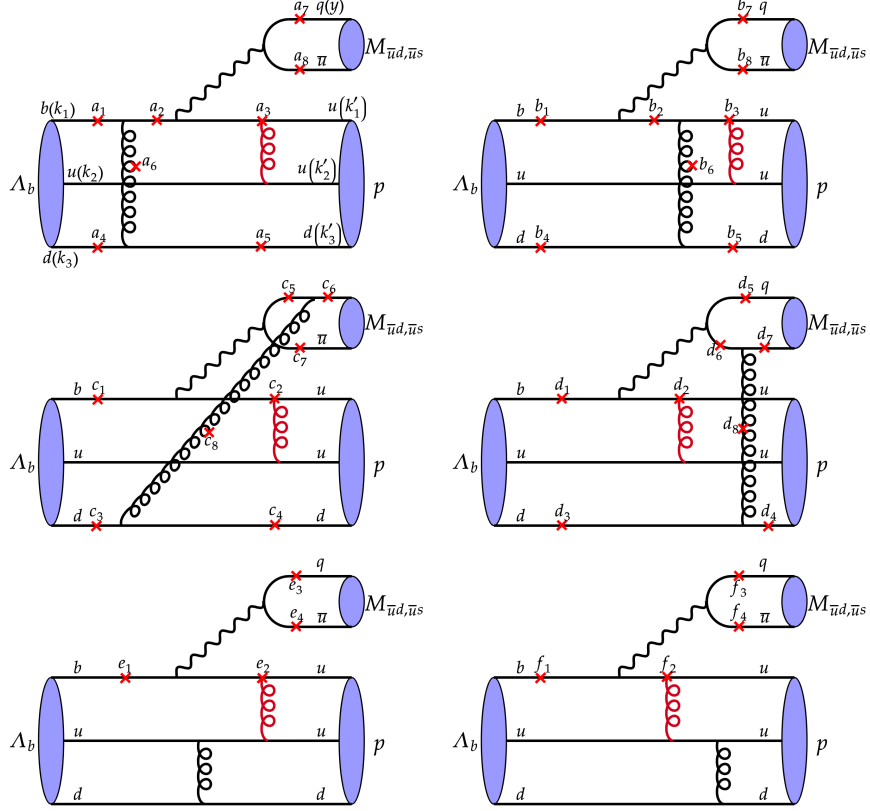


FIG. 15: Feynman diagrams contributing to the external- W emission topology T .

diagrams for the PC_1 topology. The formula for the sum of the factorizable $T(b2)$ diagram and the corresponding PC_1 diagram is written as

$$\mathcal{A}_{T(b2)+PC_1(b2)} = \frac{8}{3} \frac{-i}{128N_c^2} \int [dx] \int [dx'] \frac{1}{(2\pi)^5} \int b_1 db_1 \int b'_2 db'_2 \int b'_3 db'_3 (4\pi\alpha_s(t^{T(b2)}))^2 (B1) \\ (M_{T(b2)} + M_{PC_1(b2)}) F_1(C, b'_3) F_3(A, B, D, b_1, b'_2) \exp[-S^{T(b2)}([x], [x'], y, [b], [b'], b_q)].$$

The auxiliary functions F_i , with arguments

$$A = m_{\Lambda_b}^2(x_2 + x_3), \quad B = m_{\Lambda_b}^2 x_3(x'_1 + x'_3), \quad C = m_{\Lambda_b}^2 x_3 x'_3, \quad D = m_{\Lambda_b}^2 x_2 x'_2, \quad (B2)$$

from the internal particle propagators, have been given in Appendix A. The functions

$$M_{T(b2)} = \frac{G_F}{\sqrt{2}} \left\{ V_{ub} V_{uq}^* \left[\frac{1}{3} C_1 + C_2 \right] \right\} M_{T(b2)}^{LL}, \\ M_{PC_1(b2)} = -\frac{G_F}{\sqrt{2}} \left\{ V_{tb} V_{tq}^* \left[\frac{1}{3} C_3 + C_4 + \frac{1}{3} C_9 + C_{10} \right] \right\} M_{T(b2)}^{LL} \\ - \frac{G_F}{\sqrt{2}} \left\{ V_{tb} V_{tq}^* \left[-\frac{2}{3} C_5 - 2C_6 - \frac{2}{3} C_7 - C_8 \right] \right\} M_{T(b2)}^{SP}. \quad (B3)$$

are associated with the tree and penguin contributions, respectively, where the matrix element $M_{T(b2)}^{LL}$ ($M_{T(b2)}^{SP}$) corresponds to the insertion of the $(V-A) \otimes (V-A)((S-P) \otimes (S+P))$ operator. We display their explicit expressions as follows,

$$M_{T(b2)}^{LL} \equiv \langle h | (\bar{q}u)_{V-A} | 0 \rangle \langle p | (\bar{u}b)_{V-A} | \Lambda_b \rangle_{T(b2)}$$

$$\begin{aligned}
&= \left\{ 8if_P m_{\Lambda_b}^4 \psi_4 T_1 x_3 + m_p m_{\Lambda_b}^3 (-2if_P \psi_3^{-+} x_3 (P_1 + S_1 + 2T_2 + T_3 - T_7) - 2if_P \psi_3^{+-} x_3 (-A_3 + V_3)) \right. \\
&\quad + 2if_P m_p^3 m_{\Lambda_b} \psi_3^{-+} (x'_1 + x'_3) (A_6 + V_6) + m_p^2 m_{\Lambda_b}^2 (-4if_P \psi_2 x_3 (-A_4 - A_5 - V_4 + V_5) \\
&\quad \left. + 4if_P \psi_4 (x'_1 + x'_3) (-A_4 - A_5 + P_2 - S_2 - T_4 - T_8 - V_4 + V_5)) \right\} \\
&+ \left\{ 8if_P m_{\Lambda_b}^4 \psi_4 T_1 x_3 + m_p m_{\Lambda_b}^3 (2if_P \psi_3^{-+} x_3 (-P_1 - S_1 - 2T_2 - T_3 + T_7) + 2if_P \psi_3^{+-} x_3 (A_3 - V_3)) \right. \\
&\quad + 2if_P m_p^3 m_{\Lambda_b} \psi_3^{-+} (x'_1 + x'_3) (A_6 + V_6) + m_p^2 m_{\Lambda_b}^2 (4if_P \psi_2 x_3 (A_4 + A_5 + V_4 - V_5) \\
&\quad \left. - 4if_P \psi_4 (x'_1 + x'_3) (A_4 + A_5 - P_2 + S_2 + T_4 + T_8 + V_4 - V_5)) \right\} \gamma_5, \tag{B4}
\end{aligned}$$

$$\begin{aligned}
M_{T(b2)}^{SP} &\equiv \langle h | (\bar{q}u)_{S+P} | 0 \rangle \langle p | (\bar{u}b)_{S-P} | \Lambda_b \rangle_{T(b2)} \\
&= \left\{ -2if_P m_0^P (m_{\Lambda_b}^3 x_3 (4\psi_4 T_1 + \psi_3^{+-} (A_1 + V_1) (x_2 + x_3)) + m_p^3 (A_6 \psi_3^{-+} + \psi_3^{+-} V_6 + 4\psi_2 T_6 (x_2 + x_3)) \right. \\
&\quad (x'_1 + x'_3) - m_p m_{\Lambda_b}^2 (\psi_3^{-+} (P_1 + S_1 + 2T_2 + T_3 - T_7) x_3 + \psi_3^{+-} (-A_3 + V_3) x_3 + 2\psi_2 (A_2 + A_3 \\
&\quad - P_1 + S_1 + T_3 + T_7 - V_2 + V_3) x_3 (x_2 + x_3) - 2\psi_4 (A_2 + A_3 - V_2 + V_3) (x_2 + x_3) (x'_1 + x'_3)) \\
&\quad + m_p^2 m_{\Lambda_b} (2\psi_2 (A_4 + A_5 + V_4 - V_5) x_3 - 2\psi_4 (A_4 + A_5 - P_2 + S_2 + T_4 + T_8 + V_4 - V_5) (x'_1 + x'_3) \\
&\quad - \psi_3^{+-} (P_2 + S_2 + T_4 + 2T_5 - T_8) (x_2 + x_3) (x'_1 + x'_3) + \psi_3^{-+} (A_4 - V_4) (x_2 + x_3) (x'_1 + x'_3))) \right\} \\
&+ \left\{ 2if_P m_0^P (m_{\Lambda_b}^3 (4\psi_4 T_1 x_3 - \psi_3^{+-} (A_1 + V_1) x_3 (x_2 + x_3)) + m_p^3 (A_6 \psi_3^{-+} + \psi_3^{+-} V_6 - 4\psi_2 T_6 (x_2 + x_3)) \right. \\
&\quad (x'_1 + x'_3) - m_p m_{\Lambda_b}^2 (\psi_3^{-+} (P_1 + S_1 + 2T_2 + T_3 - T_7) x_3 + \psi_3^{+-} (-A_3 + V_3) x_3 - 2\psi_2 (A_2 + A_3 \\
&\quad - P_1 + S_1 + T_3 + T_7 - V_2 + V_3) x_3 (x_2 + x_3) + 2\psi_4 (A_2 + A_3 - V_2 + V_3) (x_2 + x_3) (x'_1 + x'_3)) \\
&\quad + m_p^2 m_{\Lambda_b} (2\psi_2 (A_4 + A_5 + V_4 - V_5) x_3 - 2\psi_4 (A_4 + A_5 - P_2 + S_2 + T_4 + T_8 + V_4 - V_5) (x'_1 + x'_3) \\
&\quad \left. + \psi_3^{+-} (P_2 + S_2 + T_4 + 2T_5 - T_8) (x_2 + x_3) (x'_1 + x'_3) - \psi_3^{-+} (A_4 - V_4) (x_2 + x_3) (x'_1 + x'_3))) \right\} \gamma_5. \tag{B5}
\end{aligned}$$

The non-factorizable $T(c7)$ diagram yields

$$\begin{aligned}
\mathcal{A}_{T(c7)} &= \frac{-1}{128N_c^2 \sqrt{2N_c}} \int [dx] \int [dx'] \int dy \frac{1}{(2\pi)^5} \int b_2 db_2 \int b_3 db_3 \int b_q db_q (4\pi\alpha_s(t^{T(c7)}))^2 \\
&\quad (M_{T(c7)} + M_{PC_1(c7)}) F_4(D, C, B, A, b_2, b_3, b_q) \exp[-S^{T(c7)}([x], [x'], y, [b], [b'], b_q)], \tag{B6}
\end{aligned}$$

with the arguments,

$$A = m_{\Lambda_b}^2 x'_3 (x_3 - y), \quad B = m_{\Lambda_b}^2 x'_2 (-1 + x_2 + y), \quad C = m_{\Lambda_b}^2 x_3 x'_3, \quad D = m_{\Lambda_b}^2 x_2 x'_2. \tag{B7}$$

The functions

$$\begin{aligned}
M_{T(c7)} &= \frac{G_F}{\sqrt{2}} \{ V_{ub} V_{uq}^* [f_1 C_1 + f_2 C_2] \} M_{T(c7)}^{LL}, \\
M_{PC_1(c7)} &= - \frac{G_F}{\sqrt{2}} \{ V_{tb} V_{tq}^* [f_1 C_3 + f_2 C_4 + f_1 C_9 + f_2 C_{10}] \} M_{T(c7)}^{LL} \\
&\quad - \frac{G_F}{\sqrt{2}} \{ V_{tb} V_{tq}^* [f_1 C_5 + f_2 C_6 + f_1 C_7 + f_2 C_8] \} M_{T(c7)}^{LR}, \tag{B8}
\end{aligned}$$

where $f_1 = 8/3$ and $f_2 = -2$ are the color factors, and the superscript LR refers to the contribution from the $(V - A) \otimes (V + A)$ operator, contain the matrix elements

$$M_{T(c7)}^{LL} \equiv \langle ph | (\bar{q}b)_{V-A} (\bar{u}u)_{V-A} | \Lambda_b \rangle_{T(c7)}$$

$$\begin{aligned}
&= \left\{ 8m_{\Lambda_b}(4m_p^3\psi_2T_6x'_2x'_3 + m_p^2m_{\Lambda_b}x'_3((A_4\psi_3^{-+} - 2\psi_3^{+-}T_5 - \psi_3^{-+}V_4)x'_2 - 2\psi_2(P_2 - S_2 + T_4 + T_8) \right. \\
&\quad (-1 + x_2 + y)) + m_{\Lambda_b}^3(x_3 - y)(A_1\psi_3^{-+}x'_2 + \psi_3^{-+}V_1x'_2 - 2A_1\psi_2(-1 + x_2 + y) + 2\psi_2(2T_1 + V_1) \\
&\quad (-1 + x_2 + y)) + m_p m_{\Lambda_b}^2(2\psi_4(A_3 + V_3)x'_2x'_3 - 2\psi_2(P_1 - S_1 + T_3 + T_7)x'_2(x_3 - y) \\
&\quad + \psi_3^{+-}(P_1 + S_1 + T_3 - T_7)x'_3(-1 + x_2 + y)))\phi_m^A \Big\} \\
&+ \left\{ 8m_{\Lambda_b}(-4m_p^3\psi_2T_6x'_2x'_3 + m_p^2m_{\Lambda_b}x'_3((-A_4\psi_3^{-+} + 2\psi_3^{+-}T_5 + \psi_3^{-+}V_4)x'_2 + 2\psi_2(-P_2 + S_2 - T_4 - T_8) \right. \\
&\quad (-1 + x_2 + y)) - m_{\Lambda_b}^3(x_3 - y)(A_1\psi_3^{-+}x'_2 + \psi_3^{-+}V_1x'_2 + 2A_1\psi_2(-1 + x_2 + y) - 2\psi_2(2T_1 + V_1) \\
&\quad (-1 + x_2 + y)) + m_p m_{\Lambda_b}^2(-2\psi_4(A_3 + V_3)x'_2x'_3 + 2\psi_2(P_1 - S_1 + T_3 + T_7)x'_2(x_3 - y) \\
&\quad + \psi_3^{+-}(P_1 + S_1 + T_3 - T_7)x'_3(-1 + x_2 + y)))\phi_m^A \Big\} \gamma_5, \tag{B9}
\end{aligned}$$

$$\begin{aligned}
M_{T(c7)}^{LR} &\equiv \langle ph | (\bar{q}b)_{V-A}(\bar{u}u)_{V+A} | \Lambda_b \rangle_{T(c7)} \\
&= \left\{ 8m_0(2m_p^3\psi_2(-((A_6 - V_6)x'_3(-1 + x_2 + y)(\phi_m^P - \phi_m^T)) + 2T_6x'_2(x_3 - y)(\phi_m^P + \phi_m^T)) - 2m_{\Lambda_b}^3\psi_4(-2T_1x'_3 \right. \\
&\quad (-1 + x_2 + y)(\phi_m^P - \phi_m^T) + A_1x'_2(x_3 - y)(\phi_m^P + \phi_m^T) - V_1x'_2(x_3 - y)(\phi_m^P + \phi_m^T)) + m_p^2m_{\Lambda_b}(-2\psi_3^{+-}T_5x'_2 \right. \\
&\quad (x_3 - y)(\phi_m^P + \phi_m^T) + \psi_3^{+-}x'_3(-1 + x_2 + y)((A_4 + A_5 + P_2 + S_2 - T_4 + T_8 - V_4 + V_5)\phi_m^P \\
&\quad + (A_4 - A_5 + P_2 + S_2 - T_4 + T_8 - V_4 - V_5)\phi_m^T) + \psi_3^{-+}(((A_5 - 2T_5 - V_4 + V_5)x'_2x_3 + (P_2 + S_2 - T_4 + T_8) \right. \\
&\quad (-1 + x_2)x'_3 - (A_5 - 2T_5 - V_4 + V_5)x'_2y + (P_2 + S_2 - T_4 + T_8)x'_3y)\phi_m^P - ((A_5 - 2T_5 + V_4 + V_5)x'_2x_3 \\
&\quad + (P_2 + S_2 - T_4 + T_8)(-1 + x_2)x'_3 - (A_5 - 2T_5 + V_4 + V_5)x'_2y + (P_2 + S_2 - T_4 + T_8)x'_3y)\phi_m^T \\
&\quad + A_4x'_2(x_3 - y)(\phi_m^P + \phi_m^T)) - 2\psi_2(-(((S_2 + T_4 + T_8)x'_2x_3 + (A_4 + V_4)(-1 + x_2)x'_3 - (S_2 + T_4 + T_8)x'_2y \right. \\
&\quad + (A_4 + V_4)x'_3y)\phi_m^P) + (-((S_2 + T_4 + T_8)x'_2x_3) + (A_4 + V_4)(-1 + x_2)x'_3 + (S_2 + T_4 + T_8)x'_2y \\
&\quad + (A_4 + V_4)x'_3y)\phi_m^T + P_2x'_2(x_3 - y)(\phi_m^P + \phi_m^T)) + m_p m_{\Lambda_b}^2(\psi_3^{-+}((A_2 + A_3 + P_1 + S_1 - T_3 + T_7 + V_2 - V_3)x'_2x_3 \right. \\
&\quad - 2T_2(-1 + x_2)x'_3 - ((A_2 + A_3 + P_1 + S_1 - T_3 + T_7 + V_2 - V_3)x'_2 + 2T_2x'_3)y)\phi_m^P + \psi_3^{-+}((A_2 - A_3 - P_1 \right. \\
&\quad - S_1 + T_3 - T_7 + V_2 + V_3)x'_2x_3 + 2T_2(-1 + x_2)x'_3 + (-A_2 + A_3 + P_1 + S_1 - T_3 + T_7 - V_2 - V_3)x'_2y + 2T_2x'_3y)\phi_m^T \\
&\quad + \psi_3^{+-}(((S_1 - T_3 + T_7)x'_2x_3 + (A_2 + A_3 - 2T_2 + V_2 - V_3)(-1 + x_2)x'_3 - (S_1 - T_3 + T_7)x'_2y + (A_2 + A_3 \right. \\
&\quad - 2T_2 + V_2 - V_3)x'_3y)\phi_m^P + ((S_1 - T_3 + T_7)x'_2x_3 + (A_2 - A_3 - 2T_2 + V_2 + V_3)(-1 + x_2)x'_3 - (S_1 - T_3 + T_7)x'_2y \\
&\quad + (A_2 - A_3 - 2T_2 + V_2 + V_3)x'_3y)\phi_m^T + P_1x'_2(x_3 - y)(\phi_m^P + \phi_m^T)) + 2\psi_4(-((P_1 - S_1 - T_3 - T_7)x'_3(-1 + x_2 + y) \right. \\
&\quad (\phi_m^P - \phi_m^T)) + A_3x'_2(x_3 - y)(\phi_m^P + \phi_m^T) + V_3x'_2(x_3 - y)(\phi_m^P + \phi_m^T))) \Big\} \\
&+ \left\{ 8m_0(2m_p^3\psi_2(-((A_6 - V_6)x'_3(-1 + x_2 + y)(\phi_m^P - \phi_m^T)) + 2T_6x'_2(x_3 - y)(\phi_m^P + \phi_m^T)) + 2m_{\Lambda_b}^3\psi_4(-2T_1x'_3 \right. \\
&\quad (-1 + x_2 + y)(\phi_m^P - \phi_m^T) + A_1x'_2(x_3 - y)(\phi_m^P + \phi_m^T) - V_1x'_2(x_3 - y)(\phi_m^P + \phi_m^T)) + m_p^2m_{\Lambda_b}(-2\psi_3^{+-}T_5x'_2 \right. \\
&\quad (x_3 - y)(\phi_m^P + \phi_m^T) + \psi_3^{+-}x'_3(-1 + x_2 + y)((A_4 + A_5 + P_2 + S_2 - T_4 + T_8 - V_4 + V_5)\phi_m^P \\
&\quad + (A_4 - A_5 + P_2 + S_2 - T_4 + T_8 - V_4 - V_5)\phi_m^T) + \psi_3^{-+}(((A_5 - 2T_5 - V_4 + V_5)x'_2x_3 + (P_2 + S_2 - T_4 + T_8) \right. \\
&\quad (-1 + x_2)x'_3 - (A_5 - 2T_5 - V_4 + V_5)x'_2y + (P_2 + S_2 - T_4 + T_8)x'_3y)\phi_m^P - ((A_5 - 2T_5 + V_4 + V_5)x'_2x_3 \\
&\quad + (P_2 + S_2 - T_4 + T_8)(-1 + x_2)x'_3 - (A_5 - 2T_5 + V_4 + V_5)x'_2y + (P_2 + S_2 - T_4 + T_8)x'_3y)\phi_m^T \\
&\quad + A_4x'_2(x_3 - y)(\phi_m^P + \phi_m^T)) + 2\psi_2(-(((S_2 + T_4 + T_8)x'_2x_3 + (A_4 + V_4)(-1 + x_2)x'_3 - (S_2 + T_4 + T_8)x'_2y \right. \\
&\quad + (A_4 + V_4)x'_3y)\phi_m^P) + (-((S_2 + T_4 + T_8)x'_2x_3) + (A_4 + V_4)(-1 + x_2)x'_3 + (S_2 + T_4 + T_8)x'_2y \\
&\quad + (A_4 + V_4)x'_3y)\phi_m^T + P_2x'_2(x_3 - y)(\phi_m^P + \phi_m^T)) - m_p m_{\Lambda_b}^2(\psi_3^{-+}((A_2 + A_3 + P_1 + S_1 - T_3 + T_7 + V_2 - V_3)x'_2x_3 \right. \\
&\quad - 2T_2(-1 + x_2)x'_3 - ((A_2 + A_3 + P_1 + S_1 - T_3 + T_7 + V_2 - V_3)x'_2 + 2T_2x'_3)y)\phi_m^P + \psi_3^{-+}((A_2 - A_3 - P_1 \right. \\
&\quad - S_1 + T_3 - T_7 + V_2 + V_3)x'_2x_3 + 2T_2(-1 + x_2)x'_3 + (-A_2 + A_3 + P_1 + S_1 - T_3 + T_7 - V_2 - V_3)x'_2y + 2T_2x'_3y)\phi_m^T
\end{aligned}$$

$$\begin{aligned}
& + \psi_3^{+-} (((S_1 - T_3 + T_7)x'_2 x_3 + (A_2 + A_3 - 2T_2 + V_2 - V_3)(-1 + x_2)x'_3 - (S_1 - T_3 + T_7)x'_2 y + (A_2 + A_3 \\
& - 2T_2 + V_2 - V_3)x'_3 y) \phi_m^P + ((S_1 - T_3 + T_7)x'_2 x_3 + (A_2 - A_3 - 2T_2 + V_2 + V_3)(-1 + x_2)x'_3 - (S_1 - T_3 + T_7)x'_2 y \\
& + (A_2 - A_3 - 2T_2 + V_2 + V_3)x'_3 y) \phi_m^T + P_1 x'_2(x_3 - y)(\phi_m^P + \phi_m^T)) - 2\psi_4(-((P_1 - S_1 - T_3 - T_7)x'_3(-1 + x_2 + y) \\
& (\phi_m^P - \phi_m^T)) + A_3 x'_2(x_3 - y)(\phi_m^P + \phi_m^T) + V_3 x'_2(x_3 - y)(\phi_m^P + \phi_m^T))) \Big) \gamma_5. \quad (B10)
\end{aligned}$$

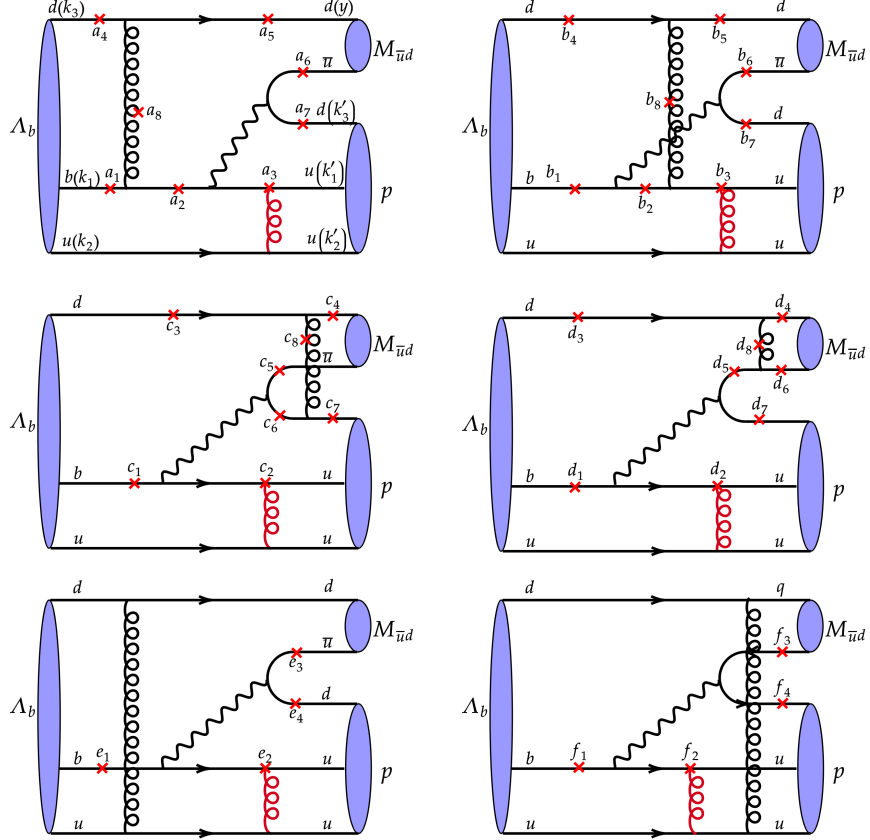


FIG. 16: Feynman diagrams contributing to the C_2 topology.

For the $C_2(c7)$ diagram in Fig. 16, we have

$$\begin{aligned}
\mathcal{A}_{C_2(c7)} = & \frac{-1}{128N_c^2} \frac{1}{\sqrt{2N_c}} \int [dx] \int [dx'] \int dy \frac{1}{(2\pi)^5} \int b_2 db_2 \int b'_2 db'_2 \int b_q db_q (4\pi\alpha_s(t^{C_2(c7)}))^2 \\
& (M_{C_2(c7)} + M_{PC_2(c7)}) F_1(D, b'_2) F_3(A, C, B, b_2, b'_2, b_q) \exp[-S^{C_2(c7)}([x], [x'], y, [b], [b'], b_q)], \quad (B11)
\end{aligned}$$

with the arguments

$$A = m_{\Lambda_b}^2 x_2(x'_2 + x'_2), \quad B = m_{\Lambda_b}^2 (x'_2 - x_3 + x'_3)(x_2 - y), \quad C = m_{\Lambda_b}^2 x_3 y, \quad D = m_{\Lambda_b}^2 x_2 x'_2. \quad (B12)$$

The functions

$$\begin{aligned} M_{C_2(c7)} &= \frac{G_F}{\sqrt{2}} \{V_{ub}V_{ud}^* [f_1 C_1 + f_2 C_2]\} M_{C_2(c7)}^{LL}, \\ M_{PC_2(c7)} &= - \frac{G_F}{\sqrt{2}} \{V_{tb}V_{td}^* [f_1 C_3 + f_2 C_4 + f_1 C_9 + f_2 C_{10}]\} M_{C_2(c7)}^{LL} \\ &\quad - \frac{G_F}{\sqrt{2}} \{V_{tb}V_{td}^* [-2f_1 C_5 - 2f_2 C_6 - 2f_1 C_7 - 2f_2 C_8]\} M_{C_2(c7)}^{SP}, \end{aligned} \quad (\text{B13})$$

contain the color factors $f_1 = -8/3$ and $f_2 = -16/3$, and the matrix elements

$$\begin{aligned} M_{C_2(c7)}^{LL} &\equiv \langle ph|(\bar{u}b)_{V-A}(\bar{d}u)_{V-A}|\Lambda_b\rangle_{C_2(c7)} \\ &= \left\{ 8m_0 m_p^3 \psi_3^{+-} (A_6 - V_6)(x'_2 + x'_3)(x'_2 - x_3 + x'_3)(\phi_m^P - \phi_m^T) + 8m_0 m_{\Lambda_b}^3 \psi_3^{-+} (A_1 - V_1)x_2(x_2 - y) \right. \\ &\quad (\phi_m^P + \phi_m^T) - 8m_p m_{\Lambda_b}^2 (m_{\Lambda_b} \psi_3^{-+} (P_1 + S_1 - 2T_2 - T_3 + T_7)(x'_2 + x'_3)(x_2 - y)\phi_m^A - m_0 \psi_3^{-+} (A_3 + V_3)x_2 \\ &\quad (x'_2 - x_3 + x'_3)(\phi_m^P - \phi_m^T) + 2m_0 \psi_2 (P_1 + S_1 - 2T_2 - T_3 + T_7)x_2(x_2 - y)(\phi_m^P + \phi_m^T) - 2m_0 \psi_4 (P_1 + S_1 \\ &\quad - 2T_2 - T_3 + T_7)(x'_2 + x'_3)(x_2 - y)(\phi_m^P + \phi_m^T)) - 8m_p^2 m_{\Lambda_b} (-2\psi_4(x'_2 + x'_3)(x'_2 - x_3 + x'_3) \\ &\quad (A_5 m_{\Lambda_b} \phi_m^A - m_{\Lambda_b} V_5 \phi_m^A - m_0 (P_2 + S_2 - T_4 - 2T_5 + T_8)(\phi_m^P - \phi_m^T)) + 2\psi_2 (A_4 m_{\Lambda_b} (x'_2 + x'_3)(x_2 - y)\phi_m^A \\ &\quad + m_{\Lambda_b} V_4 (x'_2 + x'_3)(x_2 - y)\phi_m^A - m_0 (P_2 + S_2 - T_4 - 2T_5 + T_8)x_2(x'_2 - x_3 + x'_3)(\phi_m^P - \phi_m^T)) \\ &\quad - m_0 \psi_3^{+-} (A_4 + V_4)(x'_2 + x'_3)(x_2 - y)(\phi_m^P + \phi_m^T)) \Big\} \\ &\quad + \left\{ - 8m_0 m_p^3 \psi_3^{+-} (A_6 - V_6)(x'_2 + x'_3)(x'_2 - x_3 + x'_3)(\phi_m^P - \phi_m^T) + 8m_0 m_{\Lambda_b}^3 \psi_3^{-+} (A_1 - V_1)x_2(x_2 - y) \right. \\ &\quad (\phi_m^P + \phi_m^T) - 8m_p m_{\Lambda_b}^2 (m_{\Lambda_b} \psi_3^{-+} (P_1 + S_1 - 2T_2 - T_3 + T_7)(x'_2 + x'_3)(x_2 - y)\phi_m^A + m_0 \psi_3^{-+} (A_3 + V_3)x_2 \\ &\quad (x'_2 - x_3 + x'_3)(\phi_m^P - \phi_m^T) + 2m_0 \psi_2 (P_1 + S_1 - 2T_2 - T_3 + T_7)x_2(x_2 - y)(\phi_m^P + \phi_m^T) - 2m_0 \psi_4 (P_1 + S_1 \\ &\quad - 2T_2 - T_3 + T_7)(x'_2 + x'_3)(x_2 - y)(\phi_m^P + \phi_m^T)) - 8m_p^2 m_{\Lambda_b} (-2\psi_4(x'_2 + x'_3)(x'_2 - x_3 + x'_3) \\ &\quad (A_5 m_{\Lambda_b} \phi_m^A - m_{\Lambda_b} V_5 \phi_m^A + m_0 (P_2 + S_2 - T_4 - 2T_5 + T_8)(\phi_m^P - \phi_m^T)) + 2\psi_2 (A_4 m_{\Lambda_b} (x'_2 + x'_3)(x_2 - y)\phi_m^A \\ &\quad + m_{\Lambda_b} V_4 (x'_2 + x'_3)(x_2 - y)\phi_m^A + m_0 (P_2 + S_2 - T_4 - 2T_5 + T_8)x_2(x'_2 - x_3 + x'_3)(\phi_m^P - \phi_m^T)) \\ &\quad - m_0 \psi_3^{+-} (A_4 + V_4)(x'_2 + x'_3)(x_2 - y)(\phi_m^P + \phi_m^T)) \Big\} \gamma_5, \end{aligned} \quad (\text{B14})$$

$$\begin{aligned} M_{C_2(c7)}^{SP} &\equiv \langle ph|(\bar{u}b)_{S-P}(\bar{d}u)_{S+P}|\Lambda_b\rangle_{C_2} \\ &= \left\{ 8m_p^3 T_6 (x'_2 + x'_3) (m_{\Lambda_b} \psi_3^{+-} (x'_2 - x_3 + x'_3) \phi_m^A + 2m_0 \psi_2 (x_2 - y) (\phi_m^P - \phi_m^T)) - 8m_{\Lambda_b}^3 T_1 x_2 (x'_2 - x_3 + x'_3) \right. \\ &\quad (m_{\Lambda_b} \psi_3^{-+} \phi_m^A - 2m_0 \psi_4 (\phi_m^P + \phi_m^T)) + 4m_p^2 m_{\Lambda_b} (-m_{\Lambda_b} \psi_3^{+-} (P_2 - S_2 - T_4 - T_8)(x'_2 + x'_3)(x'_2 - x_3 + x'_3) \phi_m^A \\ &\quad + 2m_{\Lambda_b} \psi_4 (A_4 + A_5 - V_4 + V_5)(x'_2 + x'_3)(x'_2 - x_3 + x'_3) \phi_m^A + m_0 \psi_3^{-+} (A_4 + A_5 - V_4 + V_5)(x'_2 + x'_3) \\ &\quad (x_2 - y) (\phi_m^P - \phi_m^T) + m_0 \psi_3^{+-} (A_4 + A_5 - V_4 + V_5) x_2 (x'_2 - x_3 + x'_3) (\phi_m^P + \phi_m^T) \\ &\quad - 2\psi_2 (m_{\Lambda_b} \phi_m^A x_2 (x'_2 - x_3 + x'_3) (A_4 + A_5 - V_4 + V_5) + m_0 (\phi_m^P - \phi_m^T) (x'_2 + x'_3) (x_2 - y) (P_2 - S_2 \\ &\quad - T_4 - T_8))) - 4m_p m_{\Lambda_b}^2 (-m_{\Lambda_b} \psi_3^{-+} (-P_1 + S_1 + T_3 + T_7) x_2 (-x'_2 + x_3 - x'_3) \phi_m^A + 2m_{\Lambda_b} \psi_2 (A_2 + A_3 \\ &\quad + V_2 - V_3) x_2 (x'_2 - x_3 + x'_3) \phi_m^A - m_0 \psi_3^{-+} (A_2 + A_3 + V_2 - V_3) (x'_2 + x'_3) (x_2 - y) (\phi_m^P - \phi_m^T) \\ &\quad - m_0 \psi_3^{+-} (A_2 + A_3 + V_2 - V_3) x_2 (x'_2 - x_3 + x'_3) (\phi_m^P + \phi_m^T) - 2\psi_4 (x'_2 - x_3 + x'_3) \\ &\quad (m_{\Lambda_b} (A_2 + A_3 + V_2 - V_3) (x'_2 + x'_3) \phi_m^A - m_0 (P_1 - S_1 - T_3 - T_7) x_2 (\phi_m^P + \phi_m^T))) \Big\} \\ &\quad + \left\{ 8m_p^3 T_6 (x'_2 + x'_3) (m_{\Lambda_b} \psi_3^{+-} (x'_2 - x_3 + x'_3) \phi_m^A + 2m_0 \psi_2 (x_2 - y) (\phi_m^P - \phi_m^T)) + 8m_{\Lambda_b}^3 T_1 x_2 (x'_2 - x_3 + x'_3) \right. \end{aligned}$$

$$\begin{aligned}
& (m_{\Lambda_b} \psi_3^{-+} \phi_m^A - 2m_0 \psi_4(\phi_m^P + \phi_m^T)) + 4m_p^2 m_{\Lambda_b} (m_{\Lambda_b} \psi_3^{+-}(P_2 - S_2 - T_4 - T_8)(x'_2 + x'_3)(x'_2 - x_3 + x'_3) \phi_m^A \\
& + 2m_{\Lambda_b} \psi_4(A_4 + A_5 - V_4 + V_5)(x'_2 + x'_3)(x'_2 - x_3 + x'_3) \phi_m^A + m_0 \psi_3^{-+}(A_4 + A_5 - V_4 + V_5)(x'_2 + x'_3) \\
& (x_2 - y)(\phi_m^P - \phi_m^T) + m_0 \psi_3^{+-}(A_4 + A_5 - V_4 + V_5)x_2(x'_2 - x_3 + x'_3)(\phi_m^P + \phi_m^T) \\
& - 2\psi_2(m_{\Lambda_b} \phi_m^A x_2(x'_2 - x_3 + x'_3)(A_4 + A_5 - V_4 + V_5) - m_0(\phi_m^P - \phi_m^T)(x'_2 + x'_3)(x_2 - y)(P_2 - S_2 \\
& - T_4 - T_8)) + 4m_p m_{\Lambda_b}^2 (m_{\Lambda_b} \psi_3^{-+}(P_1 - S_1 - T_3 - T_7)x_2(x'_2 - x_3 + x'_3) \phi_m^A + 2m_{\Lambda_b} \psi_2(A_2 + A_3 \\
& + V_2 - V_3)x_2(x'_2 - x_3 + x'_3) \phi_m^A - m_0 \psi_3^{-+}(A_2 + A_3 + V_2 - V_3)(x'_2 + x'_3)(x_2 - y)(\phi_m^P - \phi_m^T) \\
& - m_0 \psi_3^{+-}(A_2 + A_3 + V_2 - V_3)x_2(x'_2 - x_3 + x'_3)(\phi_m^P + \phi_m^T) - 2\psi_4(x'_2 - x_3 + x'_3) \\
& (m_{\Lambda_b}(A_2 + A_3 + V_2 - V_3)(x'_2 + x'_3) \phi_m^A + m_0(P_1 - S_1 - T_3 - T_7)x_2(\phi_m^P + \phi_m^T))) \Big\} \gamma_5. \quad (\text{B15})
\end{aligned}$$

The $E_2(a4)$ diagram in Fig. 17 contributes

$$\begin{aligned}
\mathcal{A}_{E_2(a4)} = & \frac{-1}{128N_c^2 \sqrt{2N_c}} \int [dx] \int [dx'] \int dy \frac{1}{(2\pi)^5} \int b_1 db_1 \int b_3 db_3 \int b'_2 db'_2 (4\pi\alpha_s(t^{E_2(a4)}))^2 \\
& (M_{E_2(a4)} + M_{PE_2(a4)}) F_1(C, b_3) F_3(A, D, B, b_1, b_3, b'_2) \exp[-S^{E_2(a4)}([x], [x'], y, [b], [b'], b_q)], \quad (\text{B16})
\end{aligned}$$

with the arguments

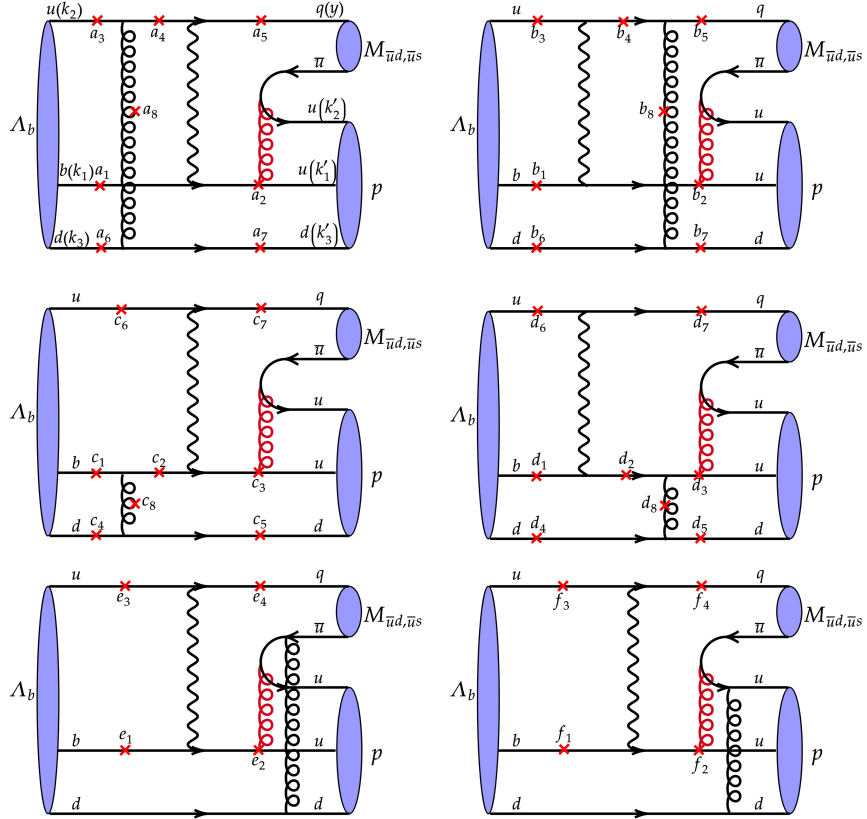
$$A = m_{\Lambda_b}^2 (x_2 + x_3) x'_3, \quad B = m_{\Lambda_b}^2 (x'_2 + x'_3) (-1 + x_2 + x_3 + y), \quad C = m_{\Lambda_b}^2 x_3 x'_3, \quad D = m_{\Lambda_b}^2 x'_2 (-1 + y). \quad (\text{B17})$$

The functions

$$\begin{aligned}
M_{E_2(a4)} &= \frac{G_F}{\sqrt{2}} \{ V_{ub} V_{uq}^* [f_1 C_1 + f_2 C_2] \} M_{E_2(a4)}^{LL}, \\
M_{PE_2(a4)} &= -\frac{G_F}{\sqrt{2}} \{ V_{tb} V_{tq}^* [f_1 C_3 + f_2 C_4 + f_1 C_9 + f_2 C_{10}] \} M_{E_2(a4)}^{LL} \\
&- \frac{G_F}{\sqrt{2}} \{ V_{tb} V_{tq}^* [-2f_1 C_5 - 2f_2 C_6 - 2f_1 C_7 - 2f_2 C_8] \} M_{E_2(a4)}^{SP}, \quad (\text{B18})
\end{aligned}$$

involve the color factors $f_1 = -8/3$ and $f_2 = -16/3$, and the matrix elements

$$\begin{aligned}
M_{E_2(a4)}^{LL} &\equiv \langle ph | (\bar{u}b)_{V-A} (\bar{q}u)_{V-A} | \Lambda_b \rangle_{E_2} \\
&= \Big\{ 8(-4m_{\Lambda_b}^4 \psi_4 T_1 x'_3 (-1 + x_2 + x_3 + y) \phi_m^A + m_{\Lambda_b}^3 (2m_p x'_3 (\psi_4(P_1 - S_1 + T_3 + T_7)(x'_2 + x'_3) \\
&+ (\psi_3^{-+} + \psi_3^{+-}) T_2 (-1 + x_2 + x_3 + y) \phi_m^A + m_0(\psi_3^{-+} + \psi_3^{+-})(A_1 - V_1)(x_2 + x_3)(-1 + x_2 + x_3 + y) \\
&(\phi_m^P - \phi_m^T)) + m_0 m_p^3 (\psi_3^{-+} + \psi_3^{+-})(A_6 - V_6) x'_3 (x'_2 + x'_3) (\phi_m^P + \phi_m^T) + m_0 m_p^2 m_{\Lambda_b} (A_4(\psi_3^{-+} + \psi_3^{+-}) x'_3 \\
&(-1 + x_2 + x_3 + y) (\phi_m^P - \phi_m^T) + \psi_3^{-+} V_4 x'_3 (-1 + x_2 + x_3 + y) (\phi_m^P - \phi_m^T) + \psi_3^{+-} V_4 x'_3 (-1 + x_2 + x_3 + y) \\
&(\phi_m^P - \phi_m^T) + 2A_4 \psi_2(x_2 + x_3)(x'_2 + x'_3) (\phi_m^P + \phi_m^T) - 2\psi_2 V_4(x_2 + x_3)(x'_2 + x'_3) (\phi_m^P + \phi_m^T) \\
&- 2\psi_4(A_5 + V_5) x'_3 (x'_2 + x'_3) (\phi_m^P + \phi_m^T)) + m_p m_{\Lambda_b}^2 (-m_p(\psi_3^{-+} + \psi_3^{+-})(P_2 + S_2 + T_4 - T_8) x'_3 (x'_2 + x'_3) \phi_m^A \\
&- 2m_0 \psi_2(A_2 + V_2)(-1 + x_2) x_2 \phi_m^P + m_0(A_3(\psi_3^{-+}(x_2 + x_3)(x'_2 + x'_3) + \psi_3^{+-}(x_2 + x_3)(x'_2 + x'_3) \\
&+ 2\psi_4 x'_3 (-1 + x_2 + x_3 + y) \phi_m^P + (2\psi_2(A_2 + V_2)x_3 + \psi_3^{+-} V_3(x_2 + x_3)(x'_2 + x'_3)) \\
&- 2(\psi_4 V_3 x'_3 (-1 + x_2 + x_3 + y) + \psi_2 V_2(x_3(2x_2 + x_3) + (x_2 + x_3)y) \\
&+ A_2 \psi_2(x_3(x_3 + y) + x_2(2x_3 + y))) \phi_m^P + A_3(\psi_3^{-+}(x_2 + x_3)(x'_2 + x'_3) + \psi_3^{+-}(x_2 + x_3)(x'_2 + x'_3) \\
&- 2\psi_4 x'_3 (-1 + x_2 + x_3 + y) \phi_m^T + (\psi_3^{+-} V_3(x_2 + x_3)(x'_2 + x'_3) + 2A_2 \psi_2(x_2 + x_3)(-1 + x_2 + x_3 + y)
\end{aligned}$$

FIG. 17: Feynman diagrams contributing to the E_2 topology.

$$\begin{aligned}
& + 2\psi_2 V_2(x_2 + x_3)(-1 + x_2 + x_3 + y) + 2\psi_4 V_3 x'_3(-1 + x_2 + x_3 + y)) \phi_m^T \\
& + \psi_3^{-+} V_3(x_2 + x_3)(x'_2 + x'_3)(\phi_m^P + \phi_m^T))) \Big\} \\
& + \Big\{ -8(4m_{\Lambda_b}^4 \psi_4 T_1 x'_3(-1 + x_2 + x_3 + y) \phi_m^A + m_{\Lambda_b}^3 (2m_p x'_3(\psi_4(P_1 - S_1 + T_3 + T_7)(x'_2 + x'_3) \\
& - (\psi_3^{-+} + \psi_3^{+-}) T_2(-1 + x_2 + x_3 + y)) \phi_m^A - m_0(\psi_3^{-+} + \psi_3^{+-})(A_1 - V_1)(x_2 + x_3)(-1 + x_2 + x_3 + y) \\
& (\phi_m^P - \phi_m^T)) + m_0 m_p^3 (\psi_3^{-+} + \psi_3^{+-})(A_6 - V_6)x'_3(x'_2 + x'_3)(\phi_m^P + \phi_m^T) + m_0 m_p^2 m_{\Lambda_b}(-A_4(\psi_3^{-+} + \psi_3^{+-})x'_3 \\
& (-1 + x_2 + x_3 + y)(\phi_m^P - \phi_m^T) - \psi_3^{-+} V_4 x'_3(-1 + x_2 + x_3 + y)(\phi_m^P - \phi_m^T) - \psi_3^{+-} V_4 x'_3(-1 + x_2 + x_3 + y) \\
& (\phi_m^P - \phi_m^T) + 2A_4 \psi_2(x_2 + x_3)(x'_2 + x'_3)(\phi_m^P + \phi_m^T) - 2\psi_2 V_4(x_2 + x_3)(x'_2 + x'_3)(\phi_m^P + \phi_m^T) \\
& - 2\psi_4(A_5 + V_5)x'_3(x'_2 + x'_3)(\phi_m^P + \phi_m^T)) + m_p m_{\Lambda_b}^2(-m_p(\psi_3^{-+} + \psi_3^{+-})(P_2 + S_2 + T_4 - T_8)x'_3(x'_2 + x'_3)\phi_m^A \\
& + 2m_0 \psi_2(A_2 + V_2)(-1 + x_2)x_2 \phi_m^P + m_0(A_3(\psi_3^{-+}(x_2 + x_3)(x'_2 + x'_3) + \psi_3^{+-}(x_2 + x_3)(x'_2 + x'_3) \\
& - 2\psi_4 x'_3(-1 + x_2 + x_3 + y)) \phi_m^P + (-2\psi_2(A_2 + V_2)x_3 + \psi_3^{+-} V_3(x_2 + x_3)(x'_2 + x'_3)) \\
& + 2(\psi_4 V_3 x'_3(-1 + x_2 + x_3 + y) + \psi_2 V_2(x_3(2x_2 + x_3) + (x_2 + x_3)y) \\
& + A_2 \psi_2(x_3(x_3 + y) + x_2(2x_3 + y))) \phi_m^P + A_3(\psi_3^{-+}(x_2 + x_3)(x'_2 + x'_3) + \psi_3^{+-}(x_2 + x_3)(x'_2 + x'_3) \\
& + 2\psi_4 x'_3(-1 + x_2 + x_3 + y)) \phi_m^T + (\psi_3^{+-} V_3(x_2 + x_3)(x'_2 + x'_3) - 2A_2 \psi_2(x_2 + x_3)(-1 + x_2 + x_3 + y) \\
& - 2\psi_2 V_2(x_2 + x_3)(-1 + x_2 + x_3 + y) - 2\psi_4 V_3 x'_3(-1 + x_2 + x_3 + y)) \phi_m^T \\
& + \psi_3^{-+} V_3(x_2 + x_3)(x'_2 + x'_3)(\phi_m^P + \phi_m^T))) \Big\} \gamma_5,
\end{aligned} \tag{B19}$$

$$\begin{aligned}
M_{E_2(a4)}^{SP} &\equiv \langle ph|(\bar{u}b)_{S-P}(\bar{q}u)_{S+P}|\Lambda_b\rangle_{E_2} \\
&= \left\{ -4m_p^3(x'_2 + x'_3)(m_{\Lambda_b}(\psi_3^{-+} + \psi_3^{+-})(A_6 - V_6)x'_3\phi_m^A - 4m_0\psi_2T_6(x_2 + x_3)(\phi_m^P - \phi_m^T)) \right. \\
&\quad - 4m_{\Lambda_b}^3(-A_1m_{\Lambda_b}(\psi_3^{-+} + \psi_3^{+-})(x_2 + x_3)(x'_2 + x'_3)\phi_m^A + m_{\Lambda_b}(\psi_3^{-+} + \psi_3^{+-})V_1(x_2 + x_3)(x'_2 + x'_3)\phi_m^A \\
&\quad - 4m_0\psi_4T_1x'_3(-1 + x_2 + x_3 + y)(\phi_m^P + \phi_m^T)) - 4m_p m_{\Lambda_b}^2(2m_{\Lambda_b}\psi_2(A_2 + V_2)(x_2 + x_3)(x'_2 + x'_3)\phi_m^A \\
&\quad + \psi_3^{-+}(A_3m_{\Lambda_b}(x_2 + x_3)(x'_2 + x'_3)\phi_m^A + m_{\Lambda_b}V_3(x_2 + x_3)(x'_2 + x'_3)\phi_m^A - m_0(2T_2x'_3 + (x_2 + x_3) \\
&\quad ((P_1 + S_1 - T_3 + T_7)x'_2 + (P_1 + S_1 - 2T_2 - T_3 + T_7)x'_3) - 2T_2x'_3y)\phi_m^P + m_0(-2T_2x'_3 + (x_2 + x_3) \\
&\quad ((P_1 + S_1 - T_3 + T_7)x'_2 + (P_1 + S_1 + 2T_2 - T_3 + T_7)x'_3) + 2T_2x'_3y)\phi_m^T) + \psi_3^{+-}(A_3m_{\Lambda_b}(x_2 + x_3)(x'_2 + x'_3)\phi_m^A \\
&\quad + m_{\Lambda_b}V_3(x_2 + x_3)(x'_2 + x'_3)\phi_m^A - m_0(2T_2x'_3 + (x_2 + x_3)((P_1 + S_1 - T_3 + T_7)x'_2 + (P_1 + S_1 - 2T_2 - T_3 + T_7)x'_3) \\
&\quad - 2T_2x'_3y)\phi_m^P + m_0(-2T_2x'_3 + (x_2 + x_3)((P_1 + S_1 - T_3 + T_7)x'_2 + (P_1 + S_1 + 2T_2 - T_3 + T_7)x'_3) + 2T_2x'_3y)\phi_m^T) \\
&\quad + 2\psi_4x'_3(-m_{\Lambda_b}(A_3 - V_3)(x'_2 + x'_3)\phi_m^A + m_0(P_1 - S_1 - T_3 - T_7)(-1 + x_2 + x_3 + y)(\phi_m^P + \phi_m^T)) \\
&\quad + 4m_p^2m_{\Lambda_b}(2m_{\Lambda_b}\psi_4(A_5 + V_5)x'_3(x'_2 + x'_3)\phi_m^A + 2\psi_2(x_2 + x_3)(x'_2 + x'_3)(m_{\Lambda_b}(-A_4 + V_4)\phi_m^A \\
&\quad - m_0(P_2 - S_2 - T_4 - T_8)(\phi_m^P - \phi_m^T)) + \psi_3^{-+}(A_4m_{\Lambda_b}x'_3(x'_2 + x'_3)\phi_m^A + m_{\Lambda_b}V_4x'_3(x'_2 + x'_3)\phi_m^A \\
&\quad - 2m_0T_5(x_2 + x_3)(x'_2 + x'_3)(\phi_m^P - \phi_m^T) + m_0(P_2 + S_2 - T_4 + T_8)x'_3(-1 + x_2 + x_3 + y)(\phi_m^P + \phi_m^T)) \\
&\quad + \psi_3^{+-}(A_4m_{\Lambda_b}x'_3(x'_2 + x'_3)\phi_m^A + m_{\Lambda_b}V_4x'_3(x'_2 + x'_3)\phi_m^A - 2m_0T_5(x_2 + x_3)(x'_2 + x'_3)(\phi_m^P - \phi_m^T) \\
&\quad + m_0(P_2 + S_2 - T_4 + T_8)x'_3(-1 + x_2 + x_3 + y)(\phi_m^P + \phi_m^T))) \right\} \\
&\quad + \left\{ 4(-m_p^3(x'_2 + x'_3)(m_{\Lambda_b}(\psi_3^{-+} + \psi_3^{+-})(A_6 - V_6)x'_3\phi_m^A - 4m_0\psi_2T_6(x_2 + x_3)(\phi_m^P - \phi_m^T)) \right. \\
&\quad + m_{\Lambda_b}^3(-A_1m_{\Lambda_b}(\psi_3^{-+} + \psi_3^{+-})(x_2 + x_3)(x'_2 + x'_3)\phi_m^A + m_{\Lambda_b}(\psi_3^{-+} + \psi_3^{+-})V_1(x_2 + x_3)(x'_2 + x'_3)\phi_m^A \\
&\quad - 4m_0\psi_4T_1x'_3(-1 + x_2 + x_3 + y)(\phi_m^P + \phi_m^T)) + m_p m_{\Lambda_b}^2(2m_{\Lambda_b}\psi_2(A_2 + V_2)(x_2 + x_3)(x'_2 + x'_3)\phi_m^A \\
&\quad - \psi_3^{-+}(A_3m_{\Lambda_b}(x_2 + x_3)(x'_2 + x'_3)\phi_m^A + m_{\Lambda_b}V_3(x_2 + x_3)(x'_2 + x'_3)\phi_m^A + m_0(2T_2x'_3 + (x_2 + x_3) \\
&\quad ((P_1 + S_1 - T_3 + T_7)x'_2 + (P_1 + S_1 - 2T_2 - T_3 + T_7)x'_3) - 2T_2x'_3y)\phi_m^P - m_0(-2T_2x'_3 + (x_2 + x_3) \\
&\quad ((P_1 + S_1 - T_3 + T_7)x'_2 + (P_1 + S_1 + 2T_2 - T_3 + T_7)x'_3) + 2T_2x'_3y)\phi_m^T) - \psi_3^{+-}(A_3m_{\Lambda_b}(x_2 + x_3)(x'_2 + x'_3)\phi_m^A \\
&\quad + m_{\Lambda_b}V_3(x_2 + x_3)(x'_2 + x'_3)\phi_m^A + m_0(2T_2x'_3 + (x_2 + x_3)((P_1 + S_1 - T_3 + T_7)x'_2 + (P_1 + S_1 - 2T_2 - T_3 + T_7)x'_3) \\
&\quad - 2T_2x'_3y)\phi_m^P - m_0(-2T_2x'_3 + (x_2 + x_3)((P_1 + S_1 - T_3 + T_7)x'_2 + (P_1 + S_1 + 2T_2 - T_3 + T_7)x'_3) + 2T_2x'_3y)\phi_m^T) \\
&\quad + 2\psi_4x'_3(-m_{\Lambda_b}(A_3 - V_3)(x'_2 + x'_3)\phi_m^A - m_0(P_1 - S_1 - T_3 - T_7)(-1 + x_2 + x_3 + y)(\phi_m^P + \phi_m^T)) \\
&\quad + m_p^2m_{\Lambda_b}(2m_{\Lambda_b}\psi_4(A_5 + V_5)x'_3(x'_2 + x'_3)\phi_m^A + 2\psi_2(x_2 + x_3)(x'_2 + x'_3)(m_{\Lambda_b}(-A_4 + V_4)\phi_m^A \\
&\quad + m_0(P_2 - S_2 - T_4 - T_8)(\phi_m^P - \phi_m^T)) - \psi_3^{-+}(A_4m_{\Lambda_b}x'_3(x'_2 + x'_3)\phi_m^A + m_{\Lambda_b}V_4x'_3(x'_2 + x'_3)\phi_m^A \\
&\quad + 2m_0T_5(x_2 + x_3)(x'_2 + x'_3)(\phi_m^P - \phi_m^T) - m_0(P_2 + S_2 - T_4 + T_8)x'_3(-1 + x_2 + x_3 + y)(\phi_m^P + \phi_m^T)) \\
&\quad - \psi_3^{+-}(A_4m_{\Lambda_b}x'_3(x'_2 + x'_3)\phi_m^A + m_{\Lambda_b}V_4x'_3(x'_2 + x'_3)\phi_m^A + 2m_0T_5(x_2 + x_3)(x'_2 + x'_3)(\phi_m^P - \phi_m^T) \\
&\quad - m_0(P_2 + S_2 - T_4 + T_8)x'_3(-1 + x_2 + x_3 + y)(\phi_m^P + \phi_m^T))) \right\} \gamma_5. \tag{B20}
\end{aligned}$$

We have, for the $B(c3)$ diagram in Fig. 18,

$$\begin{aligned}
\mathcal{A}_{B(c3)} &= \frac{-1}{128N_c^2\sqrt{2N_c}} \int [dx] \int [dx'] \int dy \frac{1}{(2\pi)^5} \int b_1 db_1 \int b_3 db_3 \int b'_2 db'_2 (4\pi\alpha_s(t^{B(c3)}))^2 \\
&\quad (M_{B(c3)} + M_{PB(c3)}) F_1(C, b_1 - b'_2) F_3(D, B, A, b_1, b_3, b'_2) \exp[-S^{B(c3)}([x], [x'], y, [b], [b'], b_q)], \tag{B21}
\end{aligned}$$

with the arguments

$$A = m_{\Lambda_b}^2 x'_2 (-1 + x_2 + y), \quad B = m_{\Lambda_b}^2 (-1 + x_2)(x'_2 - x_3), \quad C = m_{\Lambda_b}^2 x'_2 (-1 + y), \quad D = m_{\Lambda_b}^2 x_3 y. \quad (\text{B22})$$

The functions

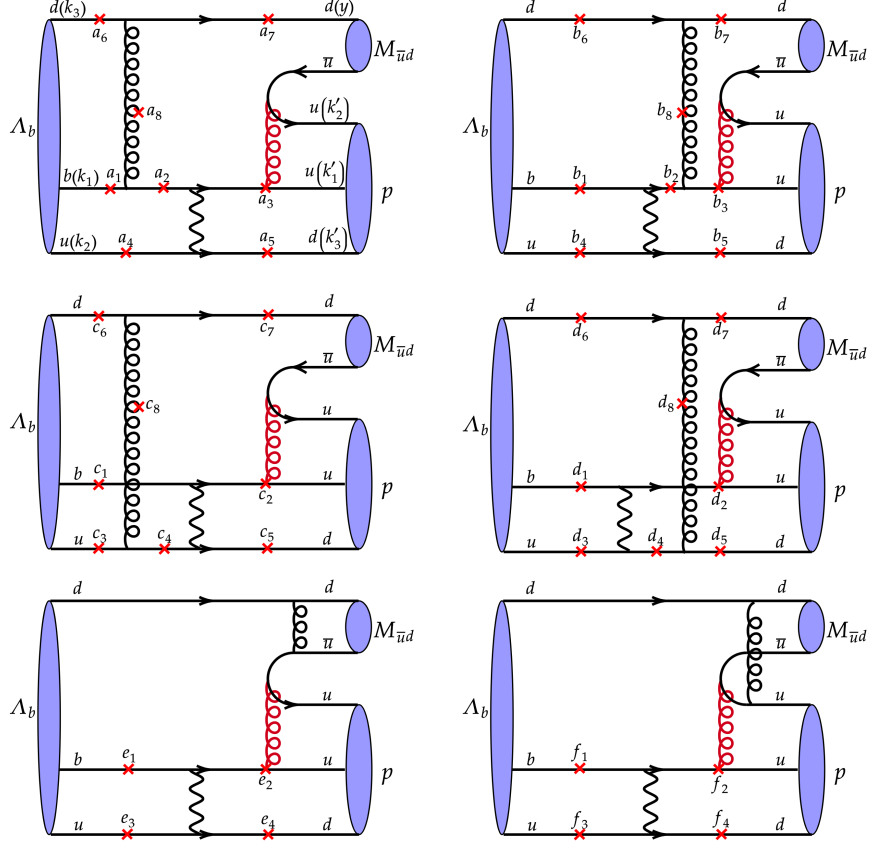


FIG. 18: Feynman diagrams contributing to the B topology.

$$\begin{aligned} M_{B(c3)} &= \frac{G_F}{\sqrt{2}} \{ V_{ub} V_{ud}^* [f_1 C_1 + f_2 C_2] \} M_{B(c3)}^{LL}, \\ M_{PB(c3)} &= -\frac{G_F}{\sqrt{2}} \{ V_{tb} V_{td}^* [f_1 C_3 + f_2 C_4 + f_2 C_9 + f_2 C_{10}] \} M_{B(c3)}^{LL} \\ &\quad - \frac{G_F}{\sqrt{2}} \{ V_{tb} V_{td}^* [-2f_1 C_5 - 2f_2 C_6 - 2f_1 C_7 - 2f_2 C_8] \} M_{B(c3)}^{SP}, \end{aligned} \quad (\text{B23})$$

contain the color factors $f_1 = -10/3$ and $f_2 = 10/3$, and the matrix elements

$$\begin{aligned} M_{B(c3)}^{LL} &\equiv \langle ph | (\bar{u}b)_{V-A} (\bar{d}u)_{V-A} | \Lambda_b \rangle_{B(c3)} \\ &= \left\{ 8m_p m_{\Lambda_b} (-2m_{\Lambda_b}^2 \psi_4 (A_2 + A_3 - V_2 + V_3) x'_2 (x'_2 - x_3) \phi_m^A - m_0 m_{\Lambda_b} \psi_3^{-+} (A_2 + A_3 - V_2 + V_3) (x'_2 - x_3) \right. \\ &\quad \left. (-1 + x_2 + y) (\phi_m^P - \phi_m^T) - 2m_0 m_{\Lambda_b} \psi_2 (P_1 + S_1 + 2T_2 + T_3 - T_7) (-1 + x_2) (-1 + x_2 + y) (\phi_m^P + \phi_m^T) \right. \\ &\quad \left. - m_p x'_2 (-2m_{\Lambda_b} \psi_2 (A_4 + A_5 + V_4 - V_5) (-1 + x_2) \phi_m^A + m_{\Lambda_b} \psi_3^{+-} (P_2 + S_2 + T_4 + 2T_5 - T_8) \right. \\ &\quad \left. (x'_2 - x_3) \phi_m^A + 2m_0 \psi_4 (P_2 + S_2 + T_4 + 2T_5 - T_8) (x'_2 - x_3) (\phi_m^P - \phi_m^T) \right\} \end{aligned}$$

$$\begin{aligned}
& + m_0 \psi_3^{+-} (A_4 + A_5 + V_4 - V_5) (-1 + x_2) (\phi_m^P + \phi_m^T)) \Big\} \\
& + \left\{ 8m_p m_{\Lambda_b} (2m_{\Lambda_b}^2 \psi_4 (A_2 + A_3 - V_2 + V_3) x'_2 (x'_2 - x_3) \phi_m^A + m_0 m_{\Lambda_b} \psi_3^{-+} (A_2 + A_3 - V_2 + V_3) (x'_2 - x_3) \right. \\
& (-1 + x_2 + y) (\phi_m^P - \phi_m^T) - 2m_0 m_{\Lambda_b} \psi_2 (P_1 + S_1 + 2T_2 + T_3 - T_7) (-1 + x_2) (-1 + x_2 + y) (\phi_m^P + \phi_m^T) \\
& - m_p x'_2 (-2m_{\Lambda_b} \psi_2 (A_4 + A_5 + V_4 - V_5) (-1 + x_2) \phi_m^A - m_{\Lambda_b} \psi_3^{+-} (P_2 + S_2 + T_4 + 2T_5 - T_8) \\
& (x'_2 - x_3) \phi_m^A - 2m_0 \psi_4 (P_2 + S_2 + T_4 + 2T_5 - T_8) (x'_2 - x_3) (\phi_m^P - \phi_m^T) \\
& \left. + m_0 \psi_3^{+-} (A_4 + A_5 + V_4 - V_5) (-1 + x_2) (\phi_m^P + \phi_m^T)) \right\} \gamma_5, \tag{B24}
\end{aligned}$$

$$\begin{aligned}
M_{B(c3)}^{SP} & \equiv \langle ph | (\bar{u}b)_{S-P} (\bar{d}u)_{S+P} | \Lambda_b \rangle_{B(c3)} \\
= & \left\{ 8m_p^3 T_6 x'_2 (x'_2 - x_3) (m_{\Lambda_b} \psi_3^{+-} \phi_m^A + 2m_0 \psi_4 (\phi_m^P - \phi_m^T)) + 16m_0 m_{\Lambda_b}^3 \psi_2 T_1 (-1 + x_2) (-1 + x_2 + y) \right. \\
& (\phi_m^P + \phi_m^T) - 4m_p^2 m_{\Lambda_b} (-2m_{\Lambda_b} \psi_2 (A_5 + V_5) (-1 + x_2) x'_2 \phi_m^A + 2\psi_4 x'_2 (x'_2 - x_3) (A_4 m_{\Lambda_b} \phi_m^A - m_{\Lambda_b} V_4 \phi_m^A \\
& + m_0 (P_2 - S_2 - T_4 - T_8) (\phi_m^P - \phi_m^T)) + m_0 \psi_3^{-+} (A_4 - V_4) (x'_2 - x_3) (-1 + x_2 + y) (\phi_m^P - \phi_m^T) \\
& + \psi_3^{+-} x'_2 (m_{\Lambda_b} (P_2 - S_2 - T_4 - T_8) (x'_2 - x_3) \phi_m^A + m_0 (A_5 + V_5) (-1 + x_2) (\phi_m^P + \phi_m^T)) \\
& - 4m_p m_{\Lambda_b}^2 (2m_{\Lambda_b} \psi_4 (A_2 + V_2) x'_2 (x'_2 - x_3) \phi_m^A + m_0 \psi_3^{-+} (A_2 + V_2) (x'_2 - x_3) (-1 + x_2 + y) (\phi_m^P - \phi_m^T) \\
& + m_0 \psi_3^{+-} (A_3 - V_3) (-1 + x_2) x'_2 (\phi_m^P + \phi_m^T) + 2\psi_2 (-1 + x_2) (-A_3 m_{\Lambda_b} x'_2 \phi_m^A + m_{\Lambda_b} V_3 x'_2 \phi_m^A \\
& + m_0 (P_1 - S_1 - T_3 - T_7) (-1 + x_2 + y) (\phi_m^P + \phi_m^T)) \Big\} \\
& + \left\{ 8m_p^3 T_6 x'_2 (x'_2 - x_3) (m_{\Lambda_b} \psi_3^{+-} \phi_m^A + 2m_0 \psi_4 (\phi_m^P - \phi_m^T)) - 16m_0 m_{\Lambda_b}^3 \psi_2 T_1 (-1 + x_2) (-1 + x_2 + y) \right. \\
& (\phi_m^P + \phi_m^T) - 4m_p^2 m_{\Lambda_b} (-2m_{\Lambda_b} \psi_2 (A_5 + V_5) (-1 + x_2) x'_2 \phi_m^A + 2\psi_4 x'_2 (x'_2 - x_3) (A_4 m_{\Lambda_b} \phi_m^A - m_{\Lambda_b} V_4 \phi_m^A \\
& - m_0 (P_2 - S_2 - T_4 - T_8) (\phi_m^P - \phi_m^T)) + m_0 \psi_3^{-+} (A_4 - V_4) (x'_2 - x_3) (-1 + x_2 + y) (\phi_m^P - \phi_m^T) \\
& + \psi_3^{+-} x'_2 (m_{\Lambda_b} (-P_2 + S_2 + T_4 + T_8) (x'_2 - x_3) \phi_m^A + m_0 (A_5 + V_5) (-1 + x_2) (\phi_m^P + \phi_m^T)) \\
& + 4m_p m_{\Lambda_b}^2 (2m_{\Lambda_b} \psi_4 (A_2 + V_2) x'_2 (x'_2 - x_3) \phi_m^A + m_0 \psi_3^{-+} (A_2 + V_2) (x'_2 - x_3) (-1 + x_2 + y) (\phi_m^P - \phi_m^T) \\
& + m_0 \psi_3^{+-} (A_3 - V_3) (-1 + x_2) x'_2 (\phi_m^P + \phi_m^T) - 2\psi_2 (-1 + x_2) (A_3 m_{\Lambda_b} x'_2 \phi_m^A - m_{\Lambda_b} V_3 x'_2 \phi_m^A \\
& \left. + m_0 (P_1 - S_1 - T_3 - T_7) (-1 + x_2 + y) (\phi_m^P + \phi_m^T)) \right\} \gamma_5. \tag{B25}
\end{aligned}$$

The formula for the $PE_1^d(c2)$ diagram in Fig. 19 is written as

$$\begin{aligned}
\mathcal{A}_{PE_1^d(c2)} = & \frac{-1}{128N_c^2} \frac{1}{\sqrt{2N_c}} \int [dx] \int [dx'] \int dy \frac{1}{(2\pi)^5} \int b_1 db_1 \int b_2 db_2 \int b_q db_q (4\pi\alpha_s(t^{PE_1^d(c2)}))^2 \\
& M_{PE_1^d(c2)} F_1(D, b_3) F_3(A, B, C, b_1, b_2, b_q) \exp[-S^{PE_1^d(c2)}([x], [x'], y, [b], [b'], b_q)], \tag{B26}
\end{aligned}$$

with the arguments

$$A = m_{\Lambda_b}^2 x'_2 (x_2 + x_3), \quad B = m_{\Lambda_b}^2 (x'_1 + x'_2) (-1 + x_2 + x_3 + y), \quad C = m_{\Lambda_b}^2 x'_1 (-1 + y), \quad D = m_{\Lambda_b}^2 x_2 x'_2. \tag{B27}$$

The functions

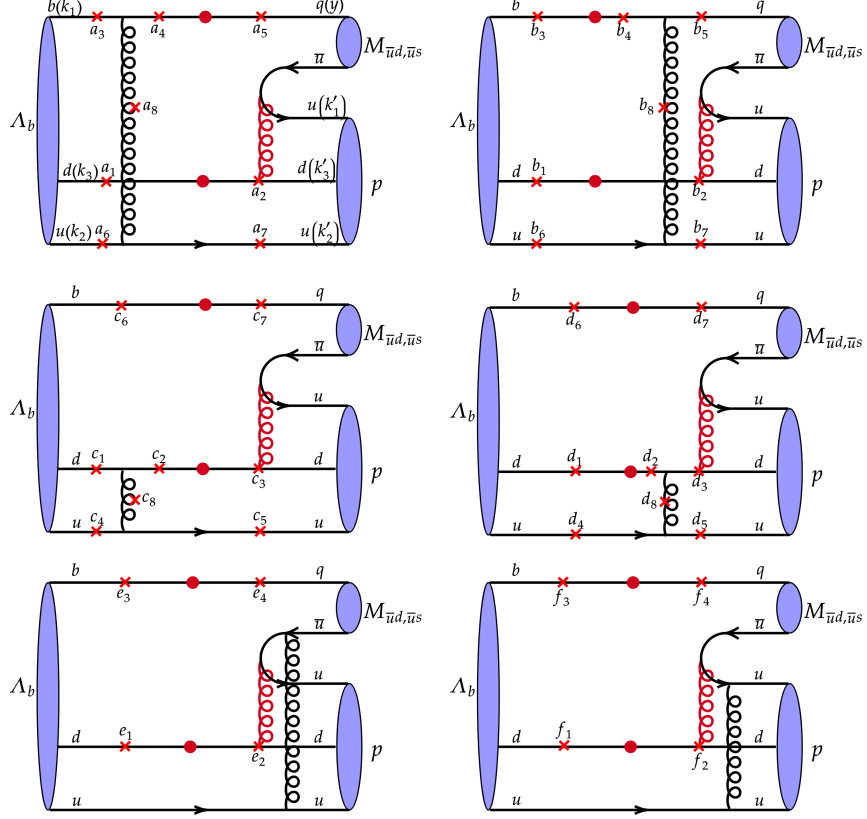


FIG. 19: Feynman diagrams in the PE_1^d topology, which also contribute to the PE_2 topology after the Feriz transformation.

$$\begin{aligned}
 M_{PE_1^d(c2)}^{p\pi} = & -\frac{G_F}{\sqrt{2}} \left\{ V_{tb} V_{td}^* \left[(f_1 + f_2)(C_3 + C_4 - \frac{1}{2}C_9 - \frac{1}{2}C_{10}) \right] \right\} M_{PE_1^d(c2)}^{LL} \\
 & -\frac{G_F}{\sqrt{2}} \left\{ V_{tb} V_{td}^* \left[f_1 C_5 + f_2 C_6 - \frac{1}{2}f_1 C_7 - \frac{1}{2}f_2 C_8 \right] \right\} M_{PE_1^d(c2)}^{LR} \\
 & -\frac{G_F}{\sqrt{2}} \{ V_{tb} V_{td}^* [-2f_2 C_5 - 2f_1 C_6 + f_2 C_7 + f_1 C_8] \} M_{PE_1^d(c2)}^{SP},
 \end{aligned} \tag{B28}$$

$$\begin{aligned}
 M_{PE_1^d(c2)}^{pK} = & -\frac{G_F}{\sqrt{2}} \left\{ V_{tb} V_{ts}^* \left[(f_1 C_3 + f_2 C_4 - \frac{1}{2}f_1 C_9 - \frac{1}{2}f_2 C_{10}) \right] \right\} M_{PE_1^d(c2)}^{LL} \\
 & -\frac{G_F}{\sqrt{2}} \left\{ V_{tb} V_{ts}^* \left[f_1 C_5 + f_2 C_6 - \frac{1}{2}f_1 C_7 - \frac{1}{2}f_2 C_8 \right] \right\} M_{PE_1^d(c2)}^{LR}.
 \end{aligned} \tag{B29}$$

contain the color factors $f_1 = 8/3$ and $f_2 = 16/3$, and the matrix elements

$$\begin{aligned}
 M_{PE_1^d(c2)}^{LL} \equiv & \langle ph | (\bar{d}b)_{V-A} (\bar{d}d)_{V-A} | \Lambda_b \rangle_{PE_1^d(c2)} \\
 = & \left\{ -8m_{\Lambda_b}^3 (-1 + x_2 + x_3 + y) (2A_1 m_{\Lambda_b} \psi_4 x'_2 \phi_m^A - 2m_{\Lambda_b} \psi_4 V_1 x'_2 \phi_m^A + A_1 m_0 (\psi_3^{-+} + \psi_3^{+-}) (x_2 + x_3) (\phi_m^P - \phi_m^T) \right. \\
 & + m_0 (\psi_3^{-+} + \psi_3^{+-}) V_1 (x_2 + x_3) (\phi_m^P - \phi_m^T) - 8m_0 m_p^3 (\psi_3^{-+} + \psi_3^{+-}) (A_6 + V_6) x'_2 (x'_1 + x'_2) (\phi_m^P + \phi_m^T) \\
 & + 8m_p m_{\Lambda_b}^2 (m_{\Lambda_b} x'_2 (-2\psi_4 (A_3 + V_3) (x'_1 + x'_2) + (\psi_3^{-+} + \psi_3^{+-}) (P_1 + S_1 - T_3 + T_7) (-1 + x_2 + x_3 + y)) \phi_m^A \\
 & + m_0 (2\psi_2 (\phi_m^P - \phi_m^T) (P_1 - S_1 + T_3 + T_7) (x_2 + x_3) (-1 + x_2 + x_3 + y) \\
 & \left. + (\psi_3^{+-} + \psi_3^{-+}) (\phi_m^P + \phi_m^T) (A_2 + V_2) (x_2 + x_3) (x'_1 + x'_2) - 2\psi_4 (\phi_m^P - \phi_m^T) (P_1 - S_1 - T_3 - T_7) \right)
 \end{aligned}$$

$$\begin{aligned}
& x'_2(-1 + x_2 + x_3 + y)) + 8m_p^2 m_{\Lambda_b} (2m_{\Lambda_b}(\psi_3^{-+} + \psi_3^{+-}) T_5 x'_2(x'_1 + x'_2) \phi_m^A \\
& + m_0(2\psi_2(S_2 + T_4 + T_8)(x'_1 + x'_2)(x_2 + x_3)(\phi_m^P + \phi_m^T) - 2P_2(x'_1 + x'_2)(-\psi_4 x'_2 + \psi_2(x_2 + x_3))(\phi_m^P + \phi_m^T) \\
& + x'_2(-2\psi_4(S_2 - T_4 - T_8)(x'_1 + x'_2)\phi_m^P + (\psi_3^{-+} + \psi_3^{+-})(A_5 + V_5)(-1 + x_2 + x_3 + y)\phi_m^P \\
& - 2\psi_4(S_2 - T_4 - T_8)(x'_1 + x'_2)\phi_m^T - (\psi_3^{-+} + \psi_3^{+-})(A_5 + V_5)(-1 + x_2 + x_3 + y)\phi_m^T)) \\
& + \left\{ -8m_{\Lambda_b}^3(-1 + x_2 + x_3 + y)(2A_1 m_{\Lambda_b} \psi_4 x'_2 \phi_m^A - 2m_{\Lambda_b} \psi_4 V_1 x'_2 \phi_m^A + A_1 m_0(\psi_3^{-+} + \psi_3^{+-})(x_2 + x_3)(\phi_m^P - \phi_m^T) \right. \\
& + m_0(\psi_3^{-+} + \psi_3^{+-})V_1(x_2 + x_3)(\phi_m^P - \phi_m^T) + 8m_0 m_p^3(\psi_3^{-+} + \psi_3^{+-})(A_6 + V_6)x'_2(x'_1 + x'_2)(\phi_m^P + \phi_m^T) \\
& - 8m_p m_{\Lambda_b}^2(-m_{\Lambda_b} x'_2(2\psi_4(A_3 + V_3)(x'_1 + x'_2) + (\psi_3^{-+} + \psi_3^{+-})(P_1 + S_1 - T_3 + T_7)(-1 + x_2 + x_3 + y))\phi_m^A \\
& + m_0(-2\psi_2(\phi_m^P - \phi_m^T)(P_1 - S_1 + T_3 + T_7)(x_2 + x_3)(-1 + x_2 + x_3 + y) \\
& + (\psi_3^{+-} + \psi_3^{-+})(\phi_m^P + \phi_m^T)(A_2 + V_2)(x_2 + x_3)(x'_1 + x'_2) + 2\psi_4(\phi_m^P - \phi_m^T)(P_1 - S_1 - T_3 - T_7) \\
& x'_2(-1 + x_2 + x_3 + y)) - 8m_p^2 m_{\Lambda_b} (2m_{\Lambda_b}(\psi_3^{-+} + \psi_3^{+-}) T_5 x'_2(x'_1 + x'_2) \phi_m^A \\
& + m_0(2\psi_2(S_2 + T_4 + T_8)(x'_1 + x'_2)(x_2 + x_3)(\phi_m^P + \phi_m^T) - 2P_2(x'_1 + x'_2)(-\psi_4 x'_2 + \psi_2(x_2 + x_3))(\phi_m^P + \phi_m^T) \\
& + x'_2(-2\psi_4(S_2 - T_4 - T_8)(x'_1 + x'_2)\phi_m^P - (\psi_3^{-+} + \psi_3^{+-})(A_5 + V_5)(-1 + x_2 + x_3 + y)\phi_m^P \\
& \left. - 2\psi_4(S_2 - T_4 - T_8)(x'_1 + x'_2)\phi_m^T + (\psi_3^{-+} + \psi_3^{+-})(A_5 + V_5)(-1 + x_2 + x_3 + y)\phi_m^T)) \right\} \gamma_5, \quad (B30)
\end{aligned}$$

$$\begin{aligned}
M_{PE_1^d(c2)}^{LR} & \equiv \langle ph | (\bar{d}b)_{V-A} (\bar{d}d)_{V-A} | \Lambda_b \rangle_{PE_1^d(c2)} \\
= & \left\{ -8m_p^3(x'_1 + x'_2)(A_6 m_{\Lambda_b}(\psi_3^{-+} + \psi_3^{+-}) x'_2 \phi_m^A + m_{\Lambda_b}(\psi_3^{-+} + \psi_3^{+-}) V_6 x'_2 \phi_m^A + 2A_6 m_0 \psi_2(x_2 + x_3) \right. \\
& (\phi_m^P - \phi_m^T) - 2m_0 \psi_2 V_6(x_2 + x_3)(\phi_m^P - \phi_m^T) + 8m_{\Lambda_b}^3(A_1 m_{\Lambda_b}(\psi_3^{-+} + \psi_3^{+-})(x'_1 + x'_2)(x_2 + x_3)\phi_m^A \\
& + m_{\Lambda_b}(\psi_3^{-+} + \psi_3^{+-})V_1(x'_1 + x'_2)(x_2 + x_3)\phi_m^A - 2A_1 m_0 \psi_4 x'_2(-1 + x_2 + x_3 + y)(\phi_m^P + \phi_m^T) \\
& + 2m_0 \psi_4 V_1 x'_2(-1 + x_2 + x_3 + y)(\phi_m^P + \phi_m^T) - 8m_p^2 m_{\Lambda_b}(m_{\Lambda_b}(x'_1 + x'_2)(-2P_2 \psi_4 x'_2 + 2\psi_4(S_2 \\
& - T_4 - T_8)x'_2 + (\psi_3^{-+} + \psi_3^{+-})(A_5 + V_5)x'_2 + 2P_2 \psi_2(x_2 + x_3) - 2\psi_2(S_2 + T_4 + T_8)(x_2 + x_3))\phi_m^A \\
& + m_0(2\psi_2(\phi_m^P - \phi_m^T)(A_5 - V_5)(x'_1 + x'_2)(x_2 + x_3) - (\psi_3^{+-} + \psi_3^{-+})(P_2 + S_2)(x'_2(-1 + 2x_2 + 2x_3 + y)\phi_m^P \\
& + x'_1(x_2 + x_3)(\phi_m^P - \phi_m^T) + x'_2(-1 + y)\phi_m^T) + (\psi_3^{+-} + \psi_3^{-+})(T_4 - T_8)(x'_1(x_2 + x_3)(\phi_m^P - \phi_m^T) \\
& + x'_2(\phi_m^P - y\phi_m^P - (-1 + 2x_2 + 2x_3 + y)\phi_m^T))) + 8m_p m_{\Lambda_b}^2(m_{\Lambda_b}(x'_1 + x'_2)(2\psi_2 S_1 x_2 - 2\psi_2 T_3 x_2 \\
& - \psi_3^{-+} V_2 x_2 + \psi_3^{+-} V_2 x_2 + 2P_1 \psi_4 x'_2 - 2\psi_4 S_1 x'_2 - 2\psi_4 T_3 x'_2 - 2\psi_4 T_7 x'_2 + 2\psi_2(S_1 - T_3 - T_7)x_3 \\
& + (\psi_3^{-+} + \psi_3^{+-})V_2 x_3 - 2P_1 \psi_2(x_2 + x_3) + A_2(\psi_3^{-+} + \psi_3^{+-})(x_2 + x_3))\phi_m^A \\
& + m_0(-2\psi_4(\phi_m^P + \phi_m^T)(A_2 - V_2)x'_2(-1 + x_2 + x_3 + y) + (\psi_3^{+-} + \psi_3^{-+})(P_1 + S_1)(x'_2(-1 + 2x_2 + 2x_3 + y)\phi_m^P \\
& + x'_1(x_2 + x_3)(\phi_m^P - \phi_m^T) + x'_2(-1 + y)\phi_m^T) + (\psi_3^{+-} + \psi_3^{-+})(T_3 - T_7)(x'_1(x_2 + x_3)(\phi_m^P - \phi_m^T) \\
& \left. + x'_2(\phi_m^P - y\phi_m^P - (-1 + 2x_2 + 2x_3 + y)\phi_m^T))) \right\} \\
& + \left\{ -8m_p^3(x'_1 + x'_2)(A_6 m_{\Lambda_b}(\psi_3^{-+} + \psi_3^{+-}) x'_2 \phi_m^A + m_{\Lambda_b}(\psi_3^{-+} + \psi_3^{+-}) V_6 x'_2 \phi_m^A + 2A_6 m_0 \psi_2(x_2 + x_3) \right. \\
& (\phi_m^P - \phi_m^T) - 2m_0 \psi_2 V_6(x_2 + x_3)(\phi_m^P - \phi_m^T) - 8m_{\Lambda_b}^3(A_1 m_{\Lambda_b}(\psi_3^{-+} + \psi_3^{+-})(x'_1 + x'_2)(x_2 + x_3)\phi_m^A \\
& + m_{\Lambda_b}(\psi_3^{-+} + \psi_3^{+-})V_1(x'_1 + x'_2)(x_2 + x_3)\phi_m^A - 2A_1 m_0 \psi_4 x'_2(-1 + x_2 + x_3 + y)(\phi_m^P + \phi_m^T) \\
& + 2m_0 \psi_4 V_1 x'_2(-1 + x_2 + x_3 + y)(\phi_m^P + \phi_m^T) + 8m_p^2 m_{\Lambda_b}(m_{\Lambda_b}(x'_1 + x'_2)(2P_2 \psi_4 x'_2 + 2\psi_4(-S_2 \\
& + T_4 + T_8)x'_2 + (\psi_3^{-+} + \psi_3^{+-})(A_5 + V_5)x'_2 - 2P_2 \psi_2(x_2 + x_3) + 2\psi_2(S_2 + T_4 + T_8)(x_2 + x_3))\phi_m^A \\
& + m_0(2\psi_2(\phi_m^P - \phi_m^T)(A_5 - V_5)(x'_1 + x'_2)(x_2 + x_3) + (\psi_3^{+-} + \psi_3^{-+})(P_2 + S_2)(x'_2(-1 + 2x_2 + 2x_3 + y)\phi_m^P \\
& + x'_1(x_2 + x_3)(\phi_m^P - \phi_m^T) + x'_2(-1 + y)\phi_m^T) - (\psi_3^{+-} + \psi_3^{-+})(T_4 - T_8)(x'_1(x_2 + x_3)(\phi_m^P - \phi_m^T) \\
& \left. + x'_2(\phi_m^P - y\phi_m^P - (-1 + 2x_2 + 2x_3 + y)\phi_m^T))) + 8m_p m_{\Lambda_b}^2(m_{\Lambda_b}(x'_1 + x'_2)(A_2 \psi_3^{-+} x_2 + A_2 \psi_3^{+-} x_2 - 2\psi_2 S_1 x_2 \right.
\end{aligned}$$

$$\begin{aligned}
& + 2\psi_2 T_3 x_2 + 2\psi_2 T_7 x_2 \\
& + \psi_3^{-+} V_2 x_2 + \psi_3^{+-} V_2 x_2 - 2P_1 \psi_4 x'_2 + 2\psi_4 S_1 x'_2 + 2\psi_4 T_3 x'_2 + 2\psi_4 T_7 x'_2 + 2\psi_2 (-S_1 + T_3 + T_7) x_3 \\
& + (\psi_3^{-+} + \psi_3^{+-})(A_2 + V_2) x_3 + 2P_1 \psi_2 (x_2 + x_3)) \phi_m^A \\
& - m_0 (2\psi_4 (\phi_m^P + \phi_m^T) (A_2 - V_2) x'_2 (-1 + x_2 + x_3 + y) + (\psi_3^{+-} + \psi_3^{-+}) (P_1 + S_1) (x'_2 (-1 + 2x_2 + 2x_3 + y) \phi_m^P \\
& + x'_1 (x_2 + x_3) (\phi_m^P - \phi_m^T) + x'_2 (-1 + y) \phi_m^T) + (\psi_3^{+-} + \psi_3^{-+}) (T_3 - T_7) (x'_1 (x_2 + x_3) (\phi_m^P - \phi_m^T) \\
& + x'_2 (\phi_m^P - y \phi_m^P - (-1 + 2x_2 + 2x_3 + y) \phi_m^T))) \Big\} \gamma_5, \tag{B31}
\end{aligned}$$

$$\begin{aligned}
M_{PE_1^d(c2)}^{SP} & \equiv \langle ph | (\bar{d}b)_{S-P} (\bar{d}d)_{S+P} | \Lambda_b \rangle_{PE_1^d(c2)}, \\
& = \Big\{ -4m_{\Lambda_b}^3 (-1 + x_2 + x_3 + y) (2A_1 m_{\Lambda_b} \psi_4 x'_2 \phi_m^A + 2m_{\Lambda_b} \psi_4 V_1 x'_2 \phi_m^A + A_1 m_0 (\psi_3^{-+} + \psi_3^{+-}) (x_2 + x_3) \\
& (\phi_m^P - \phi_m^T) + m_0 (\psi_3^{-+} + \psi_3^{+-}) V_1 (x_2 + x_3) (-\phi_m^P + \phi_m^T)) - 4m_p^3 (\psi_3^{-+} + \psi_3^{+-}) x'_2 (x'_1 + x'_2) (2m_{\Lambda_b} T_6 \phi_m^A \\
& + m_0 (A_6 - V_6) (\phi_m^P + \phi_m^T)) + 4m_p m_{\Lambda_b}^2 (m_{\Lambda_b} (\psi_3^{-+} + \psi_3^{+-}) (P_1 - S_1 + T_3 + T_7) x'_2 (-1 + x_2 + x_3 + y) \phi_m^P \\
& + m_0 (2\psi_2 (P_1 + S_1 - T_3 + T_7) (x_2 + x_3) (-1 + x_2 + x_3 + y) (\phi_m^P - \phi_m^T) + (\psi_3^{+-} + \psi_3^{-+}) (\phi_m^P + \phi_m^T) \\
& (A_2 - V_2) (x'_1 + x'_2) (x_2 + x_3) - 2\psi_4 (\phi_m^P - \phi_m^T) (P_1 + S_1 + T_3 - T_7) x'_2 (-1 + x_2 + x_3 + y))) \\
& - 4m_p^2 m_{\Lambda_b} (2A_4 m_{\Lambda_b} \psi_4 x'_2 (x'_1 + x'_2) \phi_m^A - 2m_{\Lambda_b} \psi_4 V_4 x'_2 (x'_1 + x'_2) \phi_m^A \\
& + m_0 (2\psi_2 (S_2 + T_4 - T_8) (x'_1 + x'_2) (x_2 + x_3) (\phi_m^P + \phi_m^T) + 2P_2 (x'_1 + x'_2) (-\psi_4 x'_2 + \psi_2 (x_2 + x_3)) (\phi_m^P + \phi_m^T) \\
& - x'_2 (2\psi_4 (S_2 - T_4 + T_8) (x'_1 + x'_2) \phi_m^P + (\psi_3^{-+} + \psi_3^{+-}) (A_5 - V_5) (-1 + x_2 + x_3 + y) \phi_m^P \\
& + 2\psi_4 (S_2 - T_4 + T_8) (x'_1 + x'_2) \phi_m^T - (\psi_3^{-+} + \psi_3^{+-}) (A_5 - V_5) (-1 + x_2 + x_3 + y) \phi_m^T))) \Big\} \\
& + \Big\{ -4m_{\Lambda_b}^3 (-1 + x_2 + x_3 + y) (2A_1 m_{\Lambda_b} \psi_4 x'_2 \phi_m^A + 2m_{\Lambda_b} \psi_4 V_1 x'_2 \phi_m^A + A_1 m_0 (\psi_3^{-+} + \psi_3^{+-}) (x_2 + x_3) \\
& (\phi_m^P - \phi_m^T) + m_0 (\psi_3^{-+} + \psi_3^{+-}) V_1 (x_2 + x_3) (-\phi_m^P + \phi_m^T)) - 4m_p^3 (\psi_3^{-+} + \psi_3^{+-}) x'_2 (x'_1 + x'_2) (2m_{\Lambda_b} T_6 \phi_m^A \\
& - m_0 (A_6 - V_6) (\phi_m^P + \phi_m^T)) + 4m_p m_{\Lambda_b}^2 (m_{\Lambda_b} (\psi_3^{-+} + \psi_3^{+-}) (P_1 - S_1 + T_3 + T_7) x'_2 (-1 + x_2 + x_3 + y) \phi_m^A \\
& + m_0 (2\psi_2 (P_1 + S_1 - T_3 + T_7) (x_2 + x_3) (-1 + x_2 + x_3 + y) (\phi_m^P - \phi_m^T) - (\psi_3^{+-} + \psi_3^{-+}) (\phi_m^P + \phi_m^T) \\
& (A_2 - V_2) (x'_1 + x'_2) (x_2 + x_3) - 2\psi_4 (\phi_m^P - \phi_m^T) (P_1 + S_1 + T_3 - T_7) x'_2 (-1 + x_2 + x_3 + y))) \\
& - 4m_p^2 m_{\Lambda_b} (2A_4 m_{\Lambda_b} \psi_4 x'_2 (x'_1 + x'_2) \phi_m^A - 2m_{\Lambda_b} \psi_4 V_4 x'_2 (x'_1 + x'_2) \phi_m^A \\
& + m_0 (-2\psi_2 (S_2 + T_4 - T_8) (x'_1 + x'_2) (x_2 + x_3) (\phi_m^P + \phi_m^T) - 2P_2 (x'_1 + x'_2) (-\psi_4 x'_2 + \psi_2 (x_2 + x_3)) (\phi_m^P + \phi_m^T) \\
& + x'_2 (2\psi_4 (S_2 - T_4 + T_8) (x'_1 + x'_2) \phi_m^P - (\psi_3^{-+} + \psi_3^{+-}) (A_5 - V_5) (-1 + x_2 + x_3 + y) \phi_m^P \\
& + 2\psi_4 (S_2 - T_4 + T_8) (x'_1 + x'_2) \phi_m^T + (\psi_3^{-+} + \psi_3^{+-}) (A_5 - V_5) (-1 + x_2 + x_3 + y) \phi_m^T))) \Big\} \gamma_5. \tag{B32}
\end{aligned}$$

Appendix C: Numerical results for $\Lambda_b \rightarrow pV, pA$ decays

The numerical results for the $\Lambda_b \rightarrow p\rho^-, pK^{*-}, pa_1^- (1260), pK_1^- (1270), pK_1^- (1400)$ decay amplitudes are summarized here. Several comments are in order:

- Tables **XVII** and **XX** show the invariant amplitudes for the $\Lambda_b \rightarrow p\rho^-$ and $\Lambda_b \rightarrow pK^{*-}$ modes, respectively. The $(S+P) \otimes (S-P)$ operators, coming from the Fierz transformation of the $(V-A) \otimes (V+A)$ ones, do not contribute to the factorizable penguin diagrams, because a vector meson cannot be generated by the scalar or pseudoscalar current. There is thus no hierarchy between the invariant amplitudes in the PC_1^f topology. The non-factorizable contributions are comparable to or even larger than the factorizable ones in all invariant amplitudes, contrary to the conventional power counting rules.

- The helicity amplitudes of the $\Lambda_b \rightarrow p\rho^-$ and $\Lambda_b \rightarrow pK^{*-}$ decays in Tables XVIII and XXI, respectively, reveal a hierarchical pattern for the factorizable topologies. The left-handed $(V - A) \otimes (V - A)$ current responsible for the factorizable topologies prefers the configuration with the proton spin being anti-parallel to its momentum and with a transversely polarized meson. As a consequence, the helicity amplitude $H_{-\frac{1}{2},0}$ dominates the T_f and PC_1^f topologies.
- Tables XIX and XXII are for the partial-wave amplitudes in the $\Lambda_b \rightarrow p\rho^-$ and $\Lambda_b \rightarrow pK^{*-}$ decays, respectively. The $S^L + D$ and P_1 waves are related to the $\lambda_V = 0$ helicity state, and the $P_2 - S^T$ and $P_2 + S^T$ waves are related to the $\lambda_M = 1$ and $\lambda_M = -1$ helicity states, respectively [78]. Hence, the T_f and PC_1^f topologies dominate the $S^L + D$ and P_1 wave amplitudes, but are suppressed by helicity flip effects in the P_2 and S^T waves.

TABLE XVII: Invariant amplitudes of the $\Lambda_b \rightarrow p\bar{p}$ decay.

	Real(A_1^L)	Imag(A_1^L)	Real(B_1^L)	Imag(B_1^L)	Real(A_2^L)	Imag(A_2^L)	Real(B_2^L)	Imag(B_2^L)	Real(A_1^T)	Imag(A_1^T)	Real(B_1^T)	Imag(B_1^T)
T^f	-162.20	0.00	222.31	0.00	58.98	0.00	-64.57	0.00	-162.20	0.00	222.31	0.00
T^{nf}	5.05	8.83	0.64	-17.28	-15.58	-172.86	-6.32	-25.32	1.52	-6.01	4.19	1.28
T	-157.15	8.83	222.95	-17.28	43.40	-172.86	-70.90	-25.32	-160.68	-6.01	226.51	1.28
C_2	91.63	58.69	118.67	115.65	206.61	163.16	-209.59	-180.04	25.15	73.11	19.06	128.59
E_2	-23.49	197.98	41.40	-284.37	-67.94	529.91	-74.14	486.93	-29.91	182.78	44.33	-251.50
B	-4.74	-2.65	-13.35	9.86	-12.43	-4.05	13.59	-21.22	-5.47	-8.45	-10.04	-4.43
Tree	-93.75	262.86	369.67	-176.14	169.64	516.17	-341.04	260.36	-170.92	241.42	279.86	-126.06
PC_1^f	-6.80	0.00	9.33	0.00	2.45	0.00	-2.66	0.00	-6.80	0.00	9.33	0.00
PC_1^{nf}	0.19	0.63	0.42	-1.04	-0.45	-4.76	-0.57	-0.21	-0.71	-3.67	1.27	5.27
PC_1	-6.61	0.63	9.74	-1.04	2.00	-4.76	-3.23	-0.21	-7.50	-3.67	10.60	5.27
PC_2	4.55	-1.89	2.37	8.63	7.32	9.69	-2.56	9.65	1.32	2.65	-0.20	2.89
PE_1^u	0.27	11.50	-0.99	-16.74	1.04	31.64	0.93	24.60	-0.85	8.45	0.64	-12.45
PB	-1.46	0.22	-0.39	-0.24	-4.45	0.09	0.87	-0.02	-1.24	-0.48	0.45	-0.71
$PE_1^d + PE_2$	0.46	5.02	1.75	-23.57	1.97	14.30	-3.22	38.37	0.71	5.17	0.23	-12.35
Penguin	-2.80	15.47	12.49	-32.96	7.89	31.59	-7.22	53.08	-7.57	12.12	11.71	-17.36
	$ A_1^L $	$\phi(A_1^L)^\circ$	$ B_1^L $	$\phi(B_1^L)^\circ$	$ A_2^L $	$\phi(A_2^L)^\circ$	$ B_2^L $	$\phi(B_2^L)^\circ$	$ A_1^T $	$\phi(A_1^T)^\circ$	$ B_1^T $	$\phi(B_1^T)^\circ$
T^f	162.20	180.00	222.31	0.00	58.98	0.00	64.57	180.00	162.20	180.00	222.31	0.00
T^{nf}	10.18	60.24	17.29	-87.87	173.56	-95.15	26.10	-104.03	6.20	-75.84	4.38	16.92
T	157.39	176.78	223.62	-4.43	178.22	-75.91	75.28	-160.35	160.79	-177.86	226.51	0.32
C_2	108.81	32.64	165.70	44.26	263.27	38.30	276.30	-139.34	77.31	71.02	130.00	81.57
E_2	199.37	96.77	287.37	-81.72	534.25	97.31	492.54	98.66	185.21	99.29	255.38	-80.00
B	5.43	-150.82	16.60	143.55	13.07	-161.96	25.19	-57.36	10.07	-122.92	10.97	-156.19
Tree	279.08	109.63	409.49	-25.48	543.33	71.81	429.06	142.64	295.80	125.30	306.95	-24.25
PC_1^f	6.80	180.00	9.33	0.00	2.45	0.00	2.66	180.00	6.80	180.00	9.33	0.00
PC_1^{nf}	0.66	73.47	1.12	-68.10	4.78	-95.43	0.61	-159.74	3.74	-100.92	5.42	76.46
PC_1	6.64	174.56	9.80	-6.06	5.16	-67.20	3.24	-176.28	8.35	-153.95	11.83	26.43
PC_2	4.92	-22.61	8.95	74.64	12.14	-52.92	9.99	-104.88	2.96	63.52	2.89	93.99
PE_1^u	11.51	88.68	16.77	-93.38	31.66	88.11	24.61	87.84	8.49	95.75	12.47	-87.06
PB	1.48	171.53	0.45	-148.68	4.45	178.88	0.87	-1.16	1.33	-158.77	0.84	-57.76
$PE_1^d + PE_2$	5.04	84.78	23.64	-85.75	14.44	82.15	38.51	94.79	5.22	82.23	12.35	-88.94
Penguin	15.72	100.26	35.25	-69.24	32.56	75.97	53.57	97.74	14.29	122.00	20.94	-55.99

	Real($H_{1/2,1}$)	Imag($H_{1/2,1}$)	Real($H_{-1/2,-1}$)	Imag($H_{-1/2,-1}$)	Real($H_{1/2,0}$)	Imag($H_{1/2,0}$)	Real($H_{-1/2,0}$)	Imag($H_{-1/2,0}$)
T^f	29.39	-0.00	-2084.58	0.00	-61.55	0.00	10376.39	0.00
T^{nf}	-29.27	33.29	-9.50	-45.09	235.30	1325.62	-402.27	-3099.70
T	0.12	33.29	-2094.08	-45.09	173.75	1325.62	9974.12	-3099.70
C_2	-252.02	-1070.82	75.78	-117.97	167.26	126.97	-274.43	544.89
E_2	-9.98	-28.57	-399.86	2353.61	78.59	-589.05	-148.59	354.39
B	82.07	75.56	10.74	-34.60	-145.74	-93.58	-162.44	-37.16
Tree	-179.81	-990.54	-2407.42	2155.95	273.86	769.96	9388.65	-2237.58
PC_1^f	1.17	-0.00	-87.41	0.00	-1.31	0.00	435.62	0.00
PC_1^{nf}	-1.25	-0.45	-10.48	-48.25	12.83	39.54	-7.93	-103.95
PC_1	-0.09	-0.45	-97.88	-48.25	11.52	39.54	427.69	-103.95
PC_2	-7.67	-30.60	9.53	3.92	69.14	142.60	-19.36	28.55
PE_1^u	2.58	2.52	-8.50	112.59	-17.08	-109.19	-8.21	-35.03
PB	6.03	6.43	-10.17	0.13	12.72	-1.72	-6.42	-11.94
$PE_1^d + PE_2$	-5.66	23.37	3.55	90.79	-12.30	-63.64	6.83	-19.73
Penguin	-4.80	1.27	-103.47	159.19	64.00	7.59	400.52	-142.11
	$ H_{1/2,1} $	$\phi(H_{1/2,1})^\circ$	$ H_{-1/2,-1} $	$\phi(H_{-1/2,-1})^\circ$	$ H_{1/2,0} $	$\phi(H_{1/2,0})^\circ$	$ H_{-1/2,0} $	$\phi(H_{-1/2,0})^\circ$
T^f	29.39	-0.00	2084.58	180.00	61.55	180.00	10376.39	0.00
T^{nf}	44.33	131.33	46.08	-101.90	1346.34	79.93	3125.69	-97.39
T	33.29	89.79	2094.56	-178.77	1336.96	82.53	10444.67	-17.26
C_2	1100.08	-103.24	140.21	-57.28	209.99	37.20	610.09	116.73
E_2	30.27	-109.26	2387.34	99.64	594.27	-82.40	384.28	112.75
B	111.56	42.64	36.23	-72.75	173.20	-147.30	166.64	-167.11
Tree	1006.73	-100.29	3231.68	138.15	817.21	70.42	9651.61	-13.41
PC_1^f	1.17	-0.00	87.41	180.00	1.31	180.00	435.62	0.00
PC_1^{nf}	1.33	-160.45	49.37	-102.25	41.57	72.02	104.26	-94.36
PC_1	0.45	-101.24	109.13	-153.76	41.19	73.76	440.14	-13.66
PC_2	31.55	-104.07	10.31	22.38	158.47	64.13	34.50	124.14
PE_1^u	3.61	44.35	112.91	94.31	110.52	-98.89	35.98	-103.19
PB	8.81	46.83	10.17	179.24	12.83	-7.69	13.56	-118.25
$PE_1^d + PE_2$	24.05	103.60	90.85	87.76	64.82	-100.94	20.88	-70.92
Penguin	4.97	165.21	189.86	123.02	64.45	6.77	424.99	-19.54

TABLE XVIII: Helicity amplitudes of the $\Lambda_b \rightarrow p\bar{p}^-$ decay.

	Real(S^L)	Imag(S^L)	Real(S^T)	Imag(S^T)	Real(P_1)	Imag(P_1)	Real(P_2)	Imag(P_2)	Real(D)	Imag(D)	Real($D + S^L$)	Imag($D + S^L$)
T^f	162.20	-0.00	162.20	-0.00	-309.28	0.00	157.69	0.00	150.78	-0.00	312.97	-0.00
T^{nf}	-5.05	-8.83	-1.52	6.01	5.01	53.19	2.98	0.91	-14.07	-123.86	-19.12	-132.69
T	157.15	-8.83	160.68	6.01	-304.28	53.19	160.66	0.91	136.71	-123.86	293.86	-132.69
C_2	-91.63	-58.69	-25.15	-73.11	3.21	-20.15	13.52	91.21	78.38	71.22	-13.24	12.53
E_2	23.49	-197.98	29.91	-182.78	2.10	7.04	31.45	-178.39	-30.30	226.27	-6.81	28.29
B	4.74	2.65	5.47	8.45	9.24	3.92	-7.12	-3.14	-5.24	-0.96	-0.50	1.69
Tree	93.75	-262.86	170.92	-241.42	-289.72	44.01	198.51	-89.42	179.55	172.68	273.30	-90.18
PC_1^f	6.80	-0.00	6.80	-0.00	-13.02	0.00	6.62	0.00	6.31	-0.00	13.10	-0.00
PC_1^{nf}	-0.19	-0.63	0.71	3.67	-0.15	1.93	0.90	3.74	-0.44	-3.67	-0.62	-4.30
PC_1	6.61	-0.63	7.50	3.67	-13.17	1.93	7.52	3.74	5.87	-3.67	12.48	-4.30
PC_2	4.55	1.89	-1.32	-2.65	-1.49	5.13	-0.14	2.05	1.89	5.31	-2.65	-3.42
PE_1^u	-0.27	-11.50	0.85	-8.45	0.76	4.32	0.45	-8.83	0.53	13.73	0.27	2.22
PB	1.46	-0.22	1.24	0.48	-0.19	0.41	0.32	-0.50	-2.03	-0.09	-0.57	-0.31
$PE_1^d + PE_2$	-0.46	-5.02	-0.71	-5.17	0.16	2.50	0.16	-8.76	1.03	6.33	0.57	1.32
Penguin	2.80	-15.47	7.57	-12.12	-13.93	4.03	8.31	-12.31	7.29	10.98	10.09	-4.49
	$ S^L $	$\delta^{S^L}(\circ)$	$ S^T $	$\delta^{S^T}(\circ)$	$ P_1 $	$\delta^{P_1}(\circ)$	$ P_2 $	$\delta^{P_2}(\circ)$	$ D $	$\delta^D(\circ)$	$ D + S^L $	$\delta^{D+S^L}(\circ)$
T^f	162.20	-0.00	162.20	-0.00	309.28	180.00	157.69	0.00	150.78	-0.00	312.97	-0.00
T^{nf}	10.18	-119.76	6.20	104.16	53.43	84.62	3.11	16.92	124.65	-96.48	134.06	-98.20
T	157.39	-3.22	160.79	2.14	308.89	170.08	160.66	0.32	184.47	-42.18	322.43	-24.30
C_2	108.81	-147.36	77.31	-108.98	20.40	-80.94	92.21	81.57	105.91	42.26	18.23	136.58
E_2	199.37	-83.23	185.21	-80.71	7.34	73.39	181.14	-80.00	228.29	97.63	29.10	103.54
B	5.43	29.18	10.07	57.08	10.04	22.99	7.78	-156.19	5.33	-169.67	1.76	106.49
Tree	279.08	-70.37	295.80	-54.70	293.05	171.36	217.72	-24.25	249.11	43.88	287.79	-18.26
PC_1^f	6.80	-0.00	6.80	-0.00	13.02	180.00	6.62	0.00	6.31	-0.00	13.10	-0.00
PC_1^{nf}	0.66	-106.53	3.74	79.08	1.94	94.35	3.84	76.46	3.70	-96.77	4.35	-98.23
PC_1	6.64	-5.44	8.35	26.05	13.31	171.66	8.39	26.43	6.92	-32.04	13.20	-19.02
PC_2	4.92	157.39	2.96	-116.48	5.34	-106.22	2.05	93.99	5.64	-70.40	4.33	-127.81
PE_1^u	11.51	-91.32	8.49	-84.25	4.39	80.05	8.84	-87.06	13.74	87.78	2.24	83.18
PB	1.48	-8.47	1.33	21.23	0.45	114.77	0.60	-57.76	2.04	-177.50	0.65	-151.88
$PE_1^d + PE_2$	5.04	-95.22	5.22	-97.77	2.51	86.24	8.76	-88.94	6.42	80.75	1.44	66.46
Penguin	15.72	-79.74	14.29	-58.00	14.50	163.85	14.85	-55.99	13.18	56.43	11.04	-23.98

TABLE XIX: Partial wave amplitudes of the $\Lambda_b \rightarrow p p^-$ decay.

	$\text{Real}(A_1^L)$	$\text{Imag}(A_1^L)$	$\text{Real}(B_1^L)$	$\text{Imag}(B_1^L)$	$\text{Real}(A_2^L)$	$\text{Imag}(A_2^L)$	$\text{Real}(B_2^L)$	$\text{Imag}(B_2^L)$	$\text{Real}(A_1^T)$	$\text{Imag}(A_1^T)$	$\text{Real}(B_1^T)$	$\text{Imag}(B_1^T)$
T^f	-194.45	0.00	266.80	0.00	71.23	0.00	-77.98	0.00	-194.45	0.00	266.80	0.00
T^{nf}	4.76	10.58	2.72	-20.50	-8.72	-203.69	-9.61	-29.00	2.22	-7.02	5.17	3.44
T	-189.69	10.58	269.53	-20.50	62.51	-203.69	-87.59	-29.00	-192.24	-7.02	271.98	3.44
E_2	-28.18	227.94	37.03	-316.34	-108.84	577.73	-82.87	549.87	-30.72	177.26	41.24	-260.86
Tree	-217.87	238.53	306.56	-336.84	-46.33	374.04	-170.46	520.87	-222.96	170.23	313.22	-257.41
PC_1^f	-8.16	0.00	11.19	0.00	2.97	0.00	-3.23	0.00	-8.16	0.00	11.19	0.00
PC_1^{nf}	0.06	0.60	0.49	-1.65	-0.73	-6.16	0.01	0.88	-0.25	-3.90	0.84	6.11
PC_1	-8.09	0.60	11.68	-1.65	2.25	-6.16	-3.21	0.88	-8.41	-3.90	12.03	6.11
PE_1^u	0.42	12.52	-0.67	-18.54	-0.08	35.72	1.94	26.95	-0.83	8.35	0.80	-12.48
PE_1^d	-0.38	12.18	0.71	-17.01	-0.60	30.30	-1.41	27.87	-0.32	6.16	0.35	-8.84
Penguin	-8.06	25.30	11.73	-37.20	1.57	59.85	-2.68	55.70	-9.56	10.62	13.18	-15.20
	$ A_1^L $	$\phi(A_1^L)^\circ$	$ B_1^L $	$\phi(B_1^L)^\circ$	$ A_2^L $	$\phi(A_2^L)^\circ$	$ B_2^L $	$\phi(B_2^L)^\circ$	$ A_1^T $	$\phi(A_1^T)^\circ$	$ B_1^T $	$\phi(B_1^T)^\circ$
T^f	194.45	180.00	266.80	0.00	71.23	0.00	77.98	180.00	194.45	180.00	266.80	0.00
T^{nf}	11.61	65.76	20.68	-82.43	203.88	-92.45	30.55	-108.34	7.36	-72.50	6.22	33.64
T	189.98	176.81	270.31	-4.35	213.07	-72.94	92.27	-161.68	192.37	-177.91	272.00	0.73
E_2	229.68	97.05	318.50	-83.32	587.90	100.67	556.08	98.57	179.90	99.83	264.10	-81.02
Tree	323.05	132.41	455.45	-47.69	376.90	97.06	548.05	108.12	280.52	142.64	405.43	-39.41
PC_1^f	8.16	180.00	11.19	0.00	2.97	0.00	3.23	180.00	8.16	180.00	11.19	0.00
PC_1^{nf}	0.61	83.94	1.72	-73.39	6.21	-96.72	0.88	89.06	3.91	-93.69	6.17	82.21
PC_1	8.12	175.73	11.80	-8.05	6.56	-69.97	3.33	164.62	9.27	-155.13	13.49	26.95
PE_1^u	12.53	88.10	18.56	-92.06	35.72	90.13	27.02	85.87	8.39	95.67	12.50	-86.33
PE_1^d	12.19	91.80	17.02	-87.61	30.30	91.14	27.90	92.89	6.17	92.96	8.84	-87.73
Penguin	26.56	107.67	39.01	-72.51	59.87	88.50	55.76	92.75	14.29	131.99	20.12	-49.08

TABLE XXX: Invariant amplitudes of the $\Lambda_b \rightarrow p K^{*-}$ decay.

	Real($H_{1/2,1}$)	Imag($H_{1/2,1}$)	Real($H_{-1/2,-1}$)	Imag($H_{-1/2,-1}$)	Real($H_{1/2,0}$)	Imag($H_{1/2,0}$)	Real($H_{-1/2,0}$)	Imag($H_{-1/2,0}$)
T^f	36.78	-0.00	-2491.55	0.00	-70.47	0.00	10702.76	0.00
T^{nf}	-38.20	29.82	-9.40	-61.50	133.06	1342.77	-266.10	-3118.57
T	-1.42	29.82	-2500.95	-61.50	62.59	1342.77	10436.65	-3118.57
E_2	9.97	47.66	-389.44	2352.39	125.40	-132.47	-624.29	61.91
Tree	8.55	77.48	-2890.39	2290.89	187.99	1210.31	9812.36	-3056.66
PC_1^f	1.55	-0.00	-104.51	0.00	-2.28	0.00	449.38	0.00
PC_1^{nf}	-2.21	-2.79	-5.48	-53.46	20.58	46.96	3.40	-101.76
PC_1	-0.66	-2.79	-109.99	-53.46	18.30	46.96	452.77	-101.76
PE_1^u	1.71	3.10	-9.07	111.71	21.48	-118.50	-0.13	-30.43
PE_1^d	0.46	0.59	-3.68	80.71	-5.72	-24.84	1.14	-25.57
Penguin	1.52	0.90	-122.75	138.96	34.06	-96.38	453.79	-157.76
	$ H_{1/2,1} $	$\phi(H_{1/2,1})^\circ$	$ H_{-1/2,-1} $	$\phi(H_{-1/2,-1})^\circ$	$ H_{1/2,0} $	$\phi(H_{1/2,0})^\circ$	$ H_{-1/2,0} $	$\phi(H_{-1/2,0})^\circ$
T^f	36.78	-0.00	2491.55	180.00	70.47	180.00	10702.76	0.00
T^{nf}	48.46	142.03	62.22	-98.69	1349.35	84.34	3129.90	-94.88
T	29.85	92.73	2501.71	-178.59	1344.23	87.33	10892.62	-16.64
E_2	48.69	78.18	2384.41	99.40	182.40	-46.57	627.36	174.34
Tree	77.95	83.70	3688.16	141.60	1224.82	81.17	10277.43	-17.30
PC_1^f	1.55	-0.00	104.51	180.00	2.28	180.00	449.38	0.00
PC_1^{nf}	3.56	-128.41	53.74	-95.85	51.27	66.33	101.82	-88.09
PC_1	2.86	-103.25	122.30	-154.08	50.40	68.71	464.07	-12.67
PE_1^u	3.54	61.11	112.08	94.64	120.43	-79.73	30.43	-90.25
PE_1^d	0.75	51.75	80.79	92.61	25.49	-102.97	25.59	-87.44
Penguin	1.77	30.72	185.41	131.46	102.22	-70.54	480.43	-19.17

TABLE XXI: Helicity amplitudes of the $\Lambda_b \rightarrow p K^{*-}$ decay.

	Real(S^L)	Imag(S^L)	Real(S^T)	Imag(S^T)	Real(P_1)	Imag(P_1)	Real(P_2)	Imag(P_2)	Real(D)	Imag(D)	Real($D + S^L$)	Imag($D + S^L$)
T^f	194.45	-0.00	194.45	-0.00	-367.82	0.00	188.80	0.00	178.24	-0.00	372.69	-0.00
T^{nf}	-4.76	-10.58	-2.22	7.02	4.60	61.43	3.66	2.44	-9.04	-143.75	-13.81	-154.34
T	189.69	-10.58	192.24	7.02	-363.22	61.43	192.46	2.44	169.19	-143.75	358.88	-154.34
E_2	28.18	-227.94	30.72	-177.26	17.26	2.44	29.19	-184.59	-54.11	234.67	-25.94	6.72
Tree	217.87	-238.53	222.96	-170.23	-345.96	63.87	221.64	-182.15	115.08	90.91	332.95	-147.61
PC_1^f	8.16	-0.00	8.16	-0.00	-15.47	0.00	7.92	0.00	7.47	-0.00	15.62	-0.00
PC_1^{nf}	-0.06	-0.60	0.25	3.90	-0.83	1.90	0.59	4.33	-0.53	-4.54	-0.59	-5.14
PC_1	8.09	-0.60	8.41	3.90	-16.30	1.90	8.51	4.33	6.94	-4.54	15.03	-5.14
PE_1^u	-0.42	-12.52	0.83	-8.35	-0.74	5.15	0.57	-8.83	-0.33	15.56	-0.75	3.05
PE_1^d	0.38	-12.18	0.32	-6.16	0.16	1.74	0.25	-6.25	-0.15	12.15	0.24	-0.03
Penguin	8.06	-25.30	9.56	-10.62	-16.88	8.79	9.32	-10.76	6.46	23.18	14.52	-2.12
	$ S^L $	$\delta^{S^L}(\circ)$	$ S^T $	$\delta^{S^T}(\circ)$	$ P_1 $	$\delta^{P_1}(\circ)$	$ P_2 $	$\delta^{P_2}(\circ)$	$ D $	$\delta^D(\circ)$	$ D + S^L $	$\delta^{D+S^L}(\circ)$
T^f	194.45	-0.00	194.45	-0.00	367.82	180.00	188.80	0.00	178.24	-0.00	372.69	-0.00
T^{nf}	11.61	-114.24	7.36	107.50	61.60	85.72	4.40	33.64	144.04	-93.60	154.95	-95.11
T	189.98	-3.19	192.37	2.09	368.37	170.40	192.47	0.73	222.02	-40.35	390.66	-23.27
E_2	229.68	-82.95	179.90	-80.17	17.43	8.05	186.88	-81.02	240.83	102.99	26.79	165.46
Tree	323.05	-47.59	280.52	-37.36	351.80	169.54	286.89	-39.41	146.66	38.31	364.20	-23.91
PC_1^f	8.16	-0.00	8.16	-0.00	15.47	180.00	7.92	0.00	7.47	-0.00	15.62	-0.00
PC_1^{nf}	0.61	-96.06	3.91	86.31	2.07	113.63	4.37	82.21	4.57	-96.66	5.18	-96.59
PC_1	8.12	-4.27	9.27	24.87	16.41	173.36	9.55	26.95	8.29	-33.20	15.89	-18.90
PE_1^u	12.53	-91.90	8.39	-84.33	5.20	98.16	8.85	-86.33	15.57	91.22	3.14	103.79
PE_1^d	12.19	-88.20	6.17	-87.04	1.75	84.81	6.26	-87.73	12.16	90.69	0.24	-6.07
Penguin	26.56	-72.33	14.29	-48.01	19.03	152.48	14.24	-49.08	24.06	74.43	14.67	-8.32

TABLE XXII: Partial wave amplitudes of the $\Lambda_b \rightarrow p K^{*-}$ decay.

	Real(A_1^L)	Imag(A_1^L)	Real(B_1^L)	Imag(B_1^L)	Real(A_2^L)	Imag(A_2^L)	Real(B_2^L)	Imag(B_2^L)	Real(A_1^T)	Imag(A_1^T)	Real(B_1^T)	Imag(B_1^T)
T^f	0.00	296.24	-0.00	-409.58	-0.00	-111.18	0.00	121.60	0.00	296.24	-0.00	-409.58
T^{nf}	12.02	-6.01	-26.71	-2.57	-253.52	15.21	-86.65	15.01	-11.02	-2.42	4.35	-7.12
T	12.02	290.23	-26.71	-412.15	-253.52	-95.97	-86.65	136.61	-11.02	293.83	4.35	-416.70
C_2	4.01	-109.12	75.01	-134.43	34.19	-256.32	-81.65	261.14	30.03	-66.00	107.05	-46.72
E_2	132.67	18.84	-194.56	-21.79	386.67	55.94	368.73	68.69	131.79	28.94	-191.35	-33.51
B	2.52	-14.87	1.25	-5.86	2.80	-34.90	8.93	16.22	13.09	-5.94	20.40	-3.95
Tree	151.22	185.08	-145.00	-574.24	170.14	-331.25	209.35	482.66	163.89	250.83	-59.55	-500.89
PC_1^f	0.00	12.36	0.00	-17.14	0.00	-4.64	0.00	5.03	0.00	12.36	0.00	-17.14
PC_1^{nf}	-18.38	1.34	25.60	-2.99	-51.65	5.49	-51.67	4.93	-25.22	1.38	35.43	-2.42
PC_1	-18.38	13.71	25.60	-20.12	-51.65	0.85	-51.67	9.96	-25.22	13.74	35.43	-19.55
PC_2	5.40	-2.87	-4.72	-7.81	25.32	9.16	1.15	17.40	1.97	-1.23	2.69	-2.66
PE_1^u	9.47	-1.01	-14.29	1.93	30.69	-1.02	19.59	-3.47	7.15	0.64	-11.83	-0.40
PB	-0.05	-0.65	-1.64	-2.32	-0.80	-0.27	3.00	2.77	0.06	-0.53	-0.07	-1.88
$PE_1^d + PE_2$	17.42	1.18	-4.11	0.40	42.41	3.76	3.98	-1.27	9.33	1.76	-4.17	-0.46
Penguin	13.86	10.35	0.85	-27.91	45.97	-5.85	-23.94	25.39	-6.71	14.38	22.06	-24.95
	$ A_1^L $	$\phi(A_1^L)^\circ$	$ B_1^L $	$\phi(B_1^L)^\circ$	$ A_2^L $	$\phi(A_2^L)^\circ$	$ B_2^L $	$\phi(B_2^L)^\circ$	$ A_1^T $	$\phi(A_1^T)^\circ$	$ B_1^T $	$\phi(B_1^T)^\circ$
T^f	296.24	90.00	409.58	-90.00	111.18	-90.00	121.60	90.00	296.24	90.00	409.58	-90.00
T^{nf}	13.44	-26.58	26.83	-174.50	253.97	176.57	87.95	170.17	11.28	-167.64	8.35	-58.56
T	290.48	87.63	413.02	-93.71	271.07	-159.27	161.78	122.39	294.03	92.15	416.73	-89.40
C_2	109.20	-87.90	153.94	-60.84	258.59	-82.40	273.60	107.36	72.51	-65.53	116.80	-23.58
E_2	134.00	8.08	195.77	-173.61	390.70	8.23	375.07	10.55	134.93	12.38	194.26	-170.07
B	15.08	-80.36	6.00	-77.93	35.02	-85.41	18.52	61.18	14.37	-24.43	20.78	-10.97
Tree	239.00	50.75	592.26	-104.17	372.39	-62.81	526.11	66.55	299.62	56.84	504.42	-96.78
PC_1^f	12.36	90.00	17.14	-90.00	4.64	-90.00	5.03	90.00	12.36	90.00	17.14	-90.00
PC_1^{nf}	18.43	175.82	25.78	-6.66	51.94	173.94	51.90	174.55	25.26	176.87	35.51	-3.90
PC_1	22.93	143.28	32.57	-38.17	51.65	179.06	52.62	169.09	28.72	151.41	40.47	-28.89
PC_2	6.12	-28.01	9.12	-121.17	26.93	-19.89	17.43	86.23	2.33	-31.96	3.79	-44.71
PE_1^u	9.52	-6.11	14.42	172.30	30.71	-1.91	19.90	-10.05	7.18	5.13	11.83	-178.06
PB	0.66	-94.45	2.84	-125.39	0.84	-161.57	4.09	42.72	0.53	-83.48	1.88	-92.04
$PE_1^d + PE_2$	17.46	3.88	4.13	174.38	42.57	5.06	4.18	-17.66	9.49	10.66	4.19	-173.76
Penguin	17.30	36.75	27.92	-88.26	46.34	-7.25	34.90	133.31	15.87	115.00	33.30	-48.52

TABLE XXXIII: Invariant amplitudes of the $\Lambda_b \rightarrow pa_1^- (1260)$ decay.

	Real($H_{1/2,1}$)	Imag($H_{1/2,1}$)	Real($H_{-1/2,-1}$)	Imag($H_{-1/2,-1}$)	Real($H_{1/2,0}$)	Imag($H_{1/2,0}$)	Real($H_{-1/2,0}$)	Imag($H_{-1/2,0}$)
T^f	-0.00	-59.16	0.00	3756.40	0.00	72.69	0.00	-11416.70
T^{nf}	51.32	47.69	-90.62	16.58	609.70	-103.95	-3116.18	298.85
T	51.32	-11.47	-90.62	3772.98	609.70	-31.26	-3116.18	-11117.84
C_2	-676.57	635.89	-289.78	-214.15	328.37	34.12	640.25	374.83
E_2	14.91	-35.12	1712.40	337.63	-74.15	232.15	493.87	326.34
B	-176.35	56.12	-7.80	-20.43	128.61	30.66	79.76	77.44
Tree	-786.69	645.43	1324.20	3876.03	992.53	265.67	-1902.30	-10339.24
PC_1^f	-0.00	-2.28	0.00	156.97	0.00	1.90	0.00	-477.58
PC_1^{nf}	2.51	2.03	-322.34	19.79	-30.16	-16.77	-83.72	9.55
PC_1	2.51	-0.25	-322.34	176.76	-30.16	-14.87	-83.72	-468.03
PC_2	-24.85	19.95	0.56	4.09	-142.01	43.99	6.48	21.41
PE_1^u	7.33	-2.33	99.43	5.94	-95.04	-10.79	-13.90	10.13
PB	-0.09	11.89	0.69	5.04	5.08	-21.91	-3.67	-3.27
$PE_1^d + PE_2$	-41.27	-9.25	78.91	13.37	-13.57	-9.69	-48.50	-0.58
Penguin	-56.37	20.00	-142.75	205.20	-275.70	-13.28	-143.31	-440.34
	$ H_{1/2,1} $	$\phi(H_{1/2,1})^\circ$	$ H_{-1/2,-1} $	$\phi(H_{-1/2,-1})^\circ$	$ H_{1/2,0} $	$\phi(H_{1/2,0})^\circ$	$ H_{-1/2,0} $	$\phi(H_{-1/2,0})^\circ$
T^f	59.16	-90.00	3756.40	90.00	72.69	90.00	11416.70	-90.00
T^{nf}	70.06	42.90	92.12	169.63	618.49	-9.68	3130.48	174.52
T	52.59	-12.60	3774.06	91.38	610.50	-2.94	11546.30	-105.66
C_2	928.49	136.78	360.33	-143.54	330.14	5.93	741.90	30.35
E_2	38.15	-66.99	1745.36	11.15	243.70	107.71	591.94	33.46
B	185.07	162.35	21.87	-110.89	132.22	13.41	111.17	44.15
Tree	1017.57	140.63	4095.99	71.14	1027.47	14.98	10512.78	-100.43
PC_1^f	2.28	-90.00	156.97	90.00	1.90	90.00	477.58	-90.00
PC_1^{nf}	3.23	38.99	322.95	176.49	34.51	-150.93	84.26	173.49
PC_1	2.52	-5.68	367.62	151.26	33.63	-153.76	475.46	-100.14
PC_2	31.86	141.24	4.13	82.19	148.66	162.79	22.37	73.17
PE_1^u	7.69	-17.63	99.60	3.42	95.65	-173.52	17.20	143.93
PB	11.89	90.44	5.09	82.19	22.49	-76.95	4.91	-138.30
$PE_1^d + PE_2$	42.29	-167.36	80.04	9.61	16.68	-144.46	48.50	-179.32
Penguin	59.81	160.46	249.97	124.82	276.02	-177.24	463.07	-108.03

TABLE XXXIV: Helicity amplitudes of the $\Lambda_b \rightarrow pa_1^-$ (1260) decay.

	Real(S^L)	Imag(S^L)	Real(S^T)	Imag(S^T)	Real(P_1)	Imag(P_1)	Real(P_2)	Imag(P_2)	Real(D)	Imag(D)	Real($D + S^L$)	Imag($D + S^L$)
T^f	-0.00	-296.24	-0.00	-296.24	0.00	545.91	0.00	-287.06	-0.00	-256.66	-0.00	-552.90
T^{nf}	-12.02	6.01	11.02	2.42	120.62	-9.38	3.05	-4.99	-167.28	13.37	-179.30	19.38
T	-12.02	-290.23	11.02	-293.83	120.62	536.53	3.05	-292.05	-167.28	-243.29	-179.30	-533.52
C_2	-4.01	109.12	-30.03	66.00	-46.61	-19.68	75.03	-32.74	19.01	-92.73	15.01	16.40
E_2	-132.67	-18.84	-131.79	-28.94	-20.20	-26.88	-134.11	-23.49	160.01	23.37	27.33	4.53
B	-2.52	14.87	-13.09	5.94	-10.03	-5.20	14.30	-2.77	0.17	-12.62	-2.35	2.25
Tree	-151.22	-185.08	-163.89	-250.83	43.78	484.77	-41.73	-351.05	11.92	-325.26	-139.31	-510.34
PC_1^f	-0.00	-12.36	-0.00	-12.36	0.00	22.89	0.00	-12.01	-0.00	-10.71	-0.00	-23.07
PC_1^{nf}	18.38	-1.34	25.22	-1.38	5.48	0.35	24.83	-1.69	-20.96	2.61	-2.58	1.27
PC_1	18.38	-13.71	25.22	-13.74	5.48	23.24	24.83	-13.70	-20.96	-8.10	-2.58	-21.81
PC_2	-5.40	2.87	-1.97	1.23	6.52	3.15	1.89	-1.87	12.55	3.96	7.15	-1.09
PE_1^u	-9.47	1.01	-7.15	-0.64	5.24	0.03	-8.29	-0.28	13.37	-0.01	3.90	1.01
PB	0.05	0.65	-0.06	0.53	-0.07	1.21	-0.05	-1.31	-0.47	0.24	-0.42	0.90
$PE_1^d + PE_2$	-17.42	-1.18	-9.33	-1.76	2.99	0.49	-2.92	-0.32	15.74	1.62	-1.68	0.44
Penguin	-13.86	-10.35	6.71	-14.38	20.16	21.83	15.46	-17.49	20.23	-10.20	6.37	-20.55
	$ S^L $	$\phi(S^L)^\circ$	$ S^T $	$\phi(S^T)^\circ$	$ P_1 $	$\phi(P_1)^\circ$	$ P_2 $	$\phi(P_2)^\circ$	$ D $	$\phi(D)^\circ$	$ D + S^L $	$\phi(D + S^L)^\circ$
T^f	296.24	-90.00	296.24	-90.00	545.91	90.00	287.06	-90.00	256.66	-90.00	552.90	-90.00
T^{nf}	13.44	153.42	11.28	12.36	120.98	-4.45	5.85	-58.56	167.81	175.43	180.34	173.83
T	290.48	-92.37	294.03	-87.85	549.92	77.33	292.06	-89.40	295.25	-124.51	562.84	-108.58
C_2	109.20	92.10	72.51	114.47	50.60	-157.11	81.86	-23.58	94.66	-78.41	22.23	47.53
E_2	134.00	-171.92	134.93	-167.62	33.62	-126.93	136.15	-170.07	161.71	8.31	27.71	9.42
B	15.08	99.64	14.37	155.57	11.30	-152.58	14.56	-10.97	12.62	-89.21	3.25	136.24
Tree	239.00	-129.25	299.62	-123.16	486.74	84.84	353.52	-96.78	325.48	-87.90	529.01	-105.27
PC_1^f	12.36	-90.00	12.36	-90.00	22.89	90.00	12.01	-90.00	10.71	-90.00	23.07	-90.00
PC_1^{nf}	18.43	-4.18	25.26	-3.13	5.49	3.62	24.89	-3.90	21.12	172.90	2.87	153.83
PC_1	22.93	-36.72	28.72	-28.59	23.88	76.73	28.36	-28.89	22.47	-158.87	21.96	-96.74
PC_2	6.12	151.99	2.33	148.04	7.24	-25.76	2.65	-44.71	13.16	-17.52	7.23	-8.65
PE_1^u	9.52	173.89	7.18	-174.87	5.24	0.35	8.29	-178.06	13.37	-0.03	4.03	14.46
PB	0.66	85.55	0.53	96.52	1.21	93.21	1.32	-92.04	0.53	152.67	0.99	115.12
$PE_1^d + PE_2$	17.46	-176.12	9.49	-169.34	3.03	9.40	2.94	-173.76	15.82	5.88	1.74	165.37
Penguin	17.30	-143.25	15.87	-65.00	29.72	47.27	23.34	-48.52	22.66	-26.76	21.52	-72.78

TABLE XXXV: Partial wave amplitudes of the $\Lambda_b \rightarrow pa_1^- (1260)$ decay.

	Real(A_1^L)	Imag(A_1^L)	Real(B_1^L)	Imag(B_1^L)	Real(A_2^L)	Imag(A_2^L)	Real(B_2^L)	Imag(B_2^L)	Real(A_1^T)	Imag(A_1^T)	Real(B_1^T)	Imag(B_1^T)
T^f	0.00	378.38	-0.00	-524.96	-0.00	-143.60	0.00	157.06	0.00	378.38	-0.00	-524.96
T^{nf}	-34.43	2.18	29.72	-4.78	-37.64	9.01	-362.56	37.73	-25.06	0.73	38.14	-10.20
T	-34.43	380.56	29.72	-529.74	-37.64	-134.59	-362.56	194.79	-25.06	379.10	38.14	-535.15
E_2	-144.36	-33.42	201.71	43.50	-450.06	-98.06	-382.73	-118.18	-57.35	-4.77	77.80	12.11
Tree	-178.79	347.14	231.43	-486.24	-487.70	-232.65	-745.29	76.62	-82.41	374.33	115.94	-523.04
PC_1^f	0.00	15.86	0.00	-22.01	0.00	-5.99	0.00	6.50	0.00	15.86	0.00	-22.01
PC_1^{nf}	9.57	0.85	12.46	-1.08	-21.33	1.48	-34.10	3.09	-11.29	0.32	16.50	-0.96
PC_1	-9.57	16.71	12.46	-23.09	-21.33	-4.50	-34.10	9.58	-11.29	16.19	16.50	-22.98
PE_1^u	-7.06	0.05	9.94	-0.25	-24.37	-1.55	-15.22	-0.52	-1.84	-0.16	2.23	-0.01
PE_1^d	-6.21	-0.29	8.85	0.45	-20.05	-0.01	-13.70	-1.91	-0.48	0.12	0.45	-0.20
Penguin	-22.85	16.47	31.25	-22.89	-65.75	-6.06	-63.02	7.16	-13.60	16.14	19.18	-23.18
	$ A_1^L $	$\phi(A_1^L)^\circ$	$ B_1^L $	$\phi(B_1^L)^\circ$	$ A_2^L $	$\phi(A_2^L)^\circ$	$ B_2^L $	$\phi(B_2^L)^\circ$	$ A_1^T $	$\phi(A_1^T)^\circ$	$ B_1^T $	$\phi(B_1^T)^\circ$
T^f	378.38	90.00	524.96	-90.00	143.60	-90.00	157.06	90.00	378.38	90.00	524.96	-90.00
T^{nf}	34.50	176.37	30.11	-9.14	38.70	166.54	364.52	174.06	25.07	178.34	39.48	-14.97
T	382.12	95.17	530.57	-86.79	139.76	-105.62	411.57	151.75	379.93	93.78	536.51	-85.92
E_2	148.18	-166.96	206.35	12.17	460.62	-167.71	400.56	-162.84	57.55	-175.24	78.74	8.85
Tree	390.48	117.25	538.50	-64.55	540.35	-154.50	749.21	174.13	383.30	102.42	535.73	-77.50
PC_1^f	15.86	90.00	22.01	-90.00	5.99	-90.00	6.50	90.00	15.86	90.00	22.01	-90.00
PC_1^{nf}	9.61	174.95	12.51	-4.95	21.38	176.02	34.24	174.82	11.29	178.37	16.53	-3.34
PC_1	19.26	119.81	26.24	-61.65	21.80	-168.08	35.42	164.30	19.73	124.89	28.29	-54.31
PE_1^u	7.06	179.62	9.94	-1.43	24.42	-176.36	15.23	-178.04	1.84	-175.11	2.23	-0.31
PE_1^d	6.22	-177.32	8.86	2.92	20.05	-179.98	13.83	-172.08	0.49	166.43	0.50	-23.40
Penguin	28.16	144.22	38.73	-36.22	66.03	-174.73	63.43	173.52	21.11	130.12	30.09	-50.39

TABLE XXVI: Invariant amplitudes of the $\Lambda_b \rightarrow p K_1(1270)^-$ decay with mixing angle $\theta_K = 30^\circ$.

	Real($H_{1/2,1}$)	Imag($H_{1/2,1}$)	Real($H_{-1/2,-1}$)	Imag($H_{-1/2,-1}$)	Real($H_{1/2,0}$)	Imag($H_{1/2,0}$)	Real($H_{-1/2,0}$)	Imag($H_{-1/2,0}$)
T^f	-0.00	-68.10	0.00	4803.85	0.00	88.95	0.00	-14484.42
T^{nf}	-10.66	41.32	-333.38	50.67	-3199.56	248.60	-2531.08	292.08
T	-10.66	-26.78	-333.38	4854.52	-3199.56	337.54	-2531.08	-14192.34
E_2	18.28	-23.92	-720.14	-85.37	275.50	-302.29	-710.87	-451.08
Tree	7.62	-50.69	-1053.51	4769.15	-2924.06	35.25	-3241.95	-14643.42
PC_1^f	-0.00	-2.85	0.00	201.41	0.00	2.65	0.00	-607.92
PC_1^{nf}	-1.77	2.28	-147.09	6.42	-132.76	15.41	-87.73	6.22
PC_1	-1.77	-0.57	-147.09	207.84	-132.76	18.06	-87.73	-601.70
PE_1^u	1.78	1.07	-21.88	-0.96	62.30	1.90	-16.44	-19.75
PE_1^d	1.04	0.14	-5.14	1.63	44.75	-15.04	-6.60	-5.38
Penguin	1.05	0.64	-174.12	208.51	-25.71	4.92	-110.76	-626.82
	$ H_{1/2,1} $	$\phi(H_{1/2,1})^\circ$	$ H_{-1/2,-1} $	$\phi(H_{-1/2,-1})^\circ$	$ H_{1/2,0} $	$\phi(H_{1/2,0})^\circ$	$ H_{-1/2,0} $	$\phi(H_{-1/2,0})^\circ$
T^f	68.10	-90.00	4803.85	90.00	88.95	90.00	14484.42	-90.00
T^{nf}	42.67	104.47	337.20	171.36	3209.21	175.56	2547.88	173.42
T	28.82	-111.71	4865.96	93.93	3217.32	173.98	14416.27	-100.11
E_2	30.10	-52.61	725.18	-173.24	409.00	-47.65	841.91	-147.60
Tree	51.26	-81.46	4884.12	102.46	2924.27	179.31	14998.00	-102.48
PC_1^f	2.85	-90.00	201.41	90.00	2.65	90.00	607.92	-90.00
PC_1^{nf}	2.89	127.92	147.23	177.50	133.65	173.38	87.95	175.94
PC_1	1.86	-162.20	254.62	125.29	133.98	172.25	608.06	-98.30
PE_1^u	2.08	30.87	21.90	-177.49	62.33	1.74	25.69	-129.77
PE_1^d	1.05	7.68	5.40	162.38	47.21	-18.58	8.51	-140.81
Penguin	1.23	31.21	271.65	129.86	26.17	169.17	636.53	-100.02

TABLE XXVII: Helicity amplitudes of the $\Lambda_b \rightarrow pK_1(1270)^-$ decay.

	Real(S^L)	Imag(S^L)	Real(S^T)	Imag(S^T)	Real(P_1)	Imag(P_1)	Real(P_2)	Imag(P_2)	Real(D)	Imag(D)	Real($D + S^L$)	Imag($D + S^L$)
T^f	-0.00	-378.38	-0.00	-378.38	0.00	697.91	0.00	-367.80	-0.00	-328.16	-0.00	-706.54
T^{nf}	34.43	-2.18	25.06	-0.73	277.83	-26.21	26.72	-7.14	-2.02	4.29	32.41	2.11
T	34.43	-380.56	25.06	-379.10	277.83	671.70	26.72	-374.95	-2.02	-323.87	32.41	-704.43
E_2	144.36	33.42	57.35	4.77	21.11	36.52	54.51	8.49	-192.18	-40.64	-47.82	-7.21
Tree	178.79	-347.14	82.41	-374.33	298.94	708.23	81.23	-366.46	-194.20	-364.51	-15.41	-711.64
PC_1^f	-0.00	-15.86	-0.00	-15.86	0.00	29.34	0.00	-15.42	-0.00	-13.74	-0.00	-29.60
PC_1^{nf}	9.57	-0.85	11.29	-0.32	10.69	-1.05	11.56	0.68	-7.39	0.40	2.18	-0.45
PC_1	9.57	-16.71	11.29	-16.19	10.69	28.30	11.56	-16.10	-7.39	-13.34	2.18	-30.05
PE_1^u	7.06	-0.05	1.84	0.16	-2.22	0.87	1.56	-0.01	-10.88	-1.00	-3.82	-1.05
PE_1^d	6.21	0.29	0.48	-0.12	-1.85	0.99	0.32	-0.14	-8.70	0.18	-2.49	0.47
Penguin	22.85	-16.47	13.60	-16.14	6.62	30.15	13.44	-16.24	-26.97	-14.16	-4.12	-30.63
	$ S^L $	$\phi(S^L)^\circ$	$ S^T $	$\phi(S^T)^\circ$	$ P_1 $	$\phi(P_1)^\circ$	$ P_2 $	$\phi(P_2)^\circ$	$ D $	$\phi(D)^\circ$	$ D + S^L $	$\phi(D + S^L)^\circ$
T^f	378.38	-90.00	378.38	-90.00	697.91	90.00	367.80	-90.00	328.16	-90.00	706.54	-90.00
T^{nf}	34.50	-3.63	25.07	-1.66	279.06	-5.39	27.66	-14.97	4.74	115.19	32.48	3.72
T	382.12	-84.83	379.93	-86.22	726.89	67.53	375.90	-85.92	323.88	-90.36	705.18	-87.37
E_2	148.18	13.04	57.55	4.76	42.18	59.98	55.17	8.85	196.43	-168.06	48.36	-171.42
Tree	390.48	-62.75	383.30	-77.58	768.73	67.12	375.35	-77.50	413.01	-118.05	711.81	-91.24
PC_1^f	15.86	-90.00	15.86	-90.00	29.34	90.00	15.42	-90.00	13.74	-90.00	29.60	-90.00
PC_1^{nf}	9.61	-5.05	11.29	-1.63	10.74	-5.60	11.58	-3.34	7.40	176.89	2.23	-11.53
PC_1	19.26	-60.19	19.73	-55.11	30.25	69.30	19.82	-54.31	15.25	-118.99	30.13	-85.84
PE_1^u	7.06	-0.38	1.84	4.89	2.39	158.74	1.56	-0.31	10.93	-174.73	3.96	-164.63
PE_1^d	6.22	2.68	0.49	-13.57	2.10	151.84	0.35	-23.40	8.70	178.83	2.53	169.34
Penguin	28.16	-35.78	21.11	-49.88	30.87	77.62	21.08	-50.39	30.46	-152.30	30.90	-97.67

TABLE XXVIII: Partial wave of the $\Lambda_b \rightarrow p K_1(1270)^-$ decay.

	$\text{Real}(A_1^L)$	$\text{Imag}(A_1^L)$	$\text{Real}(B_1^L)$	$\text{Imag}(B_1^L)$	$\text{Real}(A_2^L)$	$\text{Imag}(A_2^L)$	$\text{Real}(B_2^L)$	$\text{Imag}(B_2^L)$	$\text{Real}(A_1^T)$	$\text{Imag}(A_1^T)$	$\text{Real}(B_1^T)$	$\text{Imag}(B_1^T)$
T^f	0.00	156.11	0.00	-216.25	0.00	-58.88	0.00	64.41	0.00	156.11	0.00	-216.25
T^{nf}	35.90	-9.89	-50.17	0.35	-320.19	26.95	88.01	2.81	-0.81	-4.76	-15.54	-2.98
T	35.90	146.23	-50.17	-215.90	-320.19	-31.92	88.01	67.22	-0.81	151.35	-15.54	-219.24
E_2	222.20	40.60	-323.31	-46.62	686.72	131.52	613.16	127.39	179.22	41.20	-257.22	-49.19
Tree	258.10	186.82	-373.48	-262.52	366.52	99.60	701.16	194.62	178.42	192.55	-272.76	-268.43
PC_1^f	0.00	6.53	0.00	-9.06	0.00	-2.46	0.00	2.67	0.00	6.53	0.00	-9.06
PC_1^{nf}	-17.15	1.77	24.90	-3.08	-55.17	6.10	-47.81	5.59	-24.97	1.49	35.31	-2.61
PC_1	-17.15	8.30	24.90	-12.14	-55.17	3.64	-47.81	8.26	-24.97	8.02	35.31	-11.67
PE_1^u	14.38	-1.36	-21.28	2.30	48.85	0.39	29.81	-4.68	9.61	1.06	-14.55	-0.48
PE_1^d	14.66	0.59	-21.25	-0.91	40.02	0.88	32.81	2.33	8.36	0.30	-12.37	-0.07
Penguin	11.89	7.53	-17.63	-10.76	33.70	4.91	14.81	5.91	-7.00	9.38	8.39	-12.23
	$ A_1^L $	$\phi(A_1^L)^\circ$	$ B_1^L $	$\phi(B_1^L)^\circ$	$ A_2^L $	$\phi(A_2^L)^\circ$	$ B_2^L $	$\phi(B_2^L)^\circ$	$ A_1^T $	$\phi(A_1^T)^\circ$	$ B_1^T $	$\phi(B_1^T)^\circ$
T^f	156.11	90.00	216.25	-90.00	58.88	-90.00	64.41	90.00	156.11	90.00	216.25	-90.00
T^{nf}	37.24	-15.40	50.17	179.60	321.33	175.19	88.05	1.83	4.83	-99.61	15.83	-169.13
T	150.57	76.21	221.65	-103.08	321.78	-174.31	110.74	37.37	151.35	90.30	219.79	-94.06
E_2	225.88	10.35	326.66	-171.79	699.20	10.84	626.25	11.74	183.90	12.95	261.88	-169.17
Tree	318.62	35.90	456.51	-144.90	379.81	15.20	727.67	15.51	262.50	47.18	382.69	-135.46
PC_1^f	6.53	90.00	9.06	-90.00	2.46	-90.00	2.67	90.00	6.53	90.00	9.06	-90.00
PC_1^{nf}	17.24	174.11	25.09	-7.06	55.51	173.69	48.14	173.33	25.01	176.60	35.40	-4.23
PC_1	19.05	154.17	27.70	-26.00	55.29	176.23	48.52	170.20	26.22	162.20	37.19	-18.29
PE_1^u	14.44	-5.39	21.40	173.83	48.85	0.45	30.18	-8.92	9.66	6.30	14.56	-178.10
PE_1^d	14.67	2.30	21.27	-177.54	40.03	1.26	32.89	4.06	8.37	2.08	12.37	-179.67
Penguin	14.07	32.36	20.65	-148.61	34.06	8.29	15.94	21.77	11.71	126.73	14.83	-55.54

TABLE XXIX: Invariant amplitudes of the $\Lambda_b \rightarrow p K_1(1400)^-$ decay with mixing abgle $\theta_K = 30^\circ$.

	Real($H_{1/2,1}$)	Imag($H_{1/2,1}$)	Real($H_{-1/2,-1}$)	Imag($H_{-1/2,-1}$)	Real($H_{1/2,0}$)	Imag($H_{1/2,0}$)	Real($H_{-1/2,0}$)	Imag($H_{-1/2,0}$)
T^f	-0.00	-33.73	0.00	1967.90	0.00	34.08	0.00	-5381.29
T^{nf}	74.68	43.86	64.35	-17.17	2370.88	-276.73	-2405.30	333.60
T	74.68	10.13	64.35	1950.73	2370.88	-242.65	-2405.30	-5047.68
E_2	1.30	-44.14	2299.26	484.10	-313.49	219.18	850.48	501.57
Tree	75.98	-34.01	2363.61	2434.83	2057.39	-23.47	-1554.81	-4546.11
PC_1^f	-0.00	-1.35	0.00	82.39	0.00	0.97	0.00	-225.54
PC_1^{nf}	2.17	2.15	-317.96	21.19	31.88	-7.79	-83.06	8.73
PC_1	2.17	0.81	-317.96	103.59	31.88	-6.82	-83.06	-216.81
PE_1^u	3.49	-4.64	126.65	8.96	-132.44	-27.29	-6.22	18.32
PE_1^d	1.71	-1.64	108.92	2.27	-52.16	9.54	-36.19	1.84
Penguin	7.36	-5.47	-82.40	114.81	-152.73	-24.57	-125.47	-196.66
	$ H_{1/2,1} $	$\phi(H_{1/2,1})^\circ$	$ H_{-1/2,-1} $	$\phi(H_{-1/2,-1})^\circ$	$ H_{1/2,0} $	$\phi(H_{1/2,0})^\circ$	$ H_{-1/2,0} $	$\phi(H_{-1/2,0})^\circ$
T^f	33.73	-90.00	1967.90	90.00	34.08	90.00	5381.29	-90.00
T^{nf}	86.61	30.43	66.60	-14.94	2386.97	-6.66	2428.32	172.10
T	75.36	7.72	1951.79	88.11	2383.26	-5.84	5591.47	-115.48
E_2	44.16	-88.32	2349.67	11.89	382.52	145.04	987.37	30.53
Tree	83.24	-24.12	3393.39	45.85	2057.52	-0.65	4804.64	-108.88
PC_1^f	1.35	-90.00	82.39	90.00	0.97	90.00	225.54	-90.00
PC_1^{nf}	3.06	44.74	318.67	176.19	32.82	-13.74	83.52	174.00
PC_1	2.32	20.38	334.41	161.96	32.60	-12.07	232.18	-110.96
PE_1^u	5.80	-53.10	126.96	4.05	135.23	-168.36	19.34	108.75
PE_1^d	2.36	-43.77	108.94	1.19	53.03	169.64	36.24	177.09
Penguin	9.17	-36.61	141.32	125.67	154.69	-170.86	233.28	-122.54

TABLE XXX: Helicity amplitudes of the $\Lambda_b \rightarrow p K_1(1400)^-$ decay.

	Real(S^L)	Imag(S^L)	Real(S^T)	Imag(S^T)	Real(P_1)	Imag(P_1)	Real(P_2)	Imag(P_2)	Real(D)	Imag(D)	Real($D + S^L$)	Imag($D + S^L$)
T^f	-0.00	-156.11	-0.00	-156.11	0.00	283.94	0.00	-150.85	-0.00	-131.44	-0.00	-287.56
T^{nf}	-35.90	9.89	0.81	4.76	1.83	-3.02	-10.84	-2.08	-217.72	22.52	-253.61	32.41
T	-35.90	-146.23	0.81	-151.35	1.83	280.92	-10.84	-152.93	-217.72	-108.92	-253.61	-255.15
E_2	-222.20	-40.60	-179.22	-41.20	-28.51	-38.27	-179.43	-34.31	284.01	55.59	61.81	14.99
Tree	-258.10	-186.82	-178.42	-192.55	-26.69	242.64	-190.27	-187.24	66.29	-53.33	-191.81	-240.15
PC_1^f	-0.00	-6.53	-0.00	-6.53	0.00	11.92	0.00	-6.32	-0.00	-5.50	-0.00	-12.03
PC_1^{nf}	17.15	-1.77	24.97	-1.49	2.72	-0.05	24.63	1.82	-23.25	2.65	-6.10	0.88
PC_1	17.15	-8.30	24.97	-8.02	2.72	11.87	24.63	-8.14	-23.25	-2.85	-6.10	-11.15
PE_1^u	-14.38	1.36	-9.61	-1.06	7.36	0.48	-10.15	-0.34	21.08	1.07	6.70	2.42
PE_1^d	-14.66	-0.59	-8.36	-0.30	4.69	-0.60	-8.63	-0.05	15.51	0.18	0.85	-0.41
Penguin	-11.89	-7.53	7.00	-9.38	14.77	11.75	5.85	-8.53	13.34	-1.60	1.45	-9.14
	$ S^L $	$\phi(S^L)^\circ$	$ S^T $	$\phi(S^T)^\circ$	$ P_1 $	$\phi(P_1)^\circ$	$ P_2 $	$\phi(P_2)^\circ$	$ D $	$\phi(D)^\circ$	$ D + S^L $	$\phi(D + S^L)^\circ$
T^f	156.11	-90.00	156.11	-90.00	283.94	90.00	150.85	-90.00	131.44	-90.00	287.56	-90.00
T^{nf}	37.24	164.60	4.83	80.39	3.53	-58.82	11.04	-169.13	218.88	174.09	255.68	172.72
T	150.57	-103.79	151.35	-89.70	280.92	89.63	153.31	-94.06	243.44	-153.42	359.75	-134.83
E_2	225.88	-169.65	183.90	-167.05	47.73	-126.69	182.68	-169.17	289.40	11.08	63.60	13.64
Tree	318.62	-144.10	262.50	-132.82	244.11	96.28	266.95	-135.46	85.08	-38.82	307.35	-128.61
PC_1^f	6.53	-90.00	6.53	-90.00	11.92	90.00	6.32	-90.00	5.50	-90.00	12.03	-90.00
PC_1^{nf}	17.24	-5.89	25.01	-3.40	2.72	-1.05	24.70	-4.23	23.40	173.50	6.17	171.82
PC_1	19.05	-25.83	26.22	-17.80	12.18	77.11	25.94	-18.29	23.42	-173.01	12.71	-118.69
PE_1^u	14.44	174.61	9.66	-173.70	7.38	3.70	10.15	-178.10	21.11	2.89	7.13	19.87
PE_1^d	14.67	-177.70	8.37	-177.92	4.73	-7.33	8.63	-179.67	15.51	0.66	0.94	-25.74
Penguin	14.07	-147.64	11.71	-53.27	18.87	38.49	10.34	-55.54	13.43	-6.86	9.25	-81.00

TABLE XXXI: Partial wave amplitudes of the $\Lambda_b \rightarrow p K_1(1400)^-$ decay.

-
- [1] J. H. Christenson, J. W. Cronin, V. L. Fitch and R. Turlay, Evidence for the 2π Decay of the K_2^0 Meson, Phys. Rev. Lett. **13**, 138-140 (1964)
- [2] B. Aubert *et al.* (BaBar Collaboration), Measurement of CP -violating asymmetries in B^0 decays to CP eigenstates, Phys. Rev. Lett. **86**, 2515-2522 (2001)
- [3] K. Abe *et al.* (Belle Collaboration), Observation of large CP violation in the neutral B meson system, Phys. Rev. Lett. **87**, 091802 (2001)
- [4] R. Aaij *et al.* (LHCb Collaboration), Observation of CP Violation in Charm Decays, Phys. Rev. Lett. **122**, 211803 (2019)
- [5] M. Ablikim *et al.* (BESIII Collaboration), Polarization and Entanglement in Baryon-Antibaryon Pair Production in Electron-Positron Annihilation, Nature Phys. **15**, 631-634 (2019)
- [6] M. Ablikim *et al.* (BESIII Collaboration), Probing CP symmetry and weak phases with entangled double-strange baryons, Nature **606**, no.7912, 64-69 (2022)
- [7] L. K. Li *et al.* (Belle Collaboration), Search for CP violation and measurement of branching fractions and decay asymmetry parameters for $\Lambda_c^+ \rightarrow \Lambda h^+$ and $\Lambda_c^+ \rightarrow \Sigma^0 h^+$ ($h = K, \pi$), Sci. Bull. **68** (2023), 583-592
- [8] R. Aaij *et al.* (LHCb Collaboration), Measurement of matter-antimatter differences in beauty baryon decays, Nature Phys. **13**, 391-396 (2017)
- [9] R. Aaij *et al.* (LHCb Collaboration), A measurement of the CP asymmetry difference in $\Lambda_c^+ \rightarrow pK^-K^+$ and $p\pi^-\pi^+$ decays, JHEP **03**, 182 (2018)
- [10] R. Aaij *et al.* (LHCb Collaboration), Search for CP violation using triple product asymmetries in $\Lambda_b^0 \rightarrow pK^-\pi^+\pi^-$, $\Lambda_b^0 \rightarrow pK^-K^+K^-$ and $\Xi_b^0 \rightarrow pK^-K^-\pi^+$ decays, JHEP **08**, 039 (2018)
- [11] R. Aaij *et al.* (LHCb Collaboration), Search for CP violation in $\Lambda_b^0 \rightarrow pK^-$ and $\Lambda_b^0 \rightarrow p\pi^-$ decays, Phys. Lett. B **787**, 124-133 (2018)
- [12] R. Aaij *et al.* (LHCb Collaboration), Measurements of CP asymmetries in charmless four-body Λ_b^0 and Ξ_b^0 decays, Eur. Phys. J. C **79**, 745 (2019)
- [13] R. Aaij *et al.* (LHCb Collaboration), Search for CP violation and observation of P violation in $\Lambda_b^0 \rightarrow p\pi^-\pi^+\pi^-$ decays, Phys. Rev. D **102**, 051101 (2020)
- [14] R. Aaij *et al.* (LHCb Collaboration), Measurement of CP asymmetries in $\Lambda_b^0 \rightarrow ph^-$ decays, Phys. Rev. D **111**, 092004 (2025)
- [15] R. Aaij *et al.* (LHCb Collaboration), Study of Λ_b^0 and Ξ_b^0 Decays to $\Lambda h^+h'^-$ and Evidence for CP Violation in $\Lambda_b^0 \rightarrow \Lambda K^+K^-$ Decays, Phys. Rev. Lett. **134**, 101802 (2025)
- [16] R. Aaij *et al.* (LHCb Collaboration), Observation of charge-parity symmetry breaking in baryon decays, [arXiv:2503.16954 [hep-ex]].
- [17] J. J. Han, J. X. Yu, Y. Li, H. n. Li, J. P. Wang, Z. J. Xiao and F. S. Yu, Establishing CP Violation in b-Baryon Decays, Phys. Rev. Lett. **134**, 221801 (2025)
- [18] J. P. Wang, Q. Qin and F. S. Yu, CP violation observables in baryon decays, [arXiv:2411.18323 [hep-ph]].
- [19] J. G. Korner and M. Kramer, Exclusive nonleptonic charm baryon decays, Z. Phys. C **55**, 659-670 (1992)
- [20] Y. J. Zhao, Z. H. Zhang and X. H. Guo, Decay-angular-distribution correlated CP violation in heavy hadron cascade decays, Phys. Rev. D **110**, no.1, 013007 (2024)
- [21] C. Q. Geng and C. W. Liu, Time-reversal asymmetries and angular distributions in $\Lambda_b \rightarrow \Lambda V$, JHEP **11**, 104 (2021)

- [22] W. Wang, Factorization of Heavy-to-Light Baryonic Transitions in SCET, Phys. Lett. B **708**, 119-126 (2012)
- [23] J. J. Han, Y. Li, H. n. Li, Y. L. Shen, Z. J. Xiao and F. S. Yu, $\Lambda_b \rightarrow p$ transition form factors in perturbative QCD, Eur. Phys. J. C **82**, no.8, 686 (2022)
- [24] M. Beneke, G. Buchalla, M. Neubert and C. T. Sachrajda, QCD factorization for $B \rightarrow \pi\pi$ decays: Strong phases and CP violation in the heavy quark limit, Phys. Rev. Lett. **83**, 1914-1917 (1999)
- [25] M. Beneke, G. Buchalla, M. Neubert and C. T. Sachrajda, QCD factorization for exclusive, nonleptonic B meson decays: General arguments and the case of heavy light final states, Nucl. Phys. B **591**, 313-418 (2000)
- [26] C. W. Bauer, S. Fleming, D. Pirjol and I. W. Stewart, An Effective field theory for collinear and soft gluons: Heavy to light decays, Phys. Rev. D **63**, 114020 (2001)
- [27] C. W. Bauer, D. Pirjol and I. W. Stewart, Soft collinear factorization in effective field theory, Phys. Rev. D **65**, 054022 (2002)
- [28] C. W. Bauer, S. Fleming, D. Pirjol, I. Z. Rothstein and I. W. Stewart, Hard scattering factorization from effective field theory, Phys. Rev. D **66**, 014017 (2002)
- [29] Y. Y. Keum, H. N. Li and A. I. Sanda, Penguin enhancement and $B \rightarrow K\pi$ decays in perturbative QCD, Phys. Rev. D **63**, 054008 (2001)
- [30] C. D. Lu, K. Ukai and M. Z. Yang, Branching ratio and CP violation of $B \rightarrow \pi\pi$ decays in perturbative QCD approach, Phys. Rev. D **63**, 074009 (2001)
- [31] Y. Y. Keum, H. n. Li and A. I. Sanda, Fat penguins and imaginary penguins in perturbative QCD, Phys. Lett. B **504**, 6-14 (2001)
- [32] Y. K. Hsiao and C. Q. Geng, Direct CP violation in Λ_b decays, Phys. Rev. D **91**, no.11, 116007 (2015)
- [33] Y. K. Hsiao, Y. Yao and C. Q. Geng, Charmless two-body anti-triplet b -baryon decays, Phys. Rev. D **95**, no.9, 093001 (2017)
- [34] C. Q. Geng, C. W. Liu and T. H. Tsai, Non-leptonic two-body decays of Λ_b^0 in light-front quark model, Phys. Lett. B **815**, 136125 (2021)
- [35] J. Zhu, H. W. Ke and Z. T. Wei, The decay of $\Lambda_b \rightarrow p K^-$ in QCD factorization approach, Eur. Phys. J. C **76**, no.5, 284 (2016)
- [36] J. Zhu, Z. T. Wei and H. W. Ke, Semileptonic and nonleptonic weak decays of Λ_b^0 , Phys. Rev. D **99**, no.5, 054020 (2019)
- [37] C. D. Lu, Y. M. Wang, H. Zou, A. Ali and G. Kramer, Anatomy of the perturbative QCD approach to the baryonic decays $\Lambda_b \rightarrow p\pi, pK$, Phys. Rev. D **80**, 034011 (2009)
- [38] G. Buchalla, A. J. Buras and M. E. Lautenbacher, Weak decays beyond leading logarithms, Rev. Mod. Phys. **68**, 1125-1144 (1996)
- [39] L. L. Chau, H. Y. Cheng and B. Tseng, Analysis of two-body decays of charmed baryons using the quark diagram scheme, Phys. Rev. D **54**, 2132-2160 (1996)
- [40] F. S. Yu, H. Y. Jiang, R. H. Li, C. D. Lü, W. Wang and Z. X. Zhao, Discovery Potentials of Doubly Charmed Baryons, Chin. Phys. C **42**, no.5, 051001 (2018)
- [41] C. P. Jia, H. Y. Jiang, J. P. Wang and F. S. Yu, Final-state rescattering mechanism of charmed baryon decays, JHEP **11**, 072 (2024)
- [42] A. K. Leibovich, Z. Ligeti, I. W. Stewart and M. B. Wise, Predictions for nonleptonic Lambda(b) and Theta(b) decays, Phys. Lett. B **586**, 337-344 (2004)
- [43] P. Ball, V. M. Braun and E. Gardi, Distribution Amplitudes of the Lambda(b) Baryon in QCD, Phys. Lett. B **665**, 197-204 (2008)
- [44] G. Bell, T. Feldmann, Y. M. Wang and M. W. Y. Yip, Light-Cone Distribution Amplitudes for Heavy-Quark Hadrons, JHEP **11**, 191 (2013)

- [45] Y. M. Wang and Y. L. Shen, Perturbative Corrections to $\Lambda_b \rightarrow \Lambda$ Form Factors from QCD Light-Cone Sum Rules, JHEP **02**, 179 (2016)
- [46] A. Ali, C. Hambrock and A. Y. Parkhomenko, Light-cone wave functions of heavy baryons, Theor. Math. Phys. **170**, 2-16 (2012)
- [47] S. Groote, J. G. Korner and O. I. Yakovlev, An Analysis of diagonal and nondiagonal QCD sum rules for heavy baryons at next-to-leading order in alpha-s, Phys. Rev. D **56**, 3943-3954 (1997)
- [48] K. S. Huang, W. Liu, Y. L. Shen and F. S. Yu, $\Lambda_b \rightarrow p, N^*(1535)$ form factors from QCD light-cone sum rules, Eur. Phys. J. C **83**, no.4, 272 (2023)
- [49] V. Braun, R. J. Fries, N. Mahnke and E. Stein, Higher twist distribution amplitudes of the nucleon in QCD, Nucl. Phys. B **589**, 381-409 (2000) [erratum: Nucl. Phys. B **607**, 433-433 (2001)]
- [50] V. M. Braun, A. Lenz and M. Wittmann, Nucleon Form Factors in QCD, Phys. Rev. D **73**, 094019 (2006)
- [51] G. S. Bali *et al.* [RQCD], Light-cone distribution amplitudes of octet baryons from lattice QCD, Eur. Phys. J. A **55**, no.7, 116 (2019)
- [52] V. L. Chernyak and A. R. Zhitnitsky, Asymptotic Behavior of Exclusive Processes in QCD, Phys. Rept. **112**, 173 (1984)
- [53] V. M. Braun and I. E. Filyanov, QCD Sum Rules in Exclusive Kinematics and Pion Wave Function, Z. Phys. C **44**, 157 (1989)
- [54] V. M. Braun and I. E. Filyanov, Conformal Invariance and Pion Wave Functions of Nonleading Twist, Z. Phys. C **48**, 239-248 (1990)
- [55] T. Kurimoto, H. n. Li and A. I. Sanda, Leading power contributions to $B \rightarrow \pi, \rho$ transition form-factors, Phys. Rev. D **65**, 014007 (2002)
- [56] P. Ball and R. Zwicky, New results on $B \rightarrow \pi, K, \eta$ decay formfactors from light-cone sum rules, Phys. Rev. D **71**, 014015 (2005)
- [57] P. Ball, V. M. Braun and A. Lenz, Higher-twist distribution amplitudes of the K meson in QCD, JHEP **05**, 004 (2006)
- [58] R. H. Li, C. D. Lu and W. Wang, Transition form factors of B decays into p-wave axial-vector mesons in the perturbative QCD approach, Phys. Rev. D **79**, 034014 (2009)
- [59] A. Ali, G. Kramer, Y. Li, C. D. Lu, Y. L. Shen, W. Wang and Y. M. Wang, Charmless non-leptonic B_s decays to PP, PV and VV final states in the pQCD approach, Phys. Rev. D **76**, 074018 (2007)
- [60] V. M. Braun and A. Lenz, On the SU(3) symmetry-breaking corrections to meson distribution amplitudes, Phys. Rev. D **70**, 074020 (2004)
- [61] P. Ball and R. Zwicky, SU(3) breaking of leading-twist K and K^* distribution amplitudes: A Reprise, Phys. Lett. B **633**, 289-297 (2006)
- [62] P. Ball and R. Zwicky, $|V_{td}/V_{ts}|$ from $B \rightarrow V\gamma$, JHEP **04**, 046 (2006)
- [63] P. Ball and G. W. Jones, Twist-3 distribution amplitudes of K^* and phi mesons, JHEP **03**, 069 (2007)
- [64] H. Y. Cheng, Mixing angle of K_1 axial vector mesons, PoS **Hadron2013**, 090 (2013)
- [65] H. Hatanaka and K. C. Yang, $B \rightarrow K(1)$ gamma Decays in the Light-Cone QCD Sum Rules, Phys. Rev. D **77**, 094023 (2008) [erratum: Phys. Rev. D **78**, 059902 (2008)]
- [66] H. Y. Cheng, Revisiting Axial-Vector Meson Mixing, Phys. Lett. B **707**, 116-120 (2012)
- [67] Y. J. Shi, J. Zeng and Z. F. Deng, Revisiting $K1(1270)$ - $K1(1400)$ mixing with QCD sum rules, Phys. Rev. D **109**, no.1, 016027 (2024)
- [68] G. P. Lepage, A New Algorithm for Adaptive Multidimensional Integration, J. Comput. Phys. **27**, 192 (1978)
- [69] G. P. Lepage, Adaptive multidimensional integration: VEGAS enhanced, J. Comput. Phys. **439**, 110386 (2021)

- [70] H. Y. Cheng, Nonleptonic weak decays of bottom baryons, Phys. Rev. D **56**, 2799-2811 (1997) [erratum: Phys. Rev. D **99**, no.7, 079901 (2019)]
- [71] H. Y. Cheng and S. Oh, Flavor SU(3) symmetry and QCD factorization in $B \rightarrow PP$ and PV decays, JHEP **09**, 024 (2011)
- [72] C. Q. Geng, C. W. Liu and T. H. Tsai, Nonleptonic two-body weak decays of Λ_b in modified MIT bag model, Phys. Rev. D **102**, no.3, 034033 (2020)
- [73] T. D. Lee and C. N. Yang, General Partial Wave Analysis of the Decay of a Hyperon of Spin 1/2, Phys. Rev. **108**, 1645-1647 (1957)
- [74] S. M. Berman and M. Jacob, SYSTEMATICS OF ANGULAR POLARIZATION DISTRIBUTIONS IN THREE-BODY DECAYS, Phys. Rev. **139**, B1023 (1965)
- [75] R. Aaij *et al.* (LHCb Collaboration), Measurement of the b -quark production cross-section in 7 and 13 TeV pp collisions, Phys. Rev. Lett. **118** (2017) no.5, 052002 [erratum: Phys. Rev. Lett. **119** (2017) no.16, 169901]
- [76] S. Chen, Y. Li, W. Qian, Z. Shen, Y. Xie, Z. Yang, L. Zhang and Y. Zhang, Heavy Flavour Physics and CP Violation at LHCb: a Ten-Year Review, Front. Phys. **18**, 44601 (2023)
- [77] See <https://lbfence.cern.ch/alcms/public/figure/details/3837>
- [78] S. Pakvasa, S. P. Rosen and S. F. Tuan, Parity Violation and Flavor Selection Rules in Charmed Baryon Decays, Phys. Rev. D **42**, 3746-3754 (1990)